NTNU – Trondheim
Norwegian University of
Science and Technology

Design of a Surge Tank Throttle for Tonstad Hydropower Plant

Daniel Gomsrud

Civil and Environmental Engineering
Submission date: June 2015
Supervisor: Leif Lia, IVM
Co-supervisor: Kaspar Vereide, IVM

Norwegian University of Science and Technology
Department of Hydraulic and Environmental Engineering

NTNU

M.Sc. THESIS IN HYDRAULIC ENGINEERING

Candidate: Mr. Daniel Gomsrud

Title: Design of a Surge Tank Throttle for Tonstad Hydropower Plant

1. Background

Tonstad power plant is the largest power plant in Norway regarding to annual energy production. The average annual energy production is 3.6 TWh with an installed capacity of 960 MW. The power plant has been constructed in three steps. The first step (1964) included two units of total 320 MW, the second step (1971) included two additional unit of total 320 MW, and the third step (1988) included one unit of 320 MW.

The water conduit was originally designed for 640 MW, and the latest addition of 320 MW has resulted in several problems related to hydraulic transients. The implementation of the energy law in 1990, which introduced a free electricity marked in Norway has further increased these problems due to hydropeaking operation.

One of the major problems are related to the amplitude of mass oscillations in the three surge tanks. The power plant owner has experienced transport of gravel and sand from the rock trap, and down into the turbines. Restrictions on the operation are now enforced to avoid similar problems in the future. The restrictions does however result in economic losses, due to limited operation during times with beneficial marked situations.

A new measure to reduce the amplitudes of the mass oscillations are now considered. By installing a throttle in the surge tanks, it is possible to reduce the amplitudes. The throttle is normally constructed as a steel cone in the inlet to the surge tank, which reduces the cross-section of the surge tank, and thereby reduces the water flow. The effect of such throttling is site-specific, and studies with detailed information about the existing power plant are necessary before implementation.

2. Main questions for the thesis

The thesis shall cover, though not necessarily be limited to the main questions listed below.

2.1 Literature and desk study

The candidate shall carry out a literature study of waterway design and relevant theory. In addition the implementation of theory and simulation method in the numerical simulation program LVTRANS must be studied.

2.2 Main tasks

The candidate must find available background material such as former studies, reports and drawings of Tonstad power plant. Related to this material the following must be carried out:

1 Estimation of annual economic loss due to restriction on operation
2 Numerical modelling of Tonstad power plant with the software LVTRANS.
3 Calibration and validation of the numerical model
4 Determination of critical situations

5 Design of throttle
6 Evaluation of throttle effect
7 Evaluation of uncertainties
8 Conclusions
9 Proposals for future work
10 Presentation

3 Supervision and data input

Professor Leif Lia and PhD candidate Kaspar Vereide will supervise and assist the candidate, and make relevant information available.

Discussion with and input from colleagues and other research or engineering staff at NTNU is recommended. Significant inputs from other shall be referenced in a convenient manner.

The research and engineering work carried out by the candidate in connection with this thesis shall remain within an educational context. Tonstad power plant is regarded as a study object, and the candidate and the supervisors are therefore free to introduce assumptions and limitations which may be considered unrealistic or inappropriate in a contract research or a professional context.

4 Report format, references and contract

The master contract must be signed not later than 15. January. The report should be written with a text editing software, and figures, tables, photos etc. should be of good quality. The report should contain an executive summary, a table of content, a list of figures and tables, a list of references and information about other relevant sources. The report should be submitted electronically in B5-format .pdf-file in DAIM, and three paper copies should be handed in to the institute.

The executive summary should not exceed 450 words, and should be suitable for electronic reporting.

The Master's thesis should be submitted within Wednesday 10th of June 2015.

Trondheim 15. January 2015

Leif Lia
Professor
Department of Hydraulic and Environmental Engineering
NTNU

Abstract

The objective of this thesis has been to evaluate the effect of throttling the surge tanks at Tonstad Hydropower Plant, by the means of one-dimensional numerical modelling in the program LVTrans. The background of the thesis is problems with the amplitude of mass oscillations in the surge tanks at Tonstad, causing restrictions on operation, due to the fear of drawing the surge tank water level down to a level where air enters the sand trap and initiates free surface flow.

The numerical model of Tonstad hydropower plant, used for simulations, is currently running as a superset regulator at the plant. The calibration and validation shows good representation of steady state operation and period of mass oscillations. The amplitude of mass oscillations, does however show high deviations that are attributed to the inaccurate representation of transient friction in the numerical method. The simulations are interpreted relatively to minimise the error from the numerical model to the prototype, meaning that throttle effect is evaluated on the basis of improvement of mass oscillation amplitude from the restricted surge tank steady state water level. The critical situation for drawdown at this restriction level has been found to be with an output effect of 660 MW, reservoir levels at 482 m.a.s.l. in Homstøl and Ousdal, 49.5 m.a.s.l. in Sirdalsvann and with no inflow of water to the creek intakes.

An optimization of throttle losses was performed by comparing a simulation of the current situation with simulations with varying throttle losses. The throttles asymmetric geometry was calculated from tabular values. The optimization finds that an asymmetric throttle, with loss ratio 1:1.5 from upwards to downwards flow respectively, may reduce downswing of the water level by 9.6 meters. A simulation where the restriction level in the surge tanks is reduced by 8 meters, show that the surge tank water level downswing is further reduced by 5.3 meters. It is concluded that the optimized throttle allows for a reduction of the restricted water level in the surge tank from 470 to 462 m.a.s.l., provided that all reservoir gates are fully open and water level at Ousdal is equal or higher than the water level at Homstøl. Some uncertainties connected with the numerical model are high, but these are outweighed by several conservative assumptions made in the simulations.

The annual economic loss due to restricted operation is estimated to 2.5 million NOK, resulting in an allowed throttle cost of 33.3 million NOK to ensure profitability. The evaluation of surge tank throttling at Tonstad Hydropower Plant exemplifies benefits that may be achieved by detailed surge tank throttle design at other high head hydropower plants.

Sammendrag

Målet med denne masteroppgaven har vært å evaluere effekten av å installere en strupning i svingesjaktene på Tonstad Kraftverk ved å benytte endimensjonal numerisk modellering i programmet LVTrans. Bakgrunnen for oppgaven er problemer med amplituden til massesvingningene i svingekammeret, som fører til restriksjoner på kjøringen av kraftverket, fordi det fryktes at vannspeilet i svingekammeret kan bli dratt ned til et nivå der man får frispeilstrømning i sandfanget.

Den numeriske modellen som er brukt i oppgaven er i kontinuerlig drift som en overordnet regulator i kraftverket. Kalibrering og validering av modellen viser at den representerer stasjonær strømning og perioden til massesvingningene godt, men at amplituden til massesvinget viser store avvik fra målte verdier. Avvikene er begrunnet med unøyaktig beskrivelse av den transiente friksjonen i den benyttede numeriske metoden. Simuleringene er derfor tolket relativt til hverandre for å minimere feil mellom virkelighet og simuleringer. Dette betyr at strupningseffekten vurderes ved å betrakte forbedringen i amplituden til simuleringer med stasjonært nivå likt som sikkerhetsnivået i svingekamrene. Den kritiske situasjonen ved dette nivået er ved kraftverkseffekt på 660 MW, magasinnivå på 482 moh. i Ousdal og Homstøl, 49,5 moh. i Sirdalsvann og med null vannføring i bekkeinntakene.

Optimalisering av strupningstapet ble gjennomført ved å sammenligne en simulering av den nåværende situasjonen med simuleringer påført varierende strupningstap. Geometrien til den asymmetriske strupningen ble beregnet ved bruk av tabellverdier. Resultatet av optimaliseringen tilsier at en strupning med tapsforhold 1:1,5 mellom henholdsvis oppadrettet og nedadrettet strømning kan redusere nedsvinget med 9,6 meter. En simulering der sikkerhetsnivået i sjakta er flyttet 8 meter nedover viser at nedsvinget blir ytterligere redusert med 5.3 meter. Det er derfor konkludert med at den optimaliserte strupningen tillater en reduksjon av sikkerhetsnivået i svingekammeret fra 470 til 462 moh., under forutsetning av at inntakslukene i magasinene er helt åpne og at nivået i Ousdal er likt eller høyere enn nivået i Homstøl. Det er tilknyttet noen store usikkerhetsmomenter til den numeriske modellen, men disse er oppveiet av flere konservative antagelser i simuleringene.

Det økonomiske tapet av den begrensede produksjonen, på grunn av sikkerhetsnivået i svingesjaktene, er estimert til 2,5 millioner NOK, hvilket resulterer i en tillat kostnad på 33,3 millioner NOK for at en strupning skal bli lønnsom.

Preface

This thesis is submitted as the final requirement for a Master's Degree in Hydraulic and Environmental Engineering at the Norwegian University of Science and Technology. The thesis, supervised by Professor Leif Lia and Ph.D. Candidate Kaspar Vereide, is a study on the design and effect of hydraulic throttling of the surge tanks at Tonstad Hydropower Plant. This is closely related to Kaspar Vereide's work and his knowledge in the field of hydraulic transients and numerical computation has been invaluable for completion of the thesis. The work has greatly expanded my knowledge and interest in how hydraulic transients affect the design and operation of high head power plants. It has been rewarding to study an actual problem, which may be of interest beyond the academic.

I would like to thank my supervisors for their guidance and readiness to help, whenever it was needed. The extent of the thesis would not be possible without an accurate numerical model, and great thanks are expressed towards Bjørnar Svingen, who did not only provide the program, model and calibration data, but has taken the time to answer questions and help with his understanding of some results.

Lastly, I would like to thank Sira-Kvina Kraftselskap for their co-operation, hospitality and interest in the thesis, with special thanks to Rolv Guddal, Sigurd Netlandsnes, Anders Løyning and Einar Thygesen.

Trondheim 9th of June 2015

Daniel Gomsrud

Table of Contents

List of Figures

List of Tables

Abbreviations

CFD	Computational Fluid Dynamics
DCF	Discounted Cash-Flow
FRR-A	Automatic Frequency Restoration Reserves
FRR-M	Manual Frequency Restoration Reserves
HRWL	Highest regulated water level
IRR	Internal Rate of Return
LabVIEW	Laboratory Virtual Instrument Workbench
LCOE	Levelized Cost of Energy
LRWL	Lowest regulated water level
LVTrans	LabView Transient Pipe Analysis
m.a.s.l.	Meters Above Sea Level
MNOK	Million Norwegian Kroners
MOC	Method of Characteristics
NPV	Net Present Value

Definitions

Surge tank	The whole surge tank system. Includes lower and upper chambers, and the riser shaft.
Surge tank chamber	The upper or lower chamber, with surface area much bigger than in surge shaft.
Surge shaft	The vertical shaft connecting the upper and lower chamber of a surge tank together.
Loss factor	Referring to the loss formulation denoted by the coefficient C_v, where lower values equals higher loss than higher values.
Resistance coefficient	Referring to the loss formulation denoted by k, where higher values equals higher loss than lower values.

List of Symbols

Symbol	Unit	Description
A	m^2	Area
C	$-$	Loss coefficient
D	m	Diameter
H	m	Hydraulic Head
K	N/m^2	Bulk elasticity modulus
L	m	Length
Q	m^3/s	Discharge
R	$-$	Throttle loss ratio
V	m^3	Volume
a	m/s	Wave propagation velocity
c	m/s	Speed of Sound
f	$-$	Friction Factor
h	$-$	Head Loss
k	$-$	Loss Coefficient
m	kg	Mass
p	N/m^2	Pressure
t	s	Time
v	m/s	Velocity
x	m	Length in x-plane
α	°	Angle
ρ	kg/m^3	Density
τ	N/m^2	Shear Stress

List of Subscripts and Superscripts

Symbol	Description
0	Initial
L	Loss
T	Tunnel
f	Friction
ss	Surge Shaft
sys	System
th	Throttle
loc	Local

1 Introduction

With increasing demand for renewable energy, and an increasing market for energy from water, wind and solar technologies (International Energy Agency, 2014), the necessity for the regulation of power is increasing. The replacement of thermic production of energy and the increased transport capacity to the European market is expected to create higher demand and more competition for flexible Norwegian energy (Statnett SF, 2014). As seen from Figure 1.1, it is expected that unregulated power sources will constitute a big portion of the energy production during periods of the year in the Nordic countries. This will periodically lead to stoppage of a large part of the regulated hydropower, enhancing the opportunity for production and export in periods with high electricity prices. A likely result of a larger amount of unregulated power is the need for more reserve capacity.

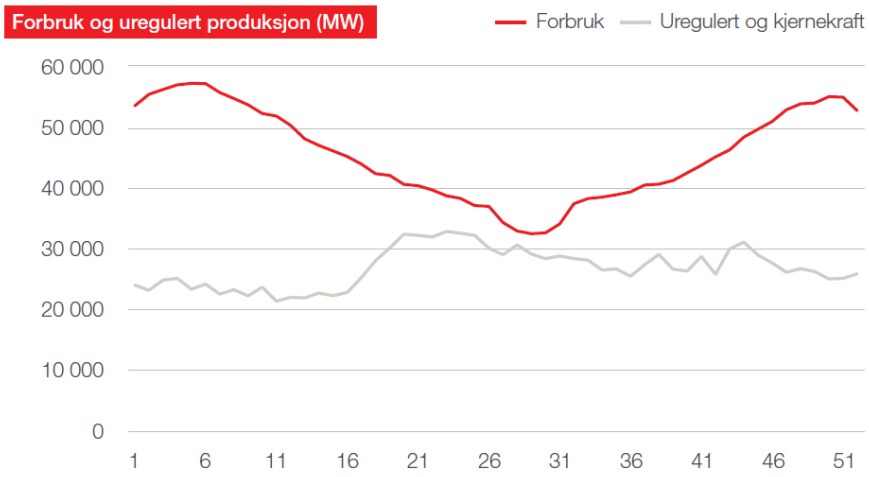

Figure 1.1: Simulated annual total demand (red) and unregulated energy production (MW), including nuclear (light grey), in the Nordic countries in 2020 (Statnett SF, 2014).

The power system needs to be in balance at all times to prevent a rise or fall in frequency, and reserve capacity is therefore important to deal with imbalances in the grid. Norway is presently obliged to have a manual reserve capacity that can handle the cut off of 1200 MW, increasing to 1400 MW when the planned connections to Germany and Great Britain are put into operation (Statnett SF, 2014). An increase of imbalances is expected, due to new connections with direct current and increased errors in demand forecast, caused by the production uncertainty of the expanded construction of small hydro and wind power.

The Norwegian primary and secondary reserve capacities, used to take care of momentary imbalances, are automatically activated due to frequency changes in the grid, which means

that generators need to have a response time of minimum 120 to 210 seconds (Statnett SF, 2013a). The tertiary reserve system, *Manual Frequency Restoration Reserves* (FRR-M) are traded on a Nordic market, and used to disengage primary and secondary reserves and to handle regional bottlenecks (Statnett SF, 2013b). FRR-M has an activation time of about 15 minutes.

The development of the European market, with expectations of higher fluctuation of prices over the day and week, and need for more power reserves, requires more robust systems that are able to withstand the effects of increasingly rapid regulation.

1.1 Background

Tonstad *Hydropower Plant* (HPP) is currently the largest power plant in Norway regarding annual production. The power plant has an average annual production of 3.6 TWh with an installed capacity of 960 MW. After an expansion of Tonstad HPP in 1988, from 640 MW to 960 MW, problems related to hydraulic transients have occurred. These problems have been further enlarged by the peaking operation of the plant after 1990 when the energy law (Olje- og energidepartementet, 1990) opened for the free electricity market. Recently the implementation of the automatic secondary reserve system, *Automatic Frequency Restoration Reserves* (FRR-A), has made it necessary to develop a waterway protection system to protect the power plant from automatic regulations that will result in transients large enough to harm the waterway (Svingen, 2015). The FRR-A and the waterway protection system have been running since January 2015.

The problems in the waterway are related to the amplitude of mass oscillations in the three surge tanks at Tonstad. The owner of the power plant has experienced mass transport from the rock traps and damage to the turbines. The cause of this is believed to be that the water level has been drawn down below the lower chambers of the surge tanks and released air into the rock trap. A result of this is that there are prevailing restrictions in the plant operation which result in an economic loss, due to the limited possibility to operate the plant at the most favourable market situations.

A measure to reduce the amplitudes of the mass oscillations is to throttle the surge tanks. An optimal surge tank throttle will produce a large controlled hydraulic loss, which may reduce the amplitudes of the mass oscillations without causing excess pressure to the neighbouring tunnels and equipment. A surge tank throttle is usually built as a steel cone which reduces the

cross-sectional area of the surge tank riser, often with asymmetric geometry that will produce different hydraulic losses in upwards and downwards directions.

The main purpose of this thesis is the investigation of the possible benefits of installing surge tank throttles at Tonstad HPP. The design and evaluation of throttles will be based on simulations from a one-dimensional numerical model, which will be calibrated, validated and applied to the critical situation. The uncertainties will be thoroughly accounted for and an estimation of economic loss, due to restricted operation, will be completed. Conclusions and proposals for future work will be made after revision of the results. The emphasis is on the improved hydraulic situation, but considerations with regards to geometry, economy and construction are made.

1.2 Tonstad Hydropower Plant

Tonstad Hydropower Plant is situated in Sirdal, in the western part of Norway. Tonstad is owned by the Sira-Kvina Hydropower Company, which owns and operates multiple hydropower plants in the Sira and Kvina watersheds, as illustrated by Figure 1.2 based on Bøe et al. (2013). The annual energy production of all seven power plants are at approximately 6.3 TWh, with an installed capacity 1,760 MW, all of which is controlled remotely from the headquarters at Tonstad (Sira-Kvina Kraftselskap, 2015).

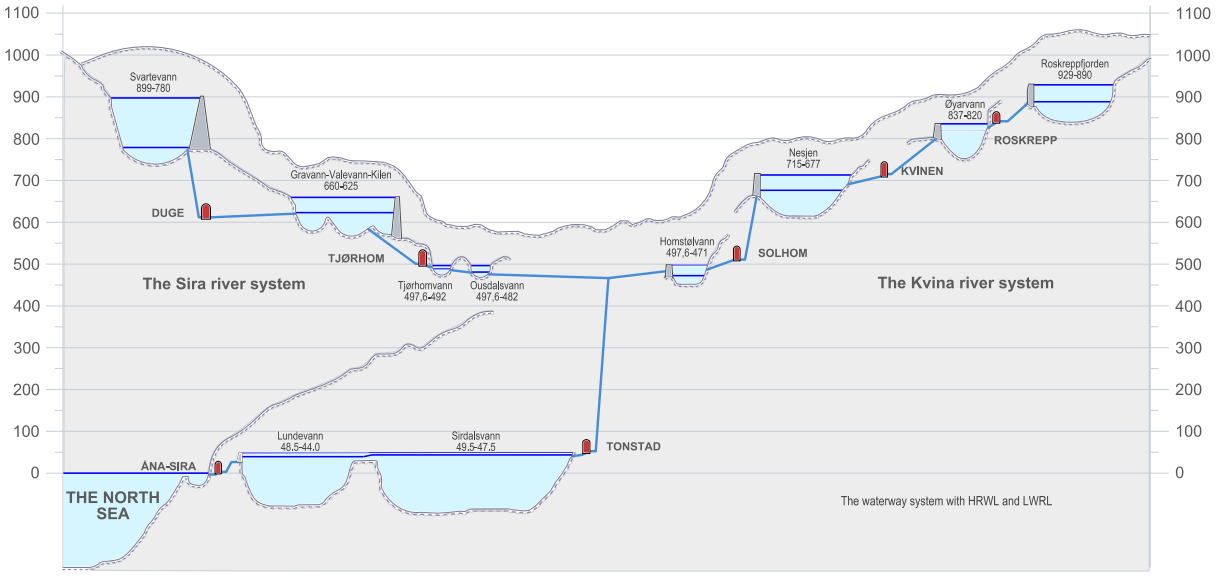

Figure 1.2: The Sira-Kvina waterway system

1.2.1 Brief History

Tonstad HPP was the first of the power plants Sira-Kvina Hydropower Company planned to build. The first electricity was produced by Tonstad in 1968 by two Francis units, while two additional units were commissioned in 1970, giving a total capacity of 640 MW and an annual output of 3.6 TWh, making it the largest power station in Norway at the time.

In 1988, exactly 25 years after the formation of Sira-Kvina Hydropower, a fith Francis turbine was opened at Tonstad HPP. The new 320 MW unit, connected to its own pressure shaft, was commissioned to, amongst other things, supply more effect and reduce flood losses.

The most recent expansion of the Tonstad waterway was the Øksendal connector, which entered service in 2010. The connector is a 6 km long tunnel that diverts water from the three moorland streams, between Ovedal and Øksendal, to the Tonstad headrace.

1.2.2 Reservoirs

The main reservoirs utilized for Tonstad Hydropower Plant is Ousdalsvann and Homstølvann, both of which are created by rock-fill dams. Ousdalsvann has a diversion tunnel, taking in water from Tjørhomvann. The outlet of Tonstad is in Sirdalsvann. In Table 1.1, the regulations of the reservoirs connected to Tonstad are listed according to the Royal Decree of 5th of July 1963 (Industridepartementet, 1963).

Table 1.1: Reservoir Regulations, Tonstad HPP

Reservoir	HRWL (m.a.s.l.)	LRWL (m.a.s.l.)
Ousdalsvann	497.6	482.0
Homstølsvann	497.6	471.0
Sirdalsvann	49.5	47.5

1.2.3 Waterway

The waterway of Tonstad HPP, shown in Figure 1.3, collects water from the main reservoirs Ousdalsvann in the Sira branch and Homstølsvann in the Kvina branch. The tunnel systems connecting the two reservoirs at the Josdal juncture are approximately 16 km and 7.5 km long for the Sira and Kvina branch, respectively. Downstream the Josdal juncture, a 100 m² tunnel stretches about 5.4 km before dividing into 3 penstocks, headed for the power station.

There are, in addition to the main tunnels, several creek intakes along the route, and a separate branch to take in Førevann and the Øksendal moors in the South, connected to the main tunnel about 4 km after the Josdal juncture.

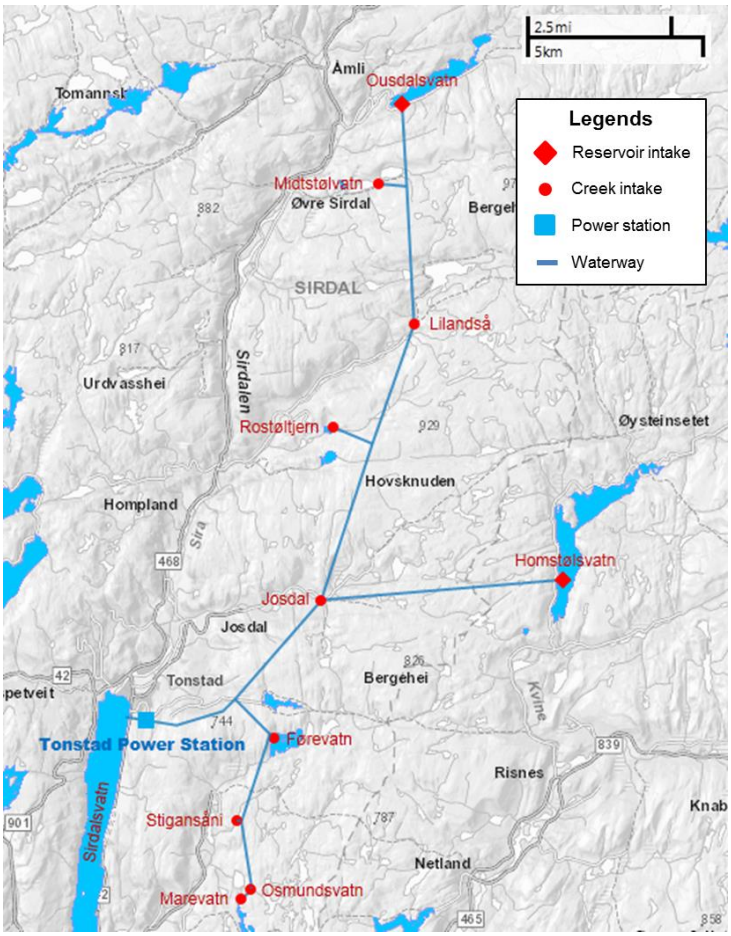

Figure 1.3: Map of Tonstad HPP waterway

About 1.5 km downstream the Førevann and the Øksendal connection to the main tunnel, the waterway branch into three separate tunnels, passing three surge tanks with intake gates, before entering the penstocks. As can be seen from the schematic representation in Figure 1.4, penstock 1 and 2, serve units 1 to 4, and penstock 3 serve unit 5 of 1988. About 30 meters downstream the turbines, three lower surge tanks are placed, before the tunnels are merged into a joint outlet to Sirdalsvann. A list of drawings portraying the waterway can be found in Appendix A.1.

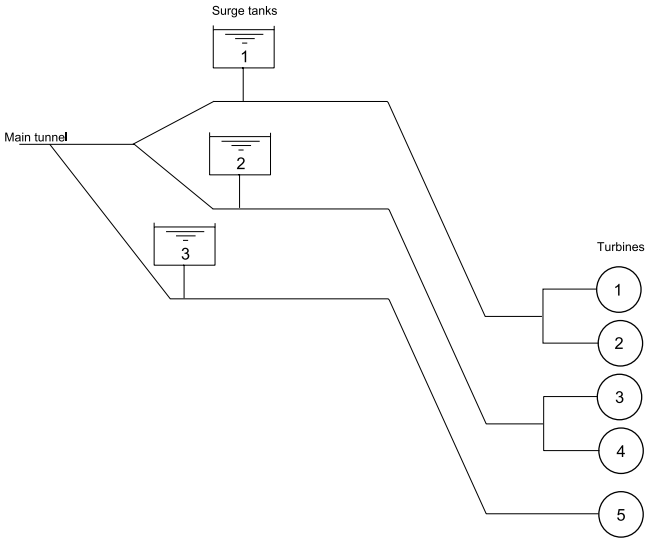

Figure 1.4: Schematic overview of surge tanks, penstocks and turbines

1.2.4 Surge Tanks

Tonstad HPP has three surge tanks upstream the turbine and three downstream. A detailed description of the upstream surge tanks are made, due to their relevance for the objective of the thesis. The surge tanks placement in the waterway is shown schematically in Figure 1.4. A References to the technical drawings describing the surge tanks are found in Appendix A.

Surge Tank 1 and 2

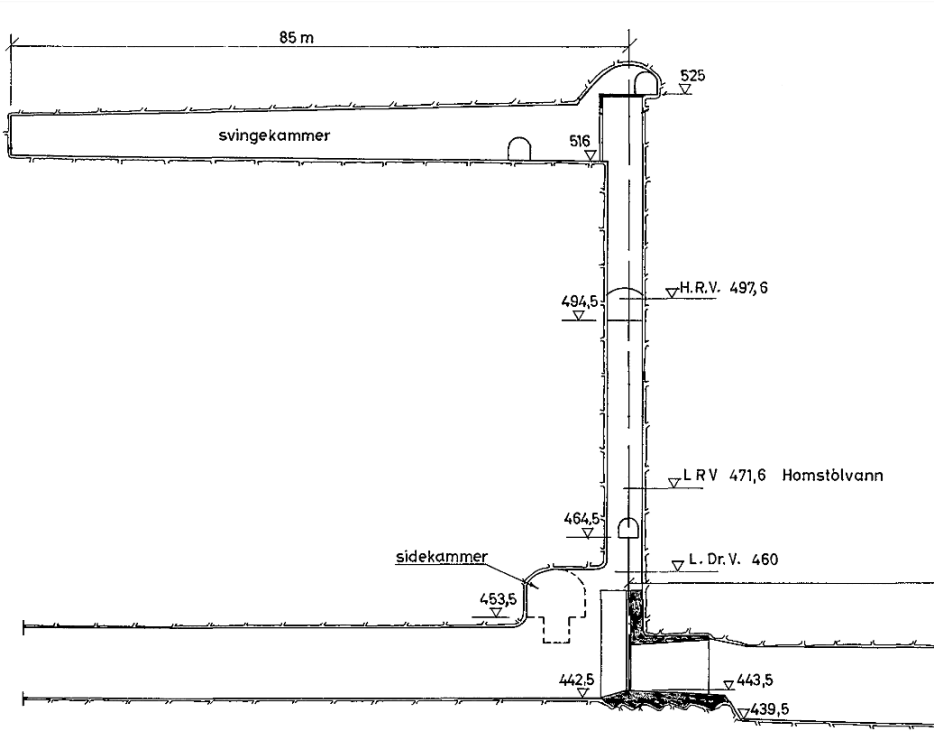

Figure 1.5: Elevation of surge tank 1 and 2

Surge tanks 1 and 2 are identically constructed, with the exception of the orientation the lower side chamber. As can be seen from the elevation in Figure 1.5, the lower chamber is included as an expansion of the headrace tunnel, joining the bottom of the surge tank riser shaft at elevation 460 m.a.s.l. The lower chamber have a total surface area of approximately 285 m². The 35 m² surge shaft is vertical, joining an upper chamber at 516 m.a.s.l. The upper chamber surface area is about 595 m², with an overflow to the entrance tunnel at 525 m.a.s.l. Surge tanks 1 and 2 are connected by a cross cut tunnel in the upper chamber and two tunnels of different sizes in the surge shaft.

There are two gates installed in each surge tank, resulting in several installations in the shaft, as shown in Figure 1.6. A concrete platform at the top of the upper chamber holds the hydraulic gate-opening equipment, connected to struts used for gate manoeuvring. These struts run through fixed guide beams at approximately every 11 meter down the shaft. The two largest circles on each side of the shaft in Figure 1.6 shows aeration pipes going from the top to the gates, and the two smaller circles represent an inspection ladder, varying at every 11th meter, starting with the right ladder. Construction details of the elevation of surge tank 1 and 2 from other angles than in Figure 1.5 can be found in Appendix B.1.

The concrete platform with the gate equipment extends vertically, as a wall, to the bottom of the upper surge chamber in the entrance to the chamber. The wall has two rectangular cut-outs with height 7.5 m and width 2.3 m.

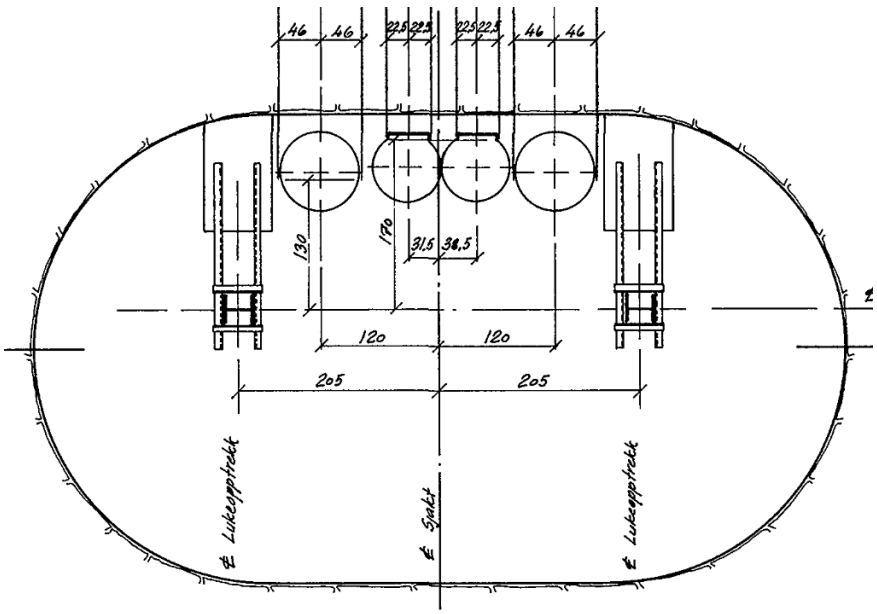

Figure 1.6: Cross-section of surge shaft 1 and 2

Surge Tank 3

Surge tank 3 is connected to the newest penstock and turbine. It is bigger than both of the other surge tanks, with slightly different layout. As seen in Figure 1.7, The lower chamber, with surface area about 500 m², is included as an expansion of the tunnel in the last 50 m before the gate. At 462 m.a.s.l., the lower chamber contracts to the 37.5 m² surge shaft, which joins the upper chamber at 516 m.a.s.l. The upper chamber extends with two tunnels, creating a total surface area of about 1250 m², with an overflow to the entrance tunnel at 525 m.a.s.l.

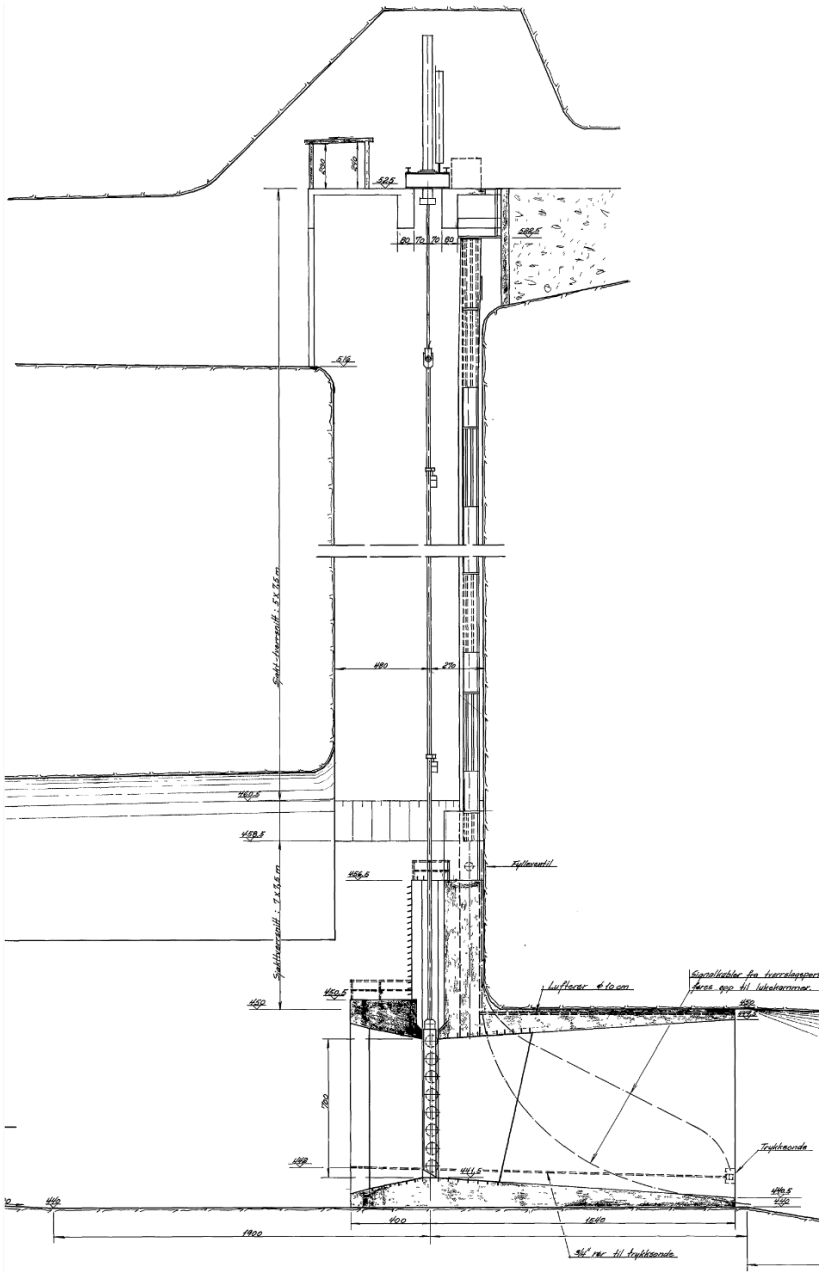

Figure 1.7: Elevation of surge tank 3

There is only one gate installed in surge tank 3, with one strut, going from the concrete plateau to the gate. The guide beam is attached across the rectangular cross-section of the shaft, shown in Figure 1.8. The aeration pipe is represented by the largest circle, and the alternating ladder as, the two smaller circles, as in surge tank 1 and 2.

There is, also in surge tank 3, a rectangular cut-out, at the wall extending from the gate equipment platform to the bottom of the upper chamber. The height of the cut-out is 7.4 m and the width 2.5 m.

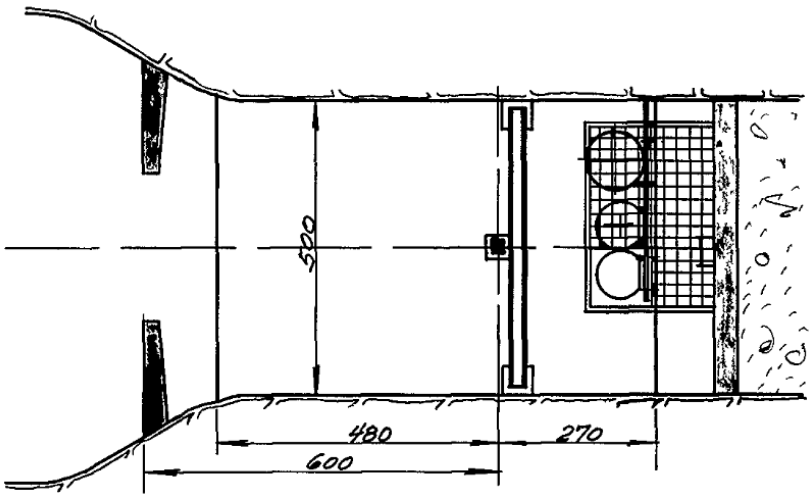

Figure 1.8: Cross-section of surge tank 3

1.2.5 Rock Traps

Immediately following the gates in the surge tanks the tunnel opens into a larger cross-section of approximately 120 m², stretching about 200 meters before entering the penstock. These tunnels have the function as a rock trap, decelerating the water allowing sedimentation, before entering the turbines. The entrance to the rock all the three rock traps is through the gate, at the highest opening at 450 m.a.s.l. Drawings of the rock traps are found in Appendix B.2.

1.2.6 Power Units

Power unit 1 to 4 are identical, while the fifth unit is bigger than the remaining. The specification of the runners, generators and step up transformers are presented in Table 1.2, Table 1.3 and Table 1.4 (Sira-Kvina Kraftselskap, 2014)

Table 1.2: Runner specifications

Description	Turbine 1-4	Turbine 5
Type	Francis	Francis
Capacity	160 MW	320 MW
Rounds per minute (RPM)	375	300
Maximum throughput	42,5 m^3/s	80 m^3/s

Table 1.3: Generator specifications

Description	Generator 1-4	Generator 5
Capacity	190 MVA	360 MVA
Voltage	12 kV	21,5 kV

Table 1.4: Transformer specifications

Description	Transformer 1-4	Transformer 5
Capacity	190 MVA	360 MVA
Voltage)	319 kV / 12 kV	320 kV / 21,5 kV

1.3 Surge Tank Throttle

To describe the effect and use of a surge tank throttle, it is firstly necessary to briefly explain the functionality of a surge tank.

High head power plants with long headrace tunnels often need a measure to control the kinetic energy caused by regulation of turbine discharge. Surge tanks are used to protect the waterway against excessive positive and negative pressures (Richter et al., 2015).

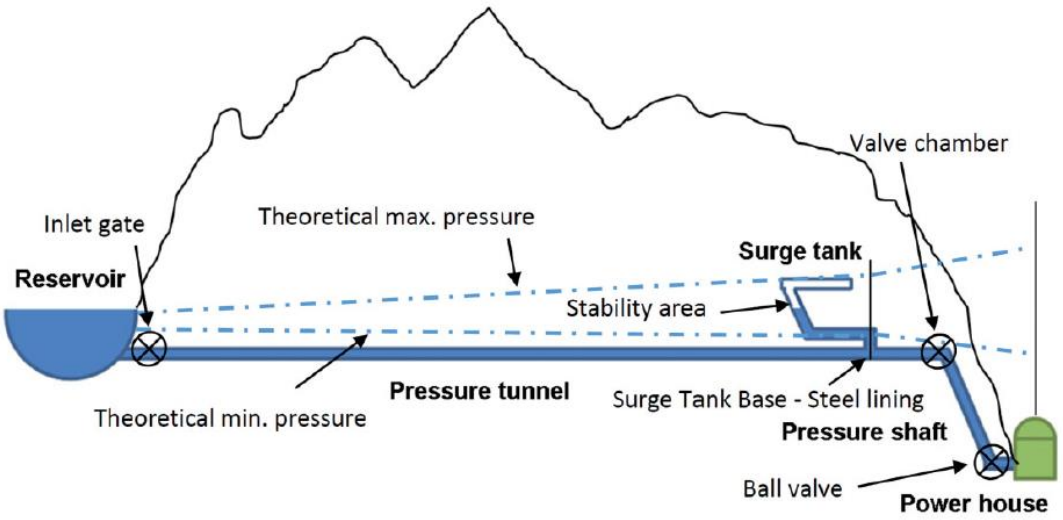

Figure 1.9: Schematic layout of a high head power plant (Richter et al., 2015)

As can be seen from Figure 1.9, a surge tank will create a water table closer to the turbine, enabling a faster response to opening and closing of the turbine. This is due to the acceleration/deceleration of less water compared to a system without a surge tank. A surge tank reduces the stress on the waterway by reducing the maximum pressure, also called water hammer, but creates mass oscillations between the reservoir and the surge tank.

When the turbine flow is altered, the kinetic energy in the water is converted into pressure energy. The surge tank reaction is either a rise or fall of water level, affiliated with closing and opening, respectively. Since the waterway can be divided into two hydraulic systems, one from the turbine to the surge tank, and the other from the surge tank to the reservoir, the potential energy from the change of water level in the surge tank will create oscillations between the reservoir and the surge tank. The potential energy in these oscillations are dissipated through hydraulic losses (Richter et al., 2015).

According to (Nabi et al., 2011), a surge tank needs to satisfy three conditions to function properly. Firstly, the surge tank needs to be at a location in which it ensures that the pressure variations, caused by water hammer, are kept within acceptable limits. Secondly, the tank must be stable, meaning it cannot allow amplification of mass oscillation, due to frequency or power regulation. Lastly, the surge tank must be proportioned, so that the maximum upsurge does not overflow (unless intended), and the lowest downsurge does not allow air entrainment into the waterway.

The classical method to ensure the stability of the mass oscillations in the surge tank is the use of the Thoma criterion. The criterion states that the cross-section of a surge tank needs to be

bigger than the Thoma cross-section, in order to be stable. The Thoma cross-section does however indicate the limit for stability, and a safety factor between 1.5 and 1.8 has been adopted (Nabi et al., 2011).

In order to reduce mass oscillations, surge tank throttles may be applied. A surge tank throttle is a construction in the surge tank used to create a large intended loss. The throttle is usually a restricting orifice, creating high local velocities and vortex formation, and can be constructed to give an asymmetric loss in the upwards and downwards direction. The function of a surge tank throttle is to contribute to the damping of the surge tank, to ensure sufficient damping capacity with regards to the mass oscillations between the surge tank and the reservoir (Richter et al., 2012).

In modern power plants, and pumped storage schemes especially, high requirements for flexibility creates the need for more effective design of surge tanks and water systems, due to the rapid shifts in start, stop and pumping. The use of throttle chamber surge tanks has been state-of-the-art in Austria, since the construction of Kaunertal hydropower plant in 1964 (Vereide et al., 2015).

When designing surge tanks with chamber configuration, Richter et al. (2012) describes three possible types of throttles being used, namely a symmetrical throttle, an asymmetrical throttle and a vortex throttle, also called reverse flow throttle. The main difference between the three is the ratios of head loss between the upsurge and downsurge directions, given as 1:1 for the symmetrical, up to 1:4 for the asymmetrical and up to 1:50 for the vortex throttle. When having an asymmetric throttle head loss, it may be necessary with an aeration shaft, parallel to the main shaft to avoid column separation and damages caused by high negative pressures.

The symmetric throttle is configured as a simple orifice, and can vary in length and shaft-to-orifice area, while the loss ratio of the asymmetric throttle is given by its asymmetric geometry. The asymmetric throttle installed in Obervermuntwerk II, in Austria is shown in Figure 1.10 (Richter, 2015). The smooth change in area, going from large to small, will cause considerably less flow resistance than the entrance with a protruding pipe and smooth expansion from the smaller to the larger area.

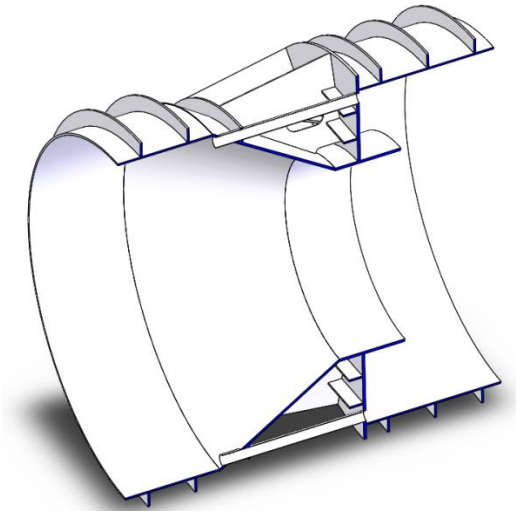

Figure 1.10: Asymmetric throttle, Obervermuntwerk II (Richter, 2015)

A vortex throttle consists of a steel torus forcing the water to exit through a pipe orthogonally to the vortex plane when emptying the chamber, inducing a loss 20 to 50 times higher than when filling it (Steyrer, 1999). An example of a vortex throttle is shown in Figure 1.11.

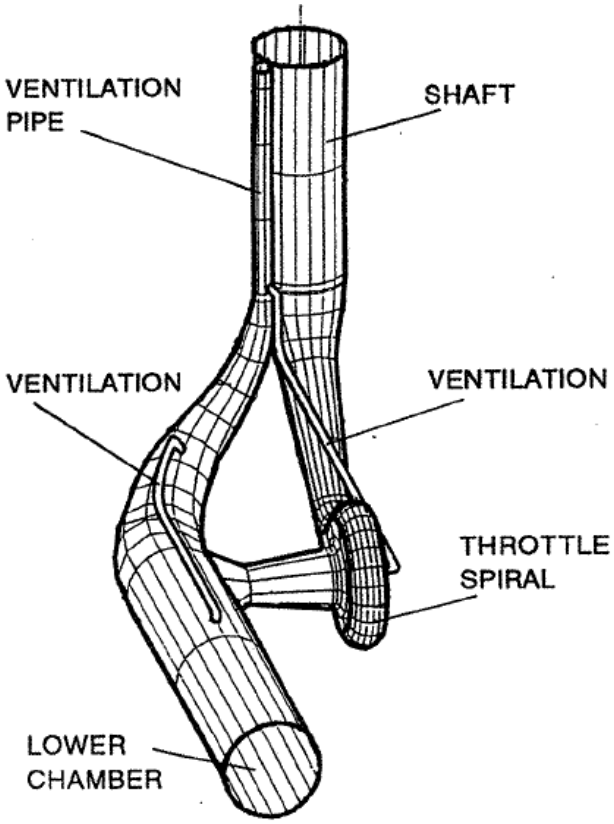

Figure 1.11: Vortex throttle (Steyrer, 1999)

There have been constructed several vortex throttles in Austria since the 1960's, making it possible to drastically reduce lower chamber excavation. It is however been shown that the large energy dissipation of the throttle, with the unsteady loss behaviour, has led to dynamic shaking, resulting in an increased use of orifice throttles (Richter et al., 2015).

2 Theory

The theory behind the methods employed in the thesis is explained in this chapter. Detailed descriptions of the governing equations are made, followed by a more idealized explanation of the phenomena of water hammer and mass oscillations. The hydraulic resistance used in the method is accounted for in general terms, but also as detailed considerations used for resistance calculations. The tools used for economic analysis is also briefly explained.

2.1 Governing Equations

The governing equations for the physics of water hammer and mass oscillations are the continuity equation and the equations of motion, which deals with the conservation of mass and change in momentum. It is also in this section included descriptions of loss formulations used in the thesis.

2.1.1 Equation of Motion

The one-dimensional differential form of the equation of motion is developed for use with programming software in accordance with (Wylie and Streeter, 1993).

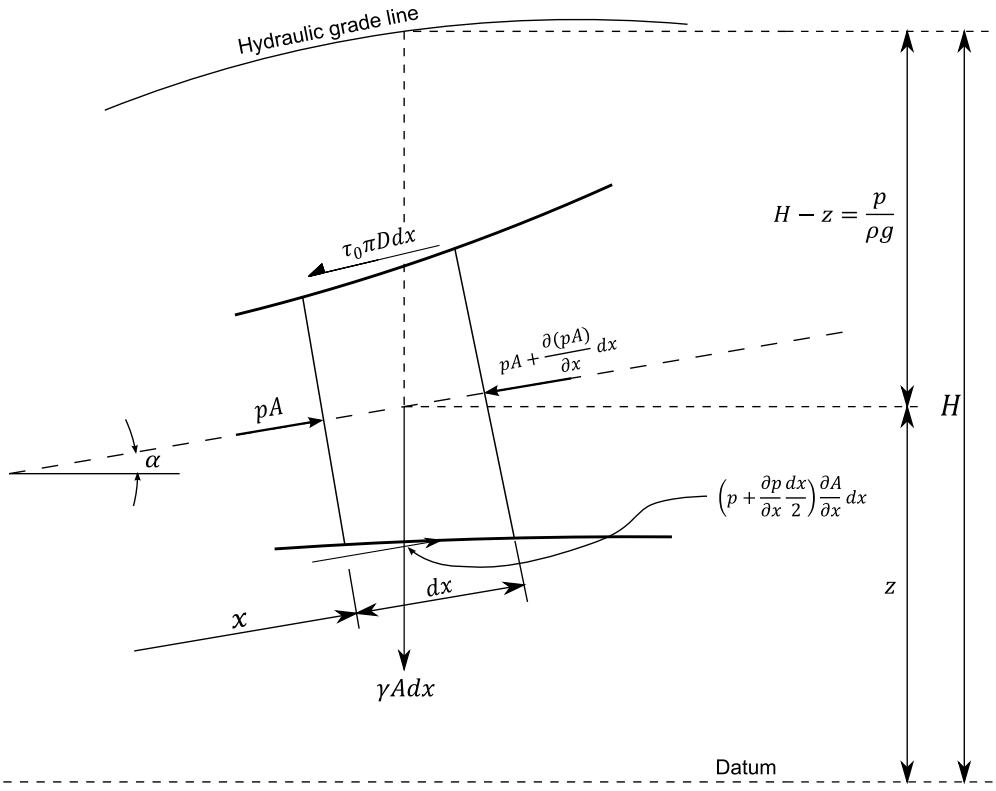

Figure 2.1: One-dimensional equation of motion diagram, from Wylie and Streeter (1993)

Figure 2.1 shows a fluid-filled cross section of a conical tube, and the derivation is also valid for a prismatic or cylindrical section. The fluid has density ρ, the centreline pressure, $p(x,t)$, is assumed equal to the average cross-sectional pressure and the average cross-sectional velocity is denoted as $v(x,t)$. The control volume is portrayed with x-direction along the centreline with the angle to the horizontal line denoted as α, and a thickness of dx.In addition to the total pressure p, the potential is showed as $H(x,t)$, as this is a common practice in hydropower purposes.

The application of Newton's 1st law on the control volume yields

$$pA + \left(pA + \frac{\partial(pA)}{\partial x}dx\right) + \left(p + \frac{\partial p}{\partial x}\frac{dx}{2}\right)\frac{\partial A}{\partial x}dx - \tau_0 \pi D dx - \rho g A dx \sin\alpha = \rho A dx \frac{dv}{dt} \qquad 2\text{-}1$$

By simplifying and neglecting second order terms, one can obtain

$$\frac{\partial p}{\partial x}A + \tau_0 \pi D + \rho g A \sin\alpha + \rho A \frac{dv}{dt} = 0 \qquad 2\text{-}2$$

An assumption is made that the shear stress is equal under steady and transient behaviour. An expression for the shear stress can be found by transforming the expression for the Darcy-Weisbach friction, in equation 2-48, into

$$\tau_0 = \frac{\rho f v|v|}{8} \qquad 2\text{-}3$$

where the absolute value sign ensure that the value of the shear stress is positive, also when the flow changes direction.

The acceleration term in equation 2-2 can further be expressed as

$$\frac{dv}{dt} = v\frac{\partial v}{\partial x} + \frac{\partial v}{\partial t} \qquad 2\text{-}4$$

By substituting equations 2-3 and 2-4 into 2-2, it takes the form

$$\frac{\partial p}{\partial x}A + \frac{\rho f v|v|}{8}\pi D + \rho g A \sin\alpha + \rho A\left(v\frac{\partial v}{\partial x} + \frac{\partial v}{\partial t}\right) = 0 \qquad 2\text{-}5$$

which can be further reduced, when $A = \frac{\pi D^2}{4}$:

$$\frac{\partial p}{\partial x} * \frac{1}{\rho} + v\frac{\partial v}{\partial x} + \frac{\partial v}{\partial t} + g\sin\alpha + \frac{fv|v|}{2D} = 0 \qquad 2\text{-}6$$

When assuming unsteady flow at low Mach-numbers, the term $v\frac{\partial v}{\partial x}$ is often excluded. Equation 2-6 can then be reduced to

$$\frac{\partial p}{\partial x} * \frac{1}{\rho} + \frac{\partial v}{\partial t} + g\sin\alpha + \frac{fv|v|}{2D} = 0 \qquad 2\text{-}7$$

By utilizing that pressure can be expressed as hydraulic head, on can derive

$$\frac{\partial p}{\partial x} = \rho g\left(\frac{\partial H}{\partial x} - \frac{\partial z}{\partial x}\right) = \rho g\left(\frac{\partial H}{\partial x} - \sin\alpha\right) \qquad 2\text{-}8$$

When equation 2-8 is substituted into equation 2-7, the simplified hydraulic-grade-line form of the equation of motion yields

$$g\frac{\partial H}{\partial x} + \frac{\partial v}{\partial t} + \frac{fv|v|}{2D} = 0 \qquad 2\text{-}9$$

While equation 2-6 is valid for any fluid, equations 2-7 and 2-9 are only valid for less compressible fluids, at low velocities.

2.1.2 Continuity Equation

As for the equation of motion, a simplified one-dimensional expression is developed for the continuity equation in coherence with Wylie and Streeter (1993). The control volume in Figure 2.2 is moving and has a fixed length of dx and varies only with the change and movement of the pipe.

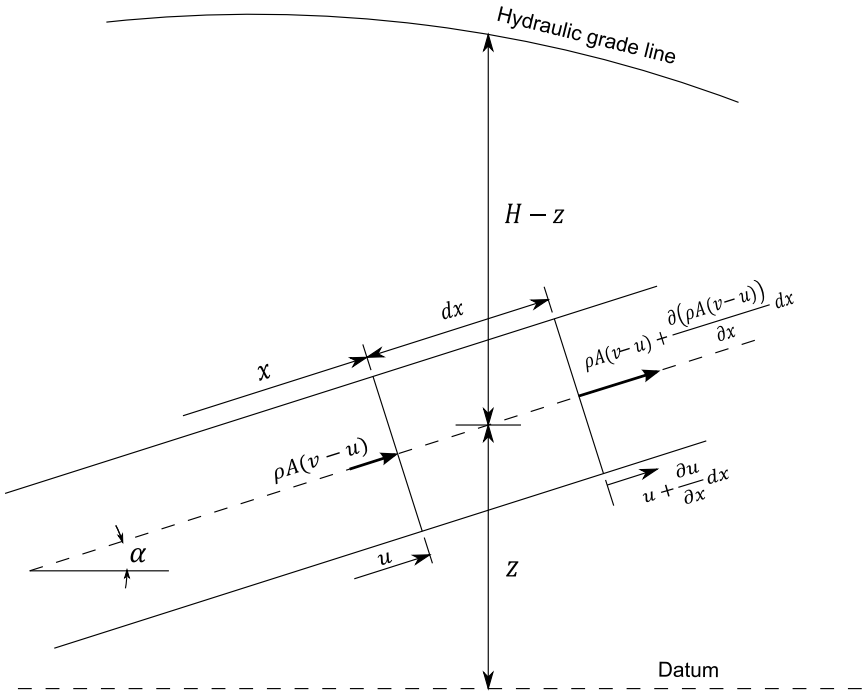

Figure 2.2: Control volume for the continuity equation, from Wylie and Streeter (1993)

The principle of mass conservation of the control volume can be explained as the mass inflow needs to be equal to the increase of mass inside the control volume. This can, for Figure 2.2, be stated as

$$-\frac{\partial\big(\rho A(v-u)\big)}{\partial x} dx = \frac{d}{dt}(\rho A\, dx) \qquad 2\text{-}10$$

where x is the upstream face of the control volume and u is the velocity of the pipe wall at x. The total derivative with respect to the axial motion from equation 2-10, can be expressed as

$$\frac{d}{dt} = u\frac{\partial}{\partial x} + \frac{\partial}{\partial t} \qquad 2\text{-}11$$

and the time rate of increase of dx as

$$\frac{d}{dt}dx = \frac{\partial u}{\partial x}dx \qquad 2\text{-}12$$

By expanding equation 2-10 and utilizing equation 2-11 and 2-12, one can derive

$$\frac{\partial(\rho A v)}{\partial x} - \frac{\partial(\rho A)}{\partial x}u - \rho A\frac{\partial u}{\partial x} + \frac{\partial(\rho A)}{\partial x}u + \frac{\partial(\rho A)}{\partial t} + \rho A\frac{\partial u}{\partial x} = 0 \qquad 2\text{-}13$$

which can be simplified to

$$\frac{\partial(\rho A v)}{\partial x} + \frac{\partial(\rho A)}{\partial t} = 0 \qquad 2\text{-}14$$

By expanding equation 2-14 to

$$\rho A\frac{\partial v}{\partial x} + v\frac{\partial(\rho A)}{\partial x} + \frac{\partial(\rho A)}{\partial t} = 0 \qquad 2\text{-}15$$

where the two last terms can be described as the total derivative of ρA with respect to the motion of a mass particle, giving

$$\rho A\frac{\partial v}{\partial x} + \frac{d(\rho A)}{dt} = 0 \qquad 2\text{-}16$$

with

$$\frac{d}{dt} = v\frac{\partial}{\partial x} + \frac{\partial}{\partial t} \qquad 2\text{-}17$$

Because no simplification assumptions are made, equation 2-16 is valid for cylindrical pipes as well as converging and diverging tubes, on a slope or horizontal. It is also full sections of any fluid, and rigid or deformable pipes.

Re-writing equation 2-16 to

$$\frac{\frac{dA}{dt}}{A} + \frac{\frac{d\rho}{dt}}{\rho} + \frac{\partial v}{\partial x} = 0 \qquad 2\text{-}18$$

enables the possibility to express the compressibility of the fluid as

$$\frac{\frac{d\rho}{dt}}{\rho} = \frac{\frac{dp}{dt}}{K} \qquad 2\text{-}19$$

This relationship with the bulk modulus, K, of the fluid excludes thermodynamic effects, thus reducing validity to only slightly compressible fluids. The first term of equation 2-18 regards the pipe wall elasticity and rate of deformation. In a prismatic tube the area only varies with pressure and we have that

$$\frac{dA}{dt} = \frac{dA}{dp}\frac{dp}{dt} \qquad 2\text{-}20$$

By substituting equations 2-19 and 2-20, equation 2-18 becomes

$$\frac{\partial v}{\partial x} + \frac{\frac{dp}{dt}}{K}\left(1 + \frac{K}{A}\frac{dA}{dp}\right) = 0 \qquad 2\text{-}21$$

The elasticity of the fluid and the pipe can be expressed by the new variable a^2,

$$a^2 = \frac{\frac{K}{\rho}}{1 + \frac{K}{A} + \frac{\Delta A}{\Delta p}} \qquad 2\text{-}22$$

With linear elastic materials for the wall and a linear elastic fluid, a^2 will be constant and the expression for the one-dimensional conservation of mass for a prismatic pipe section filled with a slightly compressible fluid becomes

$$\rho a^2 \frac{\partial v}{\partial x} + \frac{dp}{dt} = 0 \qquad 2\text{-}23$$

By setting $\frac{\partial p}{\partial t} = 0$, one can describe steady flow as a special case of unsteady flow. This will result in the simplified term

$$\rho a^2 \frac{\partial v}{\partial x} + v\frac{\partial p}{\partial x} = 0 \qquad 2\text{-}24$$

However, the equation 2-24 shows inconsistency in some cases. The density and tube area variations are normally disregarded in steady flow, giving $\frac{\partial v}{\partial x} = 0$ and consequently $\frac{\partial p}{\partial x} = 0$. It is obvious that this is not true when having a horizontal tube with friction, nor with sloped tubes. To work around the inconsistency, the complete partial differential equations for unsteady flow, 2-6 and 2-23 are combined to eliminate $\frac{\partial v}{\partial x}$ by substitution, giving

$$\frac{\partial p}{\partial x}\left(1-\left(\frac{v}{a}\right)^2\right)+\frac{v}{a^2}\frac{\partial p}{\partial t}+\rho\frac{\partial v}{\partial t}+\rho g\sin\alpha+\rho\frac{fv|v|}{2D}=0 \qquad \textit{2-25}$$

By assuming low Mach numbers, the term $\left(\frac{v}{a}\right)^2$ can be dropped without loss in accuracy. This will result in $\frac{\partial p}{\partial x}=0$, and simplification of the continuity of equation in 2-23 becomes

$$\rho a^2\frac{\partial v}{\partial x}+\frac{\partial p}{\partial t}=0 \qquad \textit{2-26}$$

valid for low Mach-number unsteady flows. As for the equation of motion the pressure term is replaced by the hydraulic head, giving the continuity equation on hydraulic grade form as

$$\frac{a^2}{g}\frac{\partial v}{\partial x}+\frac{\partial H}{\partial t}=0 \qquad \textit{2-27}$$

2.2 Water Hammer

The regulation of turbine discharge in a hydropower plant will cause pressure transients in the waterway. Closing of a valve will cause a pressure increase that will propagate in the waterway upstream the valve. This phenomenon is called water hammer. It is important to consider the compressibility of water when describing even a simple form of water hammer.

To illustrate the effect of water hammer, the simplest form is considered according to Featherstone et al. (2009). In this description of water hammer, hydraulic losses are neglected and the valve closing is considered to be instantaneous. A visual description of water hammer is found in Figure 2.3, based on Featherstone et al. (2009).

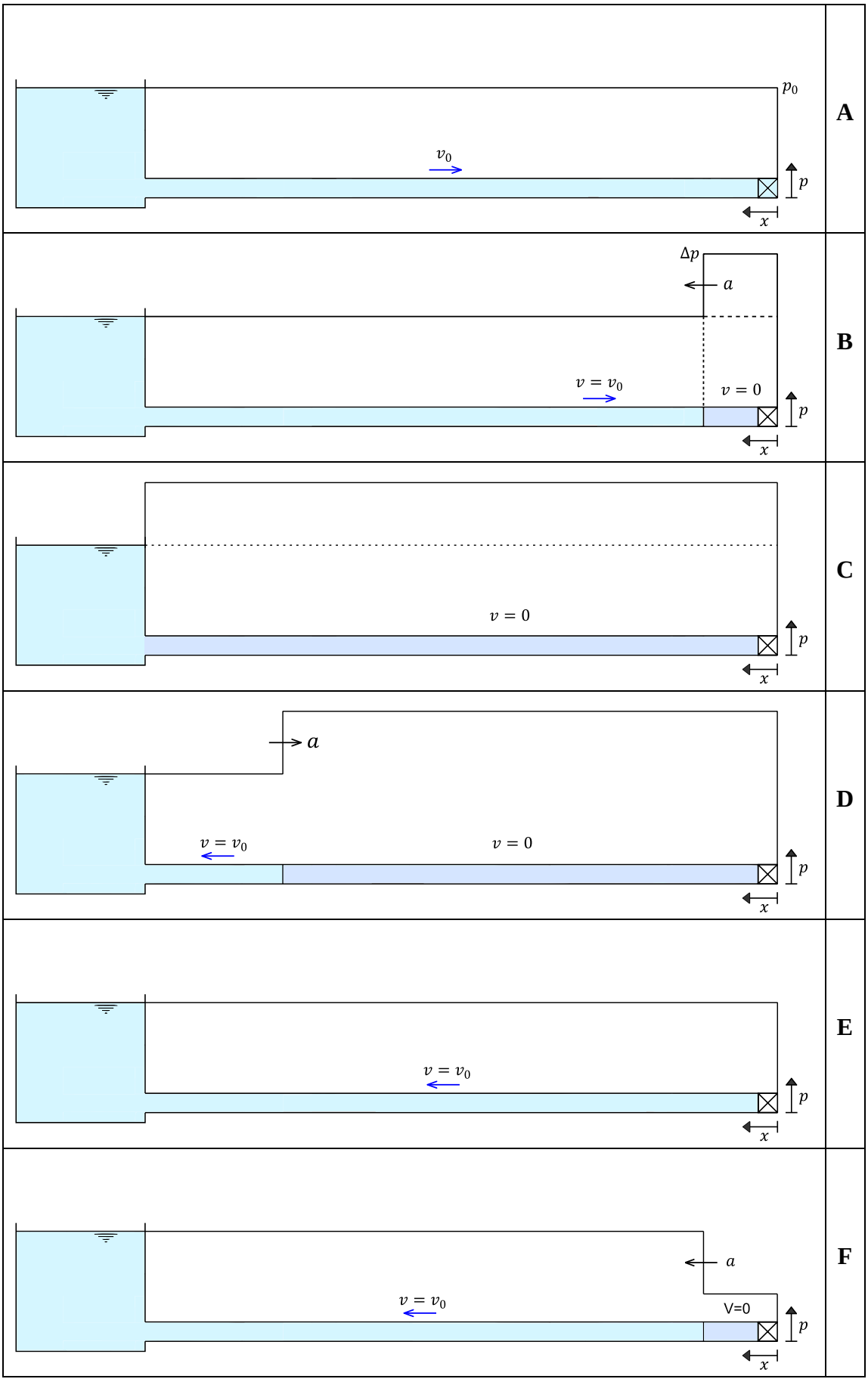

Figure 2.3: Water hammer

Figure 2.3-A displays the initial conditions of the steady state situation with the pressure line above the pipe equal to the reservoir water level. An instantaneous valve closing will cause zero velocity directly upstream the valve, and a wave of increased pressure propagates towards the reservoir with the wave speed in the fluid, denoted by a. The position of the pressure wave on the x axis at a given time, Δt, can therefore be found by $x = a\Delta t$. The water upstream the pressure wave still flows towards valve, seen in Figure 2.3-B. The pressure increase will cause a total pressure of $\Delta p + p_0$. The total time used to stop all the water in the waterway, as in Figure 2.3-C, will be $t = L/a$, with L being the length of the pipe.

The pressure wave is reflected when it has reached the reservoir and returns to the valve at $t = 2L/a$. In this process, as seen in Figure 2.3-D, the water still is flowing out of the pipe, due to the stored strain energy in the pipeline that cannot be sustained. The velocity of all the water is $v = -v_0$ when the pressure wave reaches the valve in Figure 2.3-E. Consequently a reduced pressure wave will propagate towards the reservoir with the size $p = p_0 - \Delta p$, see Figure 2.3-F.

The reduced pressure wave is, in the same way as the increased pressure wave described above, propagating to the reservoir where it again will be reflected at $t = 3L/a$ and return to the valve. At the time $t = 4L/a$. The cycle is completed with water flowing out of the pipe at the initial velocity. In a lossless system the cycle will be repeated infinitely, while it in reality is dampened out by friction. The pressure in front of the valve during the process is shown in Figure 2.4.

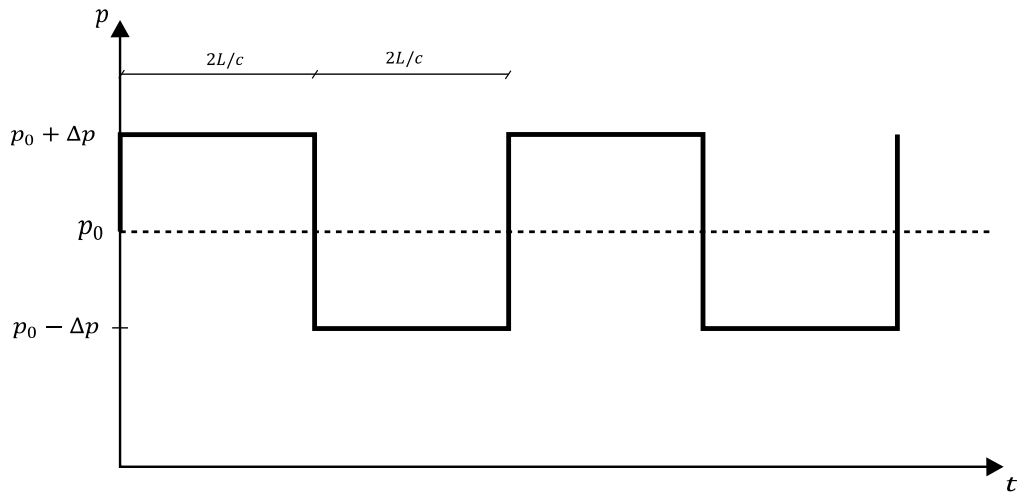

Figure 2.4: Idealised water hammer, pressure vs. time

2.2.1 Magnitude of Water Hammer Pressure

The magnitude of water hammer pressure is found by applying the momentum and continuity equation on a control volume, neglecting friction and minor effects. The following section is written in accordance with Wylie and Streeter (1993).

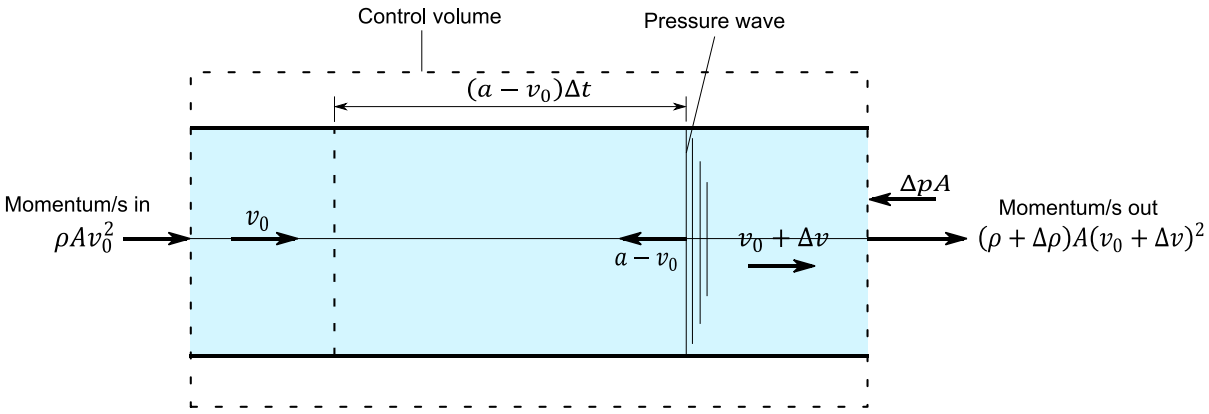

Figure 2.5: Control volume water hammer

When a valve has an instantaneous closing the water adjacent to the valve will reduce the speed from v_0 to zero, and a pressure wave will move from the valve with some wave speed of a. In Figure 2.5, a small change in valve setting is made and the absolute velocity of the wave speed is $a - v_0$. The valve pressure change, Δp, corresponds to the change in velocity, Δv. The momentum in x-direction yields that momentum influx and accumulation equals the momentum efflux of the control volume. The momentum accumulation at Δt can be described as

$$\frac{A(a - v_0)\Delta t}{\Delta t}\big((\rho + \Delta\rho)(v_0 + \Delta v) - \rho v_0\big)$$

when the volume of fluid having its momentum changed is $A(a - v_0)\Delta t$. The momentum equation applied on Figure 2.5 becomes

$$-\Delta pA = A(a - v_0)\big((\rho + \Delta\rho)(v_0 + \Delta v) - \rho v_0\big) + (\rho + \Delta\rho)A(v_0 + \Delta v)^2 - \rho A v_0^2 \qquad 2\text{-}28$$

By conservation of mass, the time rate change of mass is

$$\rho A v_0 - (\rho + \Delta\rho)A(v_0 + \Delta v) = \frac{A(a - v_0)\Delta t\,\big((\rho + \Delta\rho) - \rho\big)}{\Delta t} \qquad 2\text{-}29$$

By combination and simplification of equations 2-28 and 2-29, the pressure of water hammer is described as

$$\Delta p = -\rho a \Delta v \qquad 2\text{-}30$$

or as

$$\Delta H = -\frac{a}{g}\Delta v \qquad 2\text{-}31$$

expressed in terms of hydraulic head. The complete closure of the valve, $\Delta v = -v_0$ will then result in a pressure increase of $\Delta p = \rho a v_0$.

By assuming that the pipe is fixed, so that it will not expand, the water inflow during $\Delta t = L/a$ is $\rho A\ v_0 L/a$, which is handled by compression of the fluid, so that

$$\rho A v_0 \frac{L}{a} = LA\Delta\rho \qquad 2\text{-}32$$

By using equation 2-30, v_0, is substituted and the expression yields

$$\mathrm{a}^2 = \frac{\Delta p}{\frac{\Delta\rho}{\rho}} * \frac{1}{\rho} \qquad 2\text{-}33$$

The bulk modulus of elasticity of the fluid is defined as

$$\mathrm{K} = \frac{\Delta \mathrm{p}}{\Delta \rho / \rho} \qquad 2\text{-}34$$

resulting in a final expression for the wave speed as

$$\mathrm{a} = \sqrt{\frac{K}{\rho}} \qquad 2\text{-}35$$

2.3 Mass Oscillations

The introduction of a surge tank in a high head system, as previously described in section 1.3, will reduce problems with water hammer, but creates mass oscillation between the surge tank and the reservoirs and intakes. The description of mass oscillations is based on Nielsen (1990)

A description of the mass oscillation between the surge tank, in Figure 2.6, and the reservoir can be made by assuming that the fluid and the walls are non-compressible, due to little

significance of elastic effects. This means an infinite high bulk modulus, and thereby an infinite wave speed.

By dividing the continuity equation 2-27 with a and allowing it to approach infinite, the result is

$$\frac{\partial \mathrm{v}}{\partial \mathrm{x}} = 0 \qquad \textit{2-36}$$

meaning $Q = vA = constant$. By introducing

$$\frac{\partial H}{\partial x} = \frac{H_2 - H_1}{L} \qquad \textit{2-37}$$

the momentum equation 2-9 can be transformed to

$$\frac{\mathrm{L}}{\mathrm{gA}} \frac{dQ}{dt} = H_1 - H_2 - f \frac{L}{2gA^2D} Q|Q| \qquad \textit{2-38}$$

A simplified frictionless system for mass oscillations is displayed in Figure 2.6, where A portraits the steady state and B the transient situation after valve closing.

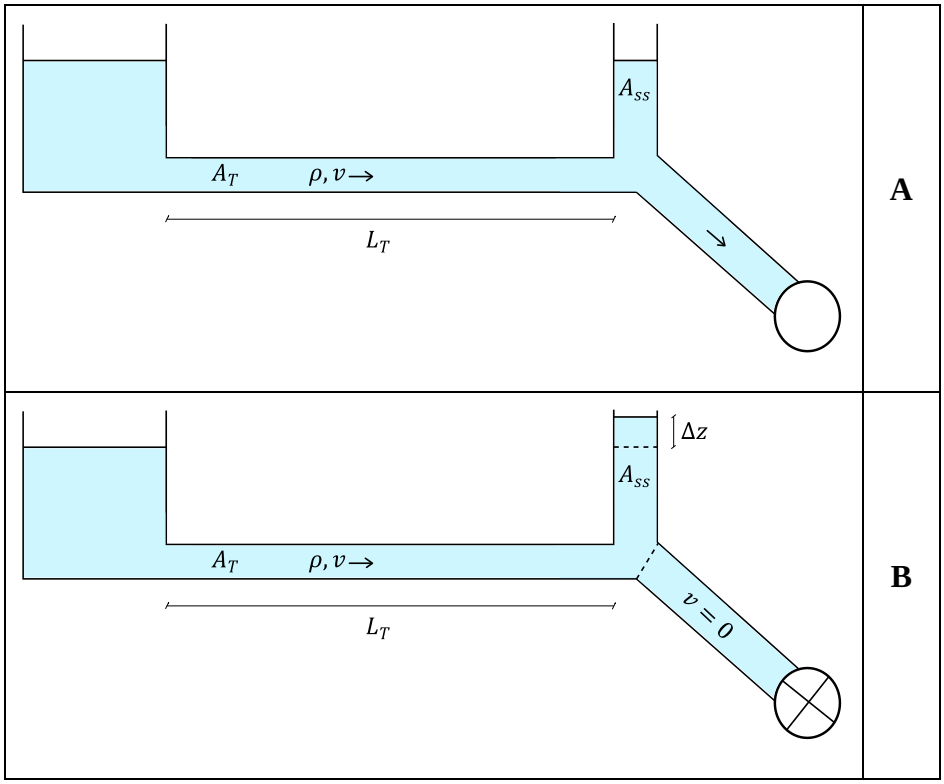

Figure 2.6: Mass oscillations in a simple system

2.3.1 Amplitude

By assuming a frictionless system, the momentum equation of the oscillations between the reservoir and the surge tank reduces to

$$\frac{\mathrm{L_T}}{\mathrm{gA_T}}\frac{dQ}{dt} = H_1 - H_2 = \Delta z \qquad \textit{2-39}$$

And the continuity for the junction from tunnel to surge tank

$$\mathrm{A_{ss}}\frac{dz}{dt} = Q = vA_T \qquad \textit{2-40}$$

when assuming a shutdown with no turbine discharge. Assuming $dz = \Delta z$, $dt = \Delta t$ and $dv = \Delta v$, an equation for a rough estimate of the surge tanks water table upswing, for shutdown, and downswing, for gate opening, becomes

$$\Delta \mathrm{z} = \pm \Delta \mathrm{Q}\sqrt{\frac{L_T/A_T}{gA_{ss}}} \qquad \textit{2-41}$$

With a lossless system this oscillation will in principle continue forever, but will in a real system be dampened by friction.

2.3.2 Period

The time-derivative of equation 2-40 yields

$$\frac{\mathrm{dQ}}{\mathrm{dt}} = A_{ss}\frac{d^2z}{dt^2} \qquad \textit{2-42}$$

which is substituted into the formulation of the momentum equation in 2-39, rearranged to the form of an harmonic differential equation:

$$L_T A_{ss}\frac{d^2z}{dt^2} + gA_T z = 0 \qquad \textit{2-43}$$

The form, natural frequency ω, and period T, of a harmonic equation is

$$m\frac{d^2x}{dt^2} + kx = 0 \qquad \textit{2-44}$$

$$\omega = \sqrt{\frac{k}{m}} \qquad 2\text{-}45$$

$$T = \frac{2\pi}{\omega} \qquad 2\text{-}46$$

respectively. When $m = LA_{ss}$ and $k = gA_T$, the period of the mass oscillations becomes

$$T = 2\pi \sqrt{\frac{L_T A_{ss}}{gA_T}} \qquad 2\text{-}47$$

2.4 Hydraulic Resistance

Idelchik (1986) argues that losses of total pressure in a hydraulic system is a result of the conversion of mechanical energy to heat, and that they are irreversible. He further explains the term fluid resistance as "the irreversible loss of total pressure (pressure drop) over a given system length" (Idelchik, 1986)

Idelchik (1986) considers two types of total pressure losses in a network of pipelines, namely pressure losses from friction and local pressure losses. The latter losses are also referred to as singular losses. It is physically speaking not possible to subdivide the total losses into these groups, but it is done for practical reasons to ease the calculations. The two types of losses are summed by the principle of superposition.

2.4.1 Friction Losses

To estimate the friction losses in a pipe one can use the Darcy-Weisbach equation, which can be derived from applying the momentum equation on a control volume, assuming fully developed and steady flow in a pipe with constant diameter (Crowe et al., 2009):

$$h_f = f\frac{L}{D}\frac{v^2}{2g} = k_f\frac{v^2}{2g} \qquad 2\text{-}48$$

The friction factor f is defined by Crowe et al. (2009) as

$$f = \frac{4\tau_0}{\rho v^2/2} \qquad 2\text{-}49$$

f is a dimensionless coefficient often used by engineers, where $\tau_0$is the wall shear stress. The friction factor for pipes can easily be estimated from the Moody diagram, which is made using the Colebrook-White formula.

2.4.2 Singular Losses

The singular losses in pipelines are induced when the configuration of the pipe changes, fluid streams meet, separate or flow past obstructions, causing phenomena that "contribute to the exchange of momentum between moving fluid particles […] , thus enhancing energy dissipation" (Idelchik, 1986).

From dimensional analysis the singular loss coefficient k, also known as the local resistance coefficient, is defined according to Crowe et al. (2009) as

$$k_{loc} = \frac{\Delta h}{\frac{v^2}{2g}} = \frac{\Delta p}{\frac{\rho v^2}{2}} \qquad \textit{2-50}$$

When applying the definition 2-50 on the flow over a component in the hydraulic system the head loss can be described as

$$h_L = k\frac{v^2}{2g} \qquad \textit{2-51}$$

where most values of k are found by experiment.

2.4.3 Throttle Losses

An empirical model of flow resistance is used to translate a loss coefficient into a geometric configuration of a throttle. The studies of Gabl et al. (2011) compares the accuracy of local head loss coefficients of a throttle with various tabular values from different authors, calculated by a three-dimensional numerical model, also referred to as *Computational Fluid Dynamics* (CFD).

The throttle is asymmetric, as shown in Figure 2.7 A-C (Gabl et al., 2011), and has an elbow leading up through the throttle to the surge shaft.

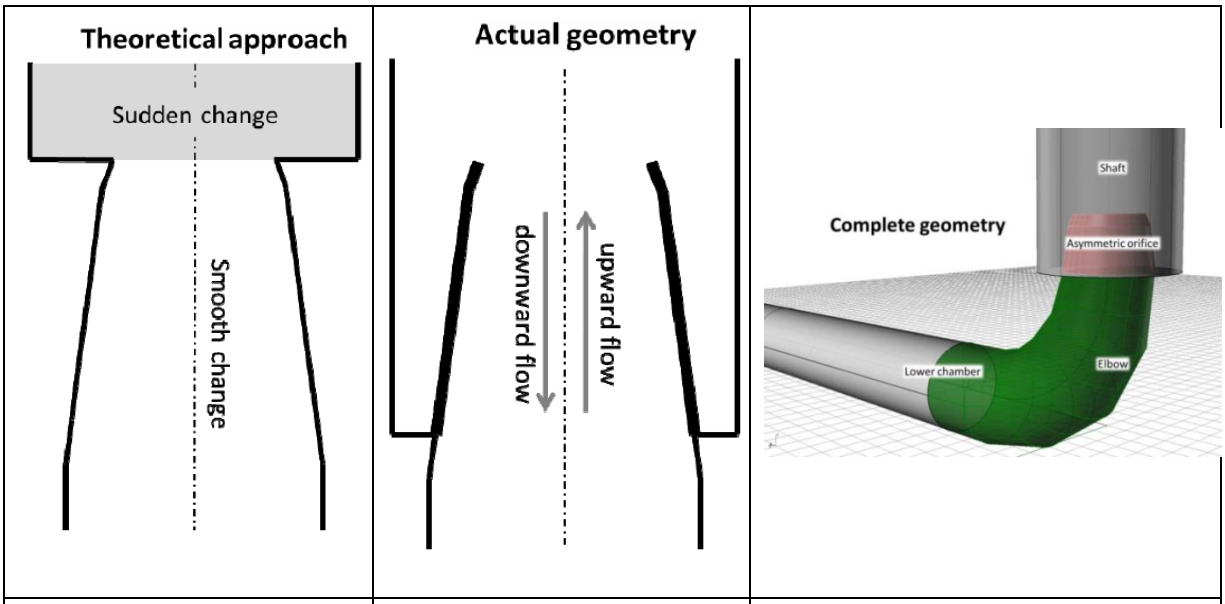

Figure 2.7 A-C: Description of throttle geometry, actual and theoretical

The result of the studies shows that the upwards flow can be portrayed accurately from tabular values used by Idelchik (1960), but that the tabular values underestimate downwards losses by about 50 % of the values from the CFD simulation. It is observed that the simplification in Figure 2.7-A exclude the effects of the protruding pipe, which may be substantial. A rough estimate based on the difference between loss coefficients for a wall-mounted inlet, shows that a sufficiently protruding pipe will increase the inlet loss by roughly 100 %. By adding these 100 % to the estimate of (Gabl et al., 2011), the difference of total loss from the CFD computations to the computed values is reduced to roughly 10 %. It is noted that this is an estimate, but serves as an indication of the magnitude of error.

Based on (Gabl et al., 2011), the method of (Idelchik, 1960) is considered the most appropriate for approximate calculation of throttle losses, compared to CFD simulation. The succeeding sections accounting for resistance coefficients, used for throttle geometry calculations, are made using the works of Idelchik (1986).

Entrance Flow

The resistance of the entrance flow to a tube or conduit is governed by the relative thickness of the inlet tube wall and the relative distance from the entrance of the tube to the wall in which it is mounted. A straight inlet section will have a maximum resistance coefficient with a thin, sharp edged, inlet tube.

The resistance coefficient of the inlet of a protruding tube, as shown in Figure 2.8, can be found from diagram 3-2 in (Idelchik, 1986).

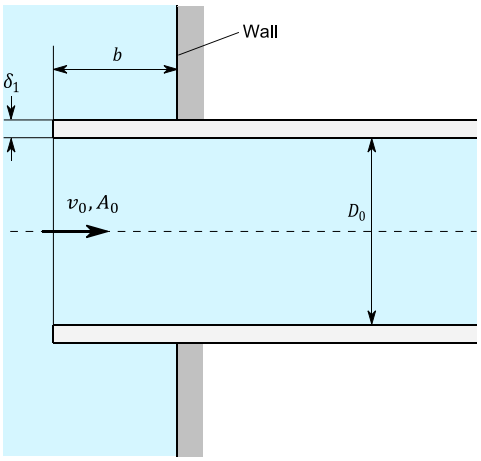

Figure 2.8: Entrance into a straight tube of constant cross-section

To achieve lower loss coefficients of the inlet, it is possible to thicken, bevel or round the inlet wall.

Flow with Smooth Change in Velocity

The flow in a diffuser goes from higher to lower velocities, because of the expansion of cross-sectional area along the length of the diffuser. Diffusers up to a certain angle will have less resistance than a straight tube with the diameter of the diffuser same as the inlet section. When the angle, α, passes a divergence limit, the resistance becomes significantly larger than a straight tube of equivalent length. This is the result of enhanced turbulent flow, separation of the boundary layer from the wall and vortex formation.

The main geometric characteristics of a diffuser are the divergence angle α and the area ratio $n_1 = A_1/A_0$, shown in Figure 2.9.

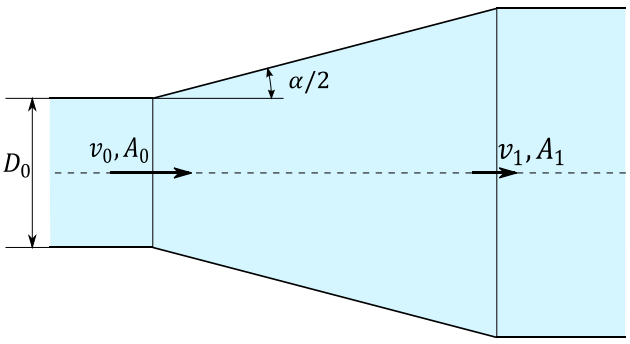

Figure 2.9: Diffuser/nozzle with circular cross-section

The resistance to flow of the diffuser in Figure 2.9 is described as

$$k = \frac{\Delta p}{\rho v_0^2/2} = k_d' k_d \qquad 2\text{-}52$$

Where k_d is found from Idelchik (1986) diagram 5-2 (a) and $k'd$ from diagram 5-2 (b/c), for a diffuser downstream a straight section. It is noted that the formulation in equation 2-52 takes into account the friction loss.

When the flow in a diffuser changes direction, going from the larger cross-section towards the smaller, it is regarded as a converging nozzle. At high Reynolds numbers, the resistance coefficient of a rectilinear converging nozzle is depended on the convergence angle α and the area ratio $n_0 = A_0/A_1$ from Figure 2.9. For engineering calculations, the resistance coefficient for a converging nozzle is

$$k = k_{loc} + k_{fr} \qquad 2\text{-}53$$

with a local resistance coefficient of

$$k_{loc} = \frac{\Delta p}{\rho v_0^2/2} = (-0.0125 n_0^4 + 0.022 n_0^3 + 0.00723 n_0^2 + 0.00444 n_0 - 0.00745) * (\alpha_p^3 - 2\pi\alpha_p^2 - 10\alpha_p) \qquad 2\text{-}54$$

where $\alpha_p = 0.01745\alpha$.

Sudden Expansion and Contraction

The sudden expansion of a pipe's cross sectional area, as shown in Figure 2.10, will lead the formation of a jet, separated from the remaining medium, which disintegrates into strong vortices along the enlarged cross-section. It is these vortices that are associated to the local loss of the sudden expansion.

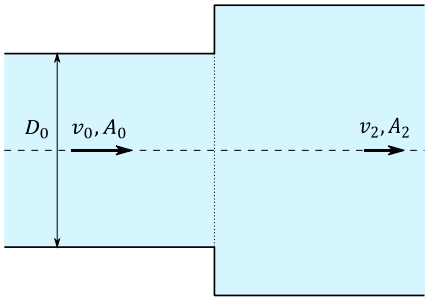

Figure 2.10: Sudden expansion/contraction of a pipe

The singular loss of an expansion at turbulent flow with uniform velocity distribution is only dependent on the area ratio $n = A_0/A_2$, and can be easily calculated by the Borda-Carnot formula. The velocity distribution is however not uniform in practical application, and an approximated value for the local resistance coefficient can be described as

$$k_{loc} = \frac{\Delta p}{\rho v_0^2/2} \approx N\left(1 - \frac{2}{3n}\right) + \frac{1}{n^2} - \frac{4}{3n} \qquad \textit{2-55}$$

where N for a circular tube is expressed as

$$N = \frac{(2m+1)^3(m+1)^3}{4m^3(2m+3)(m+3)} \qquad \textit{2-56}$$

The parameter m in equation 2-56 represents the shape of a velocity distribution in coherence with the power law, where m is an exponent that can vary from 1 to ∞, giving a fully triangular or rectangular distribution, respectively.

When the flow in Figure 2.10 changes direction, the sudden contraction of a cross-section show principally the same phenomenon as with the sudden expansion. A jet forms, but now in the reduced cross section. The main local losses now occur when the jet is expanding to fill the whole reduced cross section.

The local loss of the sudden contraction can described as

$$k_{loc} = \frac{\Delta p_{loc}}{\rho v_0^2/2} = 0.5\left(1 - \frac{A_0}{A_2}\right)^{\frac{3}{4}} \qquad \textit{2-57}$$

2.5 Economic Analysis

The economic analysis in the thesis will be based on the method of constant market prices. Prices from a given year will be used under the assumption that all prices will have the same growth in life-time of the economic analysis.

To evaluate solutions it is needed to find the *discounted cash-flow* (DCF) of all the periods in the analysis, shown generally as

$$DCF = X * \frac{1}{(1+r)^i} \qquad \textit{2-58}$$

In this formulation the X represents the cash flow of the period, and the i in which period, relative to the zero period in the model, the cash flow occurs (Pindyck and Rubinfeld, 2005).

A very important parameter in equation 2-58 is the discount rate, r. This parameter describes the required rate of return in the analysis. The rate is highly dependent on what expectations the investor has for the return on the investment, and can widely vary with different business models. For a profitable investment the minimum discount rate should be higher than the risk free investment interest, practically meaning the interest rate one could have by putting the money in a bank. In Norway the minimum required discount rate for state owned companies, in no direct competition with the private market, is 4 % for investments with life time up to 40 years (Longva and Tverstøl, 2014).

The profitability of an investment can be measured using different criteria. One of the most common is the *Net Present Value* (NPV) criterion. This is a rule that considers an investment profitable if the present value of the expected income cash flows is greater than the present value of the costs (Pindyck and Rubinfeld, 2005). This can in terms of symbols be described as

$$NVP = X_0 + \frac{X_1}{(1+r)^1} + \frac{X_2}{(1+r)^2} + \cdots + \frac{X_n}{(1+r)^n} \qquad \textit{2-59}$$

giving a profitable investment if $NPV \geq 0$. The NPV criterion is recommended by Short et al. (1995) when evaluating investments that mutually excludes one-another, because it takes into account the size of the investment.

A closely related investment criterion used to compare options is the so called *internal rate of return* (IRR), which is defined as the value of r that will give $NPV = 0$. It is important to emphasise that an investment with a higher IRR may not be more profitable than an investment with a lower, but positive IRR. An example of this is that a bigger investment with a lower IRR than a smaller investment may generate more income over the life-time, despite being less profitable according to the IRR criterion. This criterion is therefore not recommended by Short et al. (1995) for mutually excluding investments, but it is commonly used for accept/reject decisions, to ensure that the investment has a tolerated minimum rate of return.

Levelized cost of energy (LCOE) is a value that relates the cost of an investment to the energy produced, and is used to compare investments in generator produced energy. LCOE is described as the total discounted life cycle cost of an investment divided by the discounted expected production, given as

$$LCOE = \frac{\sum_{i=0}^{n} \frac{C_i}{(1+r)^i}}{\sum_{i=0}^{n} \frac{Q_i}{(1+r)^i}} \qquad \textit{2-60}$$

where C_i describes the investment costs of the period, included operation and maintenance, and Q_i the energy output created as a consequence of the investment in the period (Short et al., 1995). The LCOE is good for ranking alternatives given a limited budget, but not to choose between mutually exclusive investments, because it does not take into account the size of the investment.

3 Methodology

The methodology chapter includes numerical methods used by the employed computer program and methods used for simulations. Firstly the numerical method and model is accounted for and considerations for selecting suitable calibration data are made. Considerations for calibration and validation are made, followed by the throttle design approach taken. Lastly, the methods for analysing economic viability is explained.

3.1 Numerical Modelling

For the numerical simulations in the thesis, a computer program called *LabVIEW Transient Pipe Analysis* (LVTrans) is applied. LVTrans is a one-dimensional simulation software used for calculations on fluid-filled pipes and free flow channels, developed by Bjørnar Svingen. Its main purpose is calculations for hydropower (Svingen, 2007). The mathematical methods of describing the physics are mainly taken from the book *Fluid Transients in Systems* (Wylie and Streeter, 1993), according to Svingen (2003).

LVTrans is written in the graphical coding platform *Laboratory Virtual Instrument Workbench* (LabVIEW) (National Instruments, 2014). LabVIEW use the graphical programming language G to simulate virtual instruments, imitating physical elements. LVTrans is fully programmed in LabVIEW and the platform interface is used to build the hydraulic system and run the application.

LVTrans use the method of characteristics (MOC) to solve the differential form of the one-dimensional equations of motion and continuity (Svingen, 2003). These two equations on this form is, generally, simpler than the algebraic finite difference equations, when solving transient problems (Wylie and Streeter, 1993).

3.1.1 Method of Characteristics

In the MOC, the partial differential equations are transformed into particular total differential equations that may be solved to equations that are easily handled numerically.

The momentum and continuity equations in equation 2-9 and 2-27, respectively, are dependent on four variables, two dependent and two independent. The two dependent variables are hydraulic head and velocity, while the independent variables are made up by distance along the pipe and time. To form a solution, four equations are needed.

The simplified equations of motion and continuity are named L_1 and L_2.

$$L_1 = g\frac{\partial H}{\partial x} + \frac{\partial v}{\partial t} + \frac{fv|v|}{2D} = 0 \qquad 3\text{-}1$$

$$L_2 = \frac{a^2}{g}\frac{\partial v}{\partial x} + \frac{\partial H}{\partial t} = 0 \qquad 3\text{-}2$$

The equations are combined linearly with the multiplier $\lambda\, as$

$$L = L_1 + \lambda L_2 = \lambda\left(\frac{\partial H}{\partial x}\frac{g}{\lambda} + \frac{\partial H}{\partial t}\right) + \left(\frac{\partial v}{\partial x}\lambda\frac{a^2}{g} + \frac{\partial v}{\partial t}\right) + \frac{fv|v|}{2D} = 0 \qquad 3\text{-}3$$

By solving for λ we can obtain solutions for the equation 3-3 that differ from equation 3-1. The variables v and H are dependent on x and t. If we allow the distance along the pipe to be a function of time we can obtain the following dependencies

$$\frac{dH}{dt} = \frac{\partial H}{\partial x}\frac{dx}{dt} + \frac{\partial H}{\partial t} \qquad 3\text{-}4$$

$$\frac{dv}{dt} = \frac{\partial v}{\partial x}\frac{dx}{dt} + \frac{\partial v}{\partial t} \qquad 3\text{-}5$$

When comparing this result to equation 3-3 we can easily see that

$$\frac{dx}{dt} = \frac{g}{\lambda} = \lambda\frac{a^2}{g} \qquad 3\text{-}6$$

and equation 3-3 can be re-written as the ordinary differential equation

$$\lambda\frac{dH}{dt} + \frac{dv}{dt} + \frac{fv|v|}{2D} = 0 \qquad 3\text{-}7$$

The values of λ and $\frac{dx}{dt}$ are found from equation 3-6 to be

$$\lambda = \pm\frac{g}{a} \qquad 3\text{-}8$$

$$\frac{dx}{dt} = \pm a \qquad 3\text{-}9$$

where the positive solution in equation 3-8 corresponds to the positive solution in equation 3-9, thus giving two sets of equations:

$$C^+: \begin{cases} \frac{g}{a}\frac{dH}{dt} + \frac{dv}{dt} + \frac{fv|v|}{2D} = 0 & \textit{3-10} \\ \frac{dx}{dt} = +a & \textit{3-11} \end{cases}$$

$$C^-: \begin{cases} -\frac{g}{a}\frac{dH}{dt} + \frac{dv}{dt} + \frac{fv|v|}{2D} = 0 & \textit{3-12} \\ \frac{dx}{dt} = -a & \textit{3-13} \end{cases}$$

The two partial differential equations 3-4 and 3-5 have now been converted to two the total differential equations, valid only when equations 3-11 and 3-13 are valid. The solution can be visualized in the plane of the independent variables x and t, with equation 3-11 and 3-13 as the characteristic lines where equations 3-10 and 3-13, called compatibility equations, are valid, as shown in Figure 3.1 after Wylie and Streeter (1993).

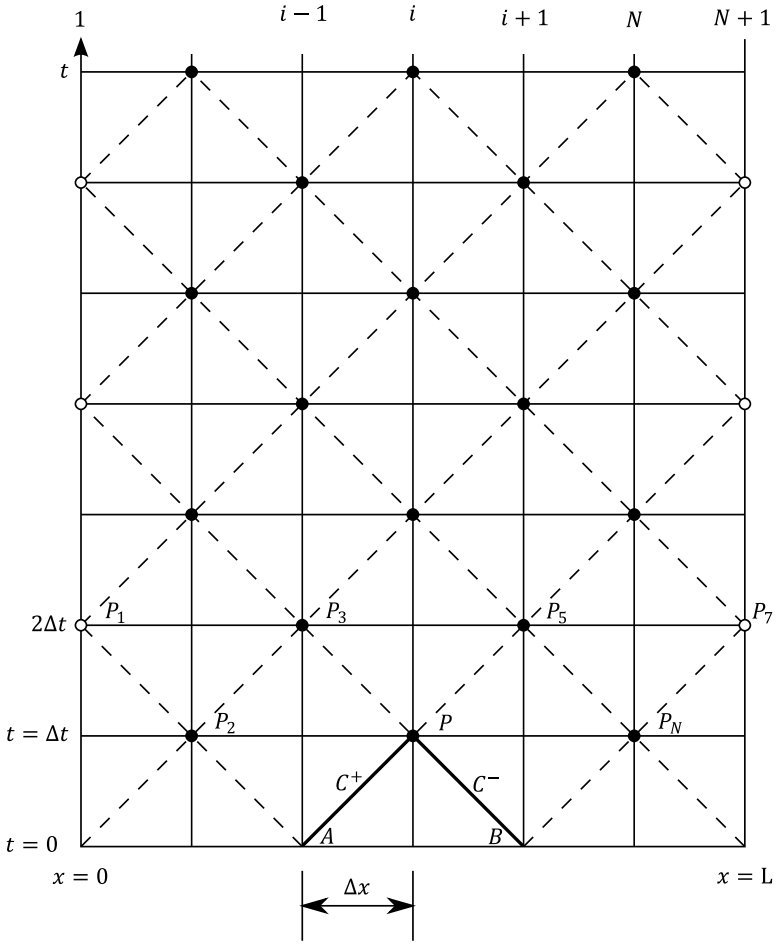

Figure 3.1: Characteristic lines in the xt-plane

As no simplifying assumptions are made in to obtain the equations in C^+ and C^-, the solution of these are equivalent with solution of L_1 and L_2.

For application on a simple pipe problem, the pipe is divided into N parts with length of Δx. The time step is found by $\Delta t = \frac{\Delta x}{a}$. If v and H are known in point A in Figure 3.1, then C^+ is valid and one can integrate equation 3-10 from A to P, resulting in an equation with the variables v and H. By assuming known variables in point B, one can integrate equation 3-12 along the C^- line, giving a second equation for the point P, resulting in solution for v and H in point P. The integration of equation 3-10 along the C^+ line can be described as

$$\int_{H_A}^{H_P} dH + \frac{a}{gA}\int_{Q_A}^{Q_P} dQ + \frac{f}{2gDA^2}\int_{x_A}^{x_P} Q|Q|\, dx = 0 \qquad \textit{3-14}$$

when $a\frac{dt}{g} = \frac{dx}{g}$ and the pipeline area is introduced to express the velocity in terms of discharge. The latter term in equation 3-14 is not known in on beforehand, so an approximation is done by the trapezoidal rule to solve the integral. By performing the integrals in equation 3-14 and a similar integration for equation 3-12, along the C^- line from point B to P, one can obtain two simple algebraic equations describing the transient propagation of hydraulic head and flow in a pipeline:

$$H_P - H_A + \frac{a}{gA}(Q_P - Q_A) + \frac{f\Delta x}{2gDA^2}Q_P|Q_A| = 0 \qquad \textit{3-15}$$

$$H_P - H_B - \frac{a}{gA}(Q_P - Q_B) - \frac{f\Delta x}{2gDA^2}Q_P|Q_B| = 0 \qquad \textit{3-16}$$

Solving for H_P yields

$$C^+: \quad H_P = H_A - B(Q_P - Q_A) - RQ_P|Q_A| = 0 \qquad \textit{3-17}$$

$$C^-: \quad H_P = H_B + B(Q_P - Q_B) + RQ_P|Q_B| = 0 \qquad \textit{3-18}$$

when introducing B and R as

$$B = \frac{a}{gA} \qquad \textit{3-19}$$

$$R = \frac{f\Delta x}{2gDA^2} \qquad \textit{3-20}$$

where B is a function of the fluid and pipeline properties, called pipeline impedance, and R is the pipeline resistance coefficient. Because the flow is equal in the points A, B and P, the equations hold for steady conditions with the steady friction over the length described by $RQ_P|Q_A|$.

In LVTrans the initial conditions at time zero are required input that enables the computation at the next time step. The two compatibility equations in 3-17 and 3-18 are solved simultaneously to find Q and H in the next time step, and can again be used to compute the values for the succeeding time step. A general simplified formulation of equations 3-17 and 3-18 can be expressed as

$$C^+: \quad H_i = C_P - B_P Q_i \qquad 3\text{-}21$$

$$C^-: \quad H_i = C_M - B_M Q_i \qquad 3\text{-}22$$

with coefficients C_P and C_M described by

$$\underset{M}{C_P} = H_{i\mp1} \pm B Q_{i\mp1} \qquad 3\text{-}23$$

and B_p and B_M as

$$\underset{M}{B_P} = B + R|Q_{i\mp1}| \qquad 3\text{-}24$$

The flow and head can then be solved for the next time step as in equation 3-25 and 3-26, respectively.

$$H_i = \frac{C_P B_M + C_M B_P}{B_P + B_M} \qquad 3\text{-}25$$

$$Q_i = \frac{C_P - C_M}{B_P + B_M} \qquad 3\text{-}26$$

3.1.2 Singular Losses

The singular losses in LVTrans are, according to Svingen (2007), described by the loss factor C_v, which is related to the flow and the resistance coefficient k, by

$$C_v = \frac{Q_0^2}{2H_0} = \frac{A^2 g}{k} \qquad 3\text{-}27$$

3.1.3 Boundary Conditions

In LVTrans the structure of the model is built with pipes connected to different components. The pipe element is the main component and it is strictly necessary to connect any other component to a pipe. As described above a characteristic grid, as in Figure 3.1, is used to solve the characteristic equations for a simple pipe. One can observe in the figure that it is only one compatibility equation is available at the start and end of a pipe element. For this reason it is necessary with boundary conditions that specify Q and H, or a relation between them, at the endpoints in Figure 3.1. These boundary conditions can be described by fairly simple equations for reservoirs, dead ends, pumps, valves etc. It is also possible to include more complex machinery and structures as turbines, air cushion chambers, surge tanks, amongst others. Comprehensive descriptions of applications and the implementation of these ca be found from Wylie and Streeter (1993).

3.1.4 Frequency-Dependent Friction

It is shown that the precision of the MOC, when evaluating an abrupt valve closure, is decreasing with time, compared to experimental results. There are some factors that may be influencing, as they are not included in the model, as listed by Wylie and Streeter (1993):

> "nonlinear inelastic behaviour of the pipe wall, nonlinear inelastic behaviour of the fluid, free gas in the liquid or release of dissolved gases during the low pressure side of the cycle, frequency-dependent wall properties, or frequency-dependent frictional losses in the fluid."

Wylie and Streeter (1993) further states that the frequency-dependent frictional losses are shown to be major in oscillating laminar flow. The pressure gradient in unsteady laminar flow affects the fluid in the boundary layer and the centre differently. The boundary layer is dominated by frictional forces with the wall, and the velocity responds in phase with the pressure gradient, due to little inertial forces. The fluid in the centre is dominated by inertial forces, as the friction is low from the adjacent fluid. As a result the velocity gradient at the wall will change before the mean velocity changes, meaning that the frictional term based on v^2 is no longer appropriate. The friction loss formulation in the MOC, in equation 2-47, assumes a velocity profile as in Figure 3.2-A, while in reality the velocity distribution looks more like Figure 3.2-B (Nielsen, 1990).

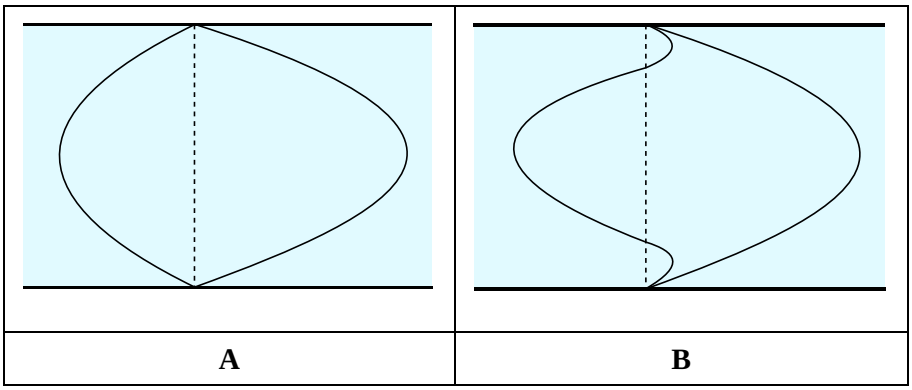

Figure 3.2: Velocity distribution during change in flow direction

There are methods developed that successfully approximate the frequency-dependent friction in laminar flow, and Brekke (1984) developed a mathematical model of turbulent frictional damping, which showed acceptable agreement with measurements at 6 hydropower plants with rough drill and blast tunnels. The analysis is however performed in the frequency-domain, and despite extensive exertions, a satisfactory modelling of turbulent flow is not available in the time-domain, with frequency as an implicit quantity.

3.2 Computer Model

The numerical model of Tonstad in LVTrans, used in this thesis, is currently running at Tonstad HPP. The model is used in a superset regulator that provides each turbine regulator with correct setpoints when a change in output power is desired (Svingen, 2015). LVTrans is used to calculate the effect of a change in setpoint in the future to check if it is satisfactory. It is in addition used in the waterway protection system to check if the mass oscillations, caused by change in plant output power, are tolerable. The LVTrans model is provided by Rainpower, with the permission of Sira Kvina. Rainpower specific components, such as PIDs and Turbines are replaced with the generic components found in LVTrans.

The model is structured such that it flows from the Homstøl and Ousdal reservoirs in the left, towards Sirdal in the right. As can be observed from Figure 3.3 and Figure 3.4, the key elements of the power plant is included, but smaller details such as thrash racks, niches, etc. are excluded. Simplifications that may have significance are the exclusion of bypass valves at the turbines and the simplified representation of the Førevann and Øksendal creek intake.

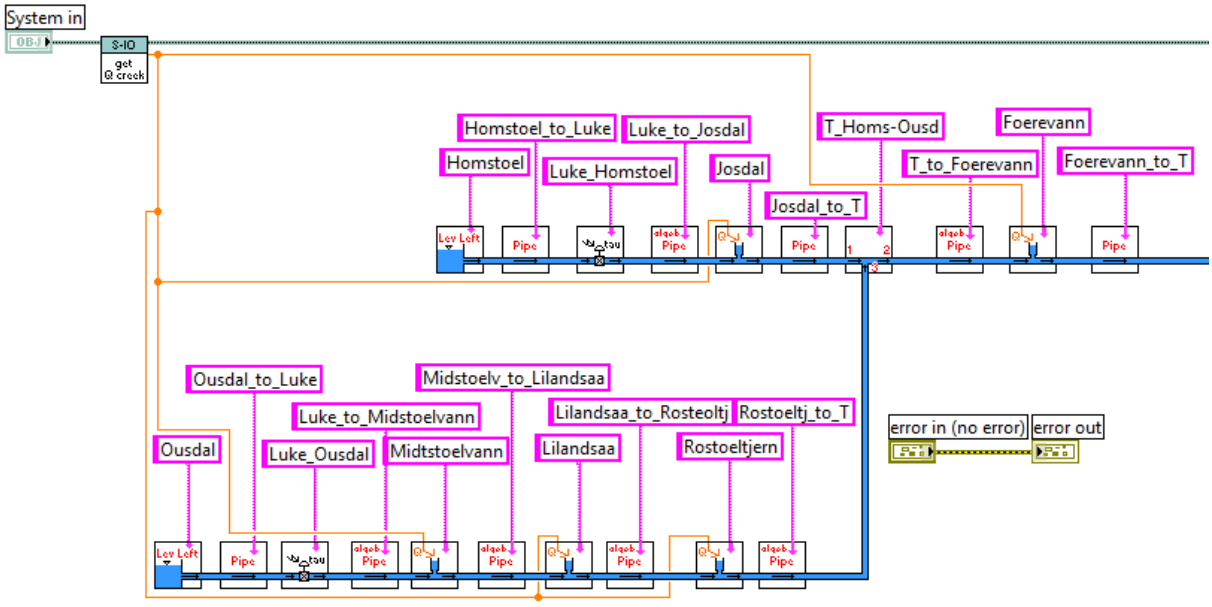

Figure 3.3: Structure of computer model, part I

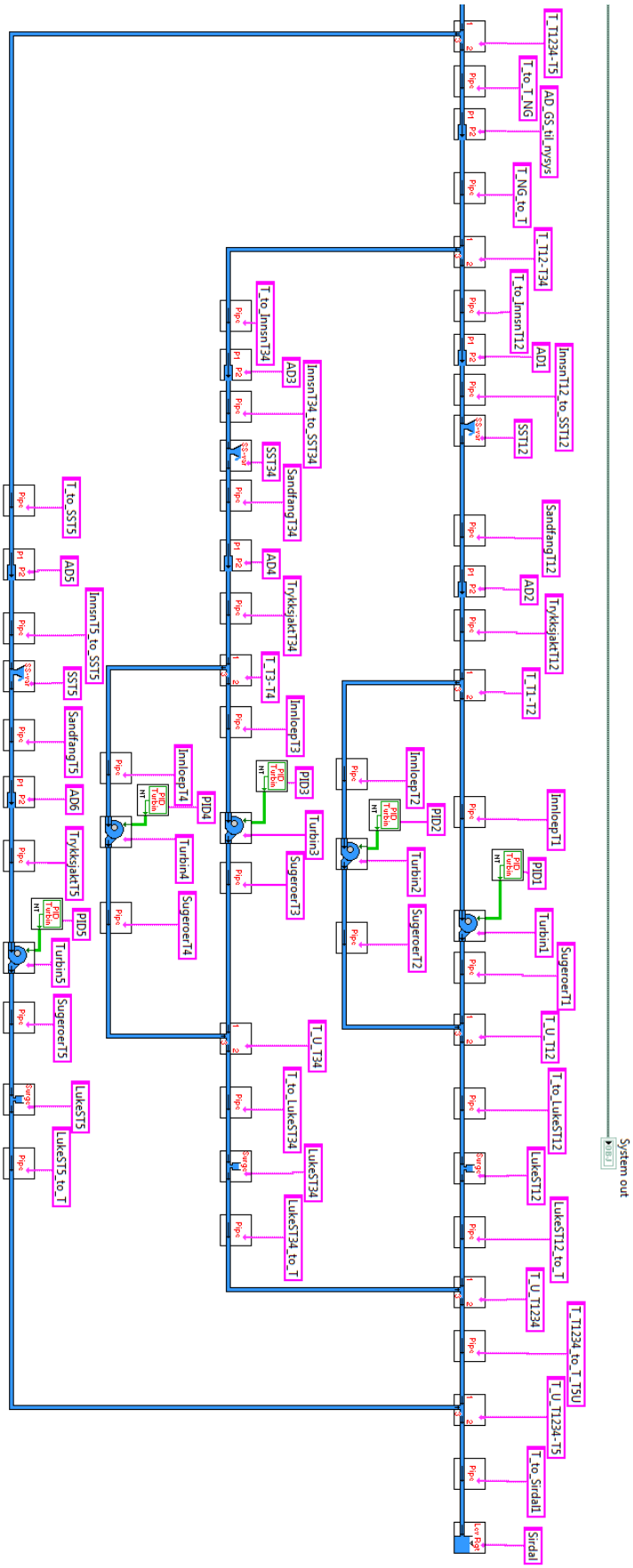

Figure 3.4: Structure of computer model, part II

An overview of the components used in the computer model is found in Table 3.1.

Table 3.1: Components in computer model

Component	Name in LVTrans	Symbol
Reservoir	Constant level	
Tunnel and pipes	Pipe	
Junction	T	
Contraction/expansion	Simple connection	
Upstream surge tank	Surge shaft variable	
Francis turbine	Francis	
PID governor	PID turbine	
Downstream surge tank	Surge shaft standard	
Valve	Valve internal servo normal	
Creek intake	Creek shaft normal	

3.2.1 Input Parameters

The most important parameters in the model will briefly be presented, but input parameters of the entire model will not be reported. The LVTrans file, will however be enclosed digitally in the supplement data, and can also be provided on inquiry.

Creek Intakes

The total inflow to the creek intakes is adjustable while LVTrans runs, with a pre-determined distribution. This distribution, given as a percentage of total inflow, can be found in Table 3.2. The total capacity of the creek intakes is calculated to 80 m^3/s from (Sira-Kvina Kraftselskap, 2008).

Table 3.2: Creek intake distribution

Creek intake	Distribution (% of total)
Midtstølsvann	8.4
Lilandså	25.6
Rostøltjern	8.7
Josdal	16.3
Førevann	41.0

Surge Tanks

There are 3 surge tanks upstream and 3 surge tanks downstream the turbine at Tonstad HPP. The area of interest is limited to the upstream surge tanks, so the downstream surge tanks are excluded from presentation here. The geometry of the surge tank is made up by area and length pairs, that together represent the change in water table area in the tank elevation. The surge tanks are roughly divided into a lower chamber, a shaft and an upper chamber in Table 3.3. The geometry parameters of the surge shafts 1 and 2 were changed to include the tunnel between the two tanks, in all simulations after the calibration. The complete list of parameters in the surge tank elements are found in Appendix C.1.

Table 3.3: Area of upstream surge tanks

Surge tank	Name in model	Lower chamber (m^2)	Shaft (m^2)	Upper chamber (m^2)
1 & 2	SST12 & SST34	285	35.0	595
3	SST5	505	37.5	1270

Turbines & PID Governors

The turbines and PID Regulators were included, in the model received from Bjørnar Svingen. No changes were made to them, other than the manipulation of the ramp, to mimic the shutdown progress in calibration and validation. It is noted that this change will have no effect on the simulation, because the ramp is not used for emergency shutdown. The table for turbines and PID input parameters is found in Appendix C.2 and C.3.

3.3 Selection of Suitable Calibration and Validation Data

To evaluate the accuracy of the numerical model, a selection of measured data from two regulation incidents are used as references. The dataset acquired from the gages at Tonstad HPP consists of multiple measurements from different parts of the hydraulic system in the period 20th of December 2014 to 19st of January 2015. The resolution of this dataset is for most measurements 1 second. The main consideration, when selecting incidents used for calibration, is the highest reduction of turbine load, measured in reduction of output power. This is done in an attempt to calibrate and validate the model as close to the simulation domain as possible to minimize scaling errors. The simulations are performed with high load rejection. Unfortunately, data from a major shut-down incident has not been available.

After analysing the data, an incident from 25th December 2014 and one from 16th January 2015 are chosen as reference datasets. The first incident consists of a reduction of approximately 260 MW distributed on two units, while the latter incident approximately consist of a 220 MW reduction. Extracts of the incidents were made with the properties listed in Table 3.4, and the extracted files are made available digitally in the supplement data.

Table 3.4: Extracted data points for reference December 2014

Description	Unit	Resolution
Output effect, units 1-5	% of nominal	1 s
Gate opening, turbines 1-5	%	1 s
Penstock pressure head, 1-5	mWC	1 s
Water Level Ousdal	m.a.s.l.	1 min
Water level Homstøl	m.a.s.l.	1 min
Water level Sirdal	m.a.s.l.	1 min
Water level, Surge tanks 1-3	m.a.s.l.	1 s
Inflow creek intake	m³/s	Daily

The calibration is performed with the incident from 25th December 2014 as a reference, and the validation with the incident from 16th January 2015. The surge tank oscillations of both incidents are shown in Figure 3.5, while the shutdown progress of the active turbines are shown separately in Figure 3.6 and Figure 3.7 for 25th December and 16th January, respectively.

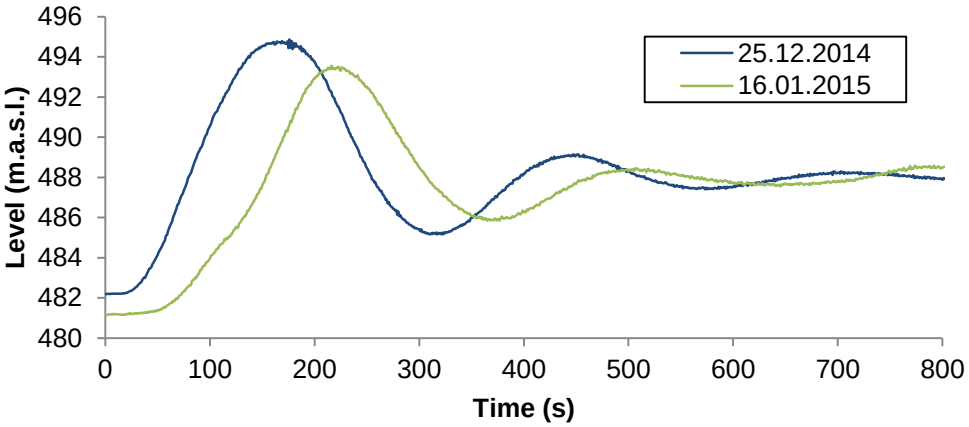

Figure 3.5: Surge tank mass oscillations, calibration & validation incident

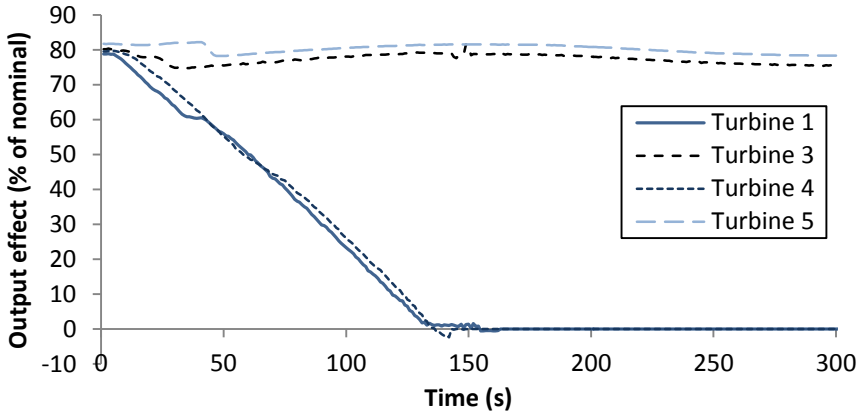

Figure 3.6: Shutdown progress 25th December 2014

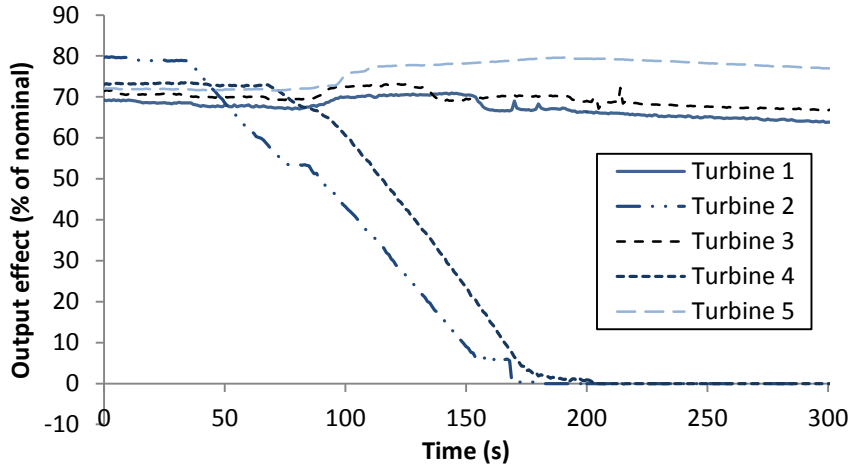

Figure 3.7: Shutdown progress 16th January 2015

3.4 Calibration

The calibration of the numerical model is important for the reliability of the results. There are several aspects that can affect the accuracy of the model versus the measured results. The model in use at Tonstad HPP is very accurate for steady state and friction coefficients are well calibrated, according Bjørnar Svingen (2015, pers. comm., 27 January). The friction parameters are therefore not changed. The system has however not been tested for accuracy at high load rejections, other than perceptive impressions under normal operations of the model at Tonstad HPP.

The most uncertain parameters of the model are the ones related to turbines, PIDs and the inflow in the creek intakes. There are carried out multiple simulations with change in different parameters to assess the importance and influence of these.

The boundary conditions for the simulations done in LVTrans, see Table 3.5, is taken from the beginning of the reference incident. It is emphasised that the values for the inflow to the creek intakes are theoretically calculated values, not measurements.

Table 3.5: Boundary conditions, calibration

Boundary condition	**25th December 2014**
Water level Ousdal (m.a.s.l.)	495.4
Water level Homstøl (m.a.s.l.)	489.2
Water level Sirdal (m.a.s.l.)	50.6
Inflow creek intakes (m^3/s)	5.3

Firstly, a simulation in LVTrans is done with no changes to the model, other than changing the boundary conditions so they correspond with Table 3.5. The shutdown procedure in Figure 3.6 is replicated by using the log of unit output effect. The replicated shutdown procedure is shown in Figure 3.8, while Figure 3.9 compares the simulations and measurements for surge tank mass oscillations.

It is noticed that the water level in Sirdalsvann, found in Table 3.5, is above the HRWL and is therefore considered to be questionable. It is possible to have water levels higher than HRWL during flood, but the energy production and the fact that the period of the year is not usually prone to floods, leaves doubt towards the correctness of these values. The effect of lowering

the steady state level within the allowed range of Sirdalsvann is tested, but results show that the steady state is not much affected. The lowering of the level in Sirdalsvann to LRWL results in a change of steady state level by 0.3 meters, which is too little to account for the change seen in Figure 3.9. A curve is added for comparison with an adjusted steady state level.

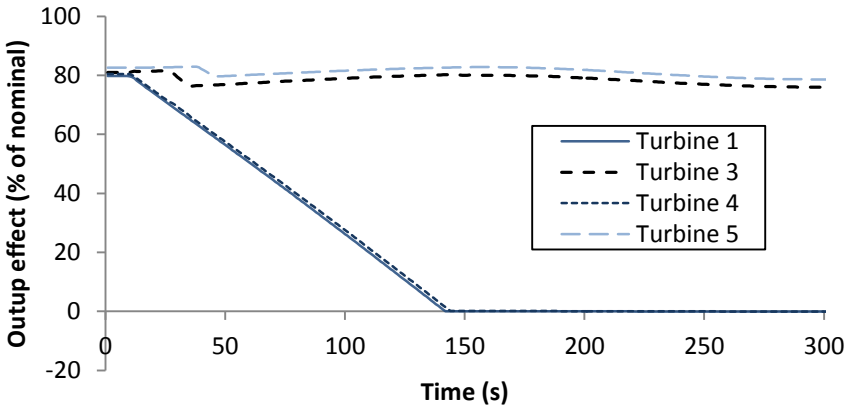

Figure 3.8: Shutdown progress of calibration simulation

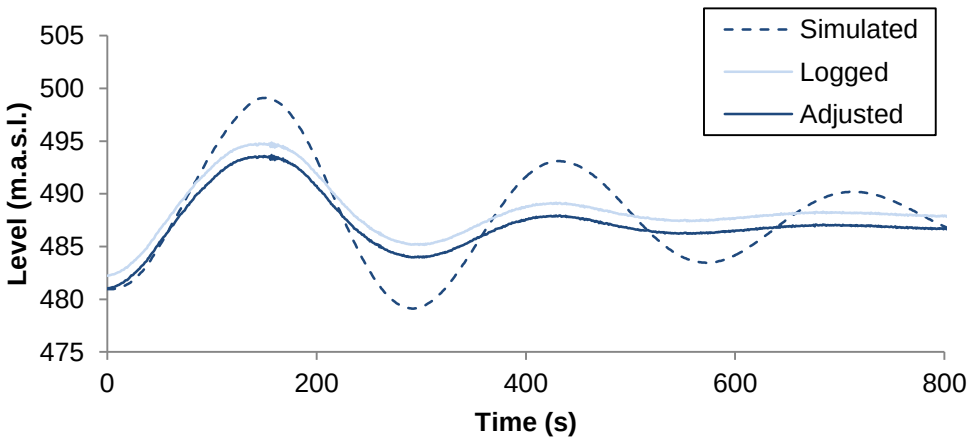

Figure 3.9: Comparison of surge tank 1 oscillation, calibration

There are high deviations from the LVTrans simulation of mass oscillations to the reference incident, as can be observed in Figure 3.9. A comparison of the amplitudes of the mass oscillation from the prototype and the simulations reveals a deviation of approximately 5.2 m

for the first peak and 5.0 m for the first local minimum. This is in terms of percentage of the prototype amplitude 76 % and 178 % for the first peak and first minimum, respectively. The reason for the deviations are not obvious, so it is therefore undergone other simulations where parameters that may have an effect on the result are varied. A simpler scenario is used for these simulations, for estimation purposes. The simplified shutdown progress only consists of the shutdown of turbines 1 and 4. The different simulations with parameter variations, listed in Table 3.6, are compared with the reference incident in the following sub-sections.

Table 3.6: Simulations with parameter variation

Simulation name	Description
Ref.	Measured values from reference incident
0	Original configuration, simplified shutdown
1	Inflow creek intake adjusted to 24.6 m^3/s
2	A 20% increase of surge tank riser area
3	A 0.01 increase of turbine efficiency
4	The addition of the tunnel connection at 494.5 m.a.s.l.

Simulation 1 – Creek Intake

As can be seen from Figure 3.9, the starting point of the shutdown, indicating the steady state level, is not correct. The steady state level is affected by the inflow to the creek intakes, and the result of controlling the steady state level by adjusting the creek inflow is examined. By increasing creek inflow to 24.6 m^3/s, the steady state aligns with the measurements in Figure 3.10. The effect on the first amplitude is minimal when shifting the curve of simulation 0 to the level of simulation 1. What is interesting is that the level of both simulations first local minimum coincides, although a noticeable change in creek inflow is made. This may suggest that an increase of inflow to the creek intakes improves the systems damping. It is noted that an increase of inflow to creek intakes by almost five times is unlikely true to account for change in the steady state level.

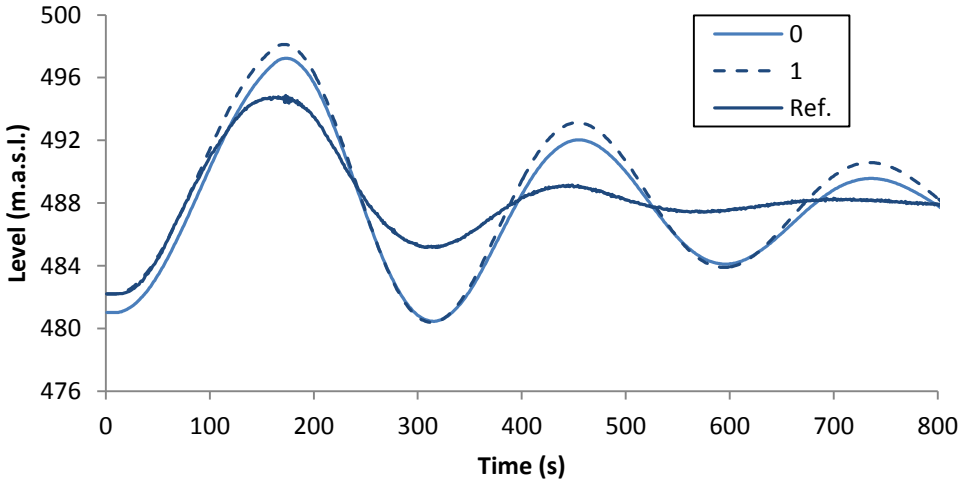

Figure 3.10: Increase of inflow to creek intakes to 24.6 m³/s

Simulation 2 – Increased Cross-Section Area of Surge Tank Riser

Simulation 2 is done under the assumption that the drawings of the surge shafts 1 and 2 portrait the minimum cross-section, and not necessary the as-built situation. An increase of 20 % is much, but it is done to investigate the effect of an increase. As can be seen from Figure 3.11, the period of the surge tank oscillations is prolonged, giving a less accurate representation than original configuration in simulation 0. The effect on the amplitude of the oscillation can be described as minimal, and a conclusion is hence made that the errors caused by deviation in the cross-section area of the surge tank risers are negligible.

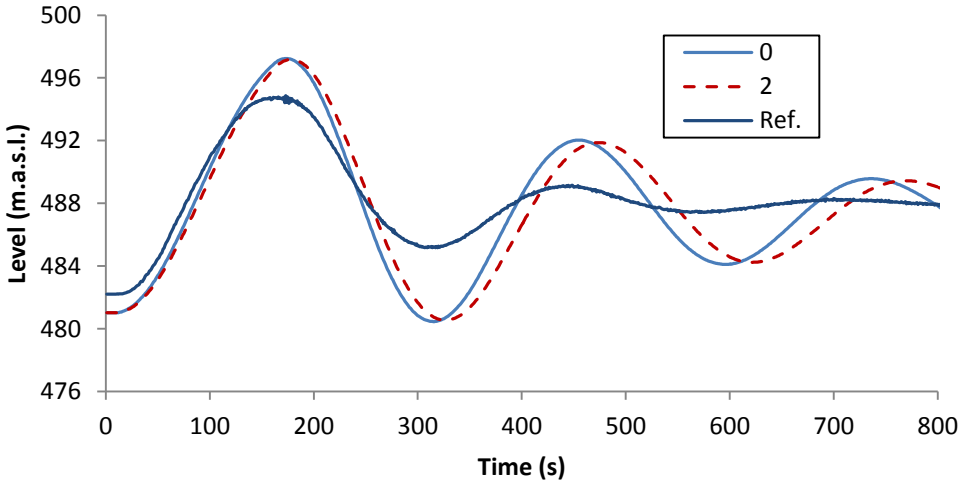

Figure 3.11: Increase of risers in surge tank 1 and 2

Simulation 3 – Increase of Turbine Efficiency

The effect of change in turbine efficiency is investigated by increasing the efficiency by 0.01, giving an input rated turbine efficiency of 0.95. An increase will cause less turbine discharge at the same output power, causing a smaller reaction to the shutdown. However, the reaction in the numerical model to the increase is so small that it is not noticeable in Figure 3.12. The conclusion drawn is that the turbine efficiency does not cause the major deviations from the reference incident.

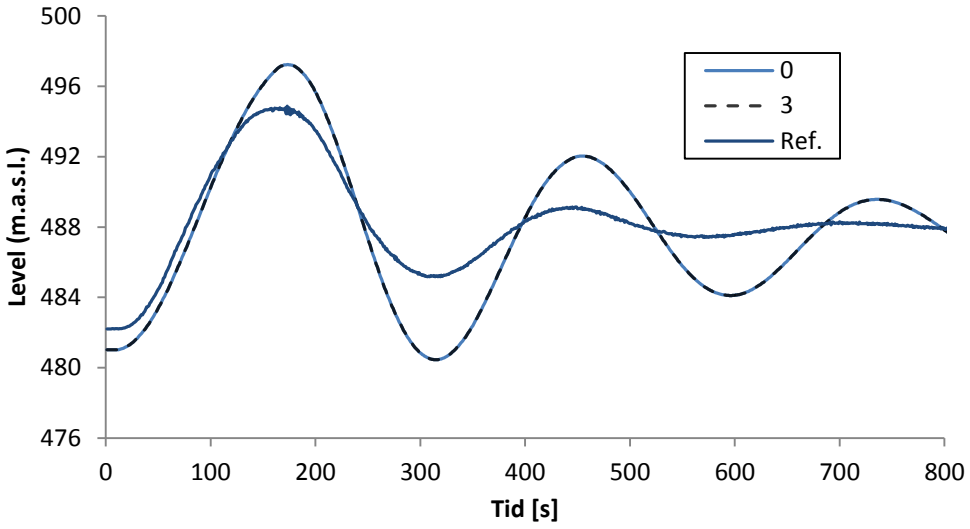

Figure 3.12: Increase of turbine efficiency

Simulation 4 – Additional Tunnel

A discovery was made that the tunnels between surge tank 1 and 2 are not included in the numerical representation of the variable surge tank in the numerical model received. The largest tunnel is located 494.5 m.a.s.l., so it will have no effect on the prototype measurements, because the water level does not pass the tunnel. Nevertheless, the effect of including the largest tunnel in the numerical model, as seen in Figure 3.13, is substantial. There is a slight effect on the period, but this would also be true if the prototype measurements had exceeded 494.5 m.a.s.l. It is therefore come to the conclusion to include the tunnel connecting surge tank 1 and 2 at 494.5 m.a.s.l. for future simulations.

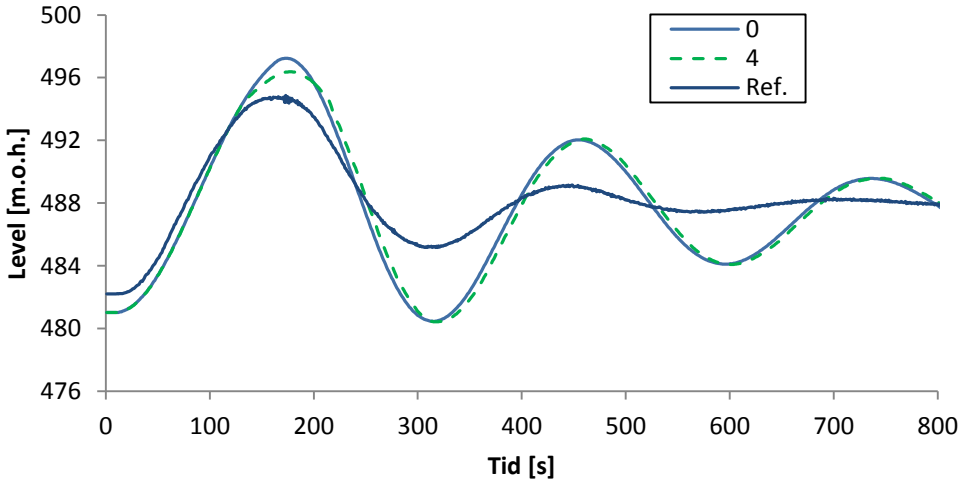

Figure 3.13: Inclusion of connection tunnel 494.5 m.a.s.l.

Findings from Parameter Variations

As a result of the above investigations, the influences of the change in a range of parameters are found. It is believed that none of the parameters varied in simulations 1 to 4, or a combination of these, are the cause of the large deviations from the reference incident. It is also considered very unlikely that the friction in the model and in the prototype are severely different, causing the deviations. This is because the steady state situation is well calibrated in the ongoing use of the superset regulator at Tonstad HPP.

The deviation in steady state level cannot be explained by either error in inflow to the creek intakes nor the fact that Sirdalsvann is above HRWL. The difference is however not so big that it is believed to affect the results severely.

Given that the above assumptions hold, the only parameter that can influence the amplitude of surge tank oscillations is a reduction in produced power of the power plant, with a resulting reduction in turbine discharge. This is very unlikely, considering that the output power is measured and regulated.

A well-known problem in the numerical simulation procedure is the underestimation of system friction during transients, due to the lack of an appropriate formulation for the frictional damping of oscillations. It has previously in simulations of other systems been the practice to assume that the error in the first period of the surge tank oscillations, due to the lack of damping of oscillatory friction, is negligible. A conclusion has hence been drawn, with input from co-supervisor Vereide and Bjørnar Svingen, that the major part of the deviations of surge tank mass oscillation amplitudes, from the numerical model to the

reference incident, is most probably caused by the underestimation of the transient friction in the MOC.

3.4.1 Calibration Considerations

It is possible to adjust the inlet and outlet loss coefficient of the surge tank to the degree that the first peak and the first minimum becomes the same as in the reference incident. This is however not done, as it does not represent transient friction believed to cause the deviation, and can therefore not be controlled when simulations outside the calibration domain is performed. It was also shown in the authors specialization project work (Gomsrud, 2014), that the loss factors needed to reduce the amplitude sufficiently, was considerably higher than values considered to be realistic.

The simulations show very good consistency with the period of the mass oscillations. The difference of the period of mass oscillations for the simulation, compared to the average period of the prototype is estimated to 5 %, which implies that the length and area of the surge tank is sufficiently calibrated with respect to the period.

Bearing in mind that the simulation results are conservative, with respect to amplitude of mass oscillations in the surge tank, it is decided to do no calibration of parameters, other than including the area of the tunnel connecting surge tank 1 and 2 at 494.5 m.a.s.l.

3.5 Validation

The validation of the numerical model is based on the reference regulation event from 16th January 2015, where a shutdown of two turbines takes place with an approximate effect regulation of 220 MW. The boundary conditions for the reference incident, shown in Table 3.7, are used for the validation.

Table 3.7: Boundary conditions, validation

Boundary condition	16th January 2015
Water level Ousdal (m.a.s.l.)	494.6
Water level Homstøl (m.a.s.l.)	491.2
Water level Sirdal (m.a.s.l.)	50.5
Inflow creek intakes (m³/s)	4.3

The shutdown is roughly imitated based on the log of output effect from the superset regulator installed at Tonstad. The progress of the shutdown of the reference event is shown in Figure 3.7 and the imitated shutdown of the validation simulation in Figure 3.14.

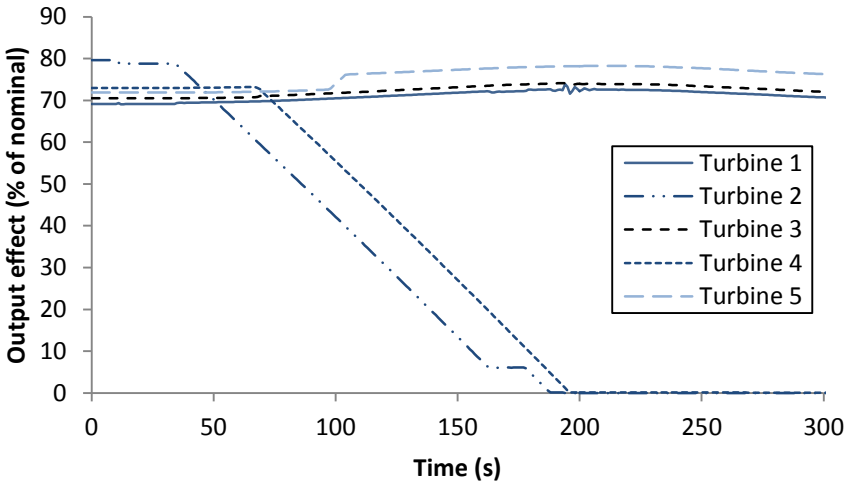

Figure 3.14: Shutdown progress of validation simulation

The result of the validation shows consistence with finding from the calibration. The water level in the surge tank, as shown in the comparison in Figure 3.15, displays that the period of mass oscillations shows high accuracy, with a deviation of 0.2 % from the average period of the logged values. The deviations of the amplitude show similar characteristics as seen from the calibration. The deviation of amplitude of the validation simulation to the measurements is 5.7 meters at the first peak and 5.2 meters at the first local minimum, resulting in a percentage of 41 % and 154 %, respectively. This is lower than deviations from the calibration, indicating that the deviations may increase with increased regulated effect, with a decrease of 40 MW from the calibration to the validation. The results further substantiate the conclusion, from the calibration, that the numerical model is decidedly conservative with regards to interpretations of absolute values.

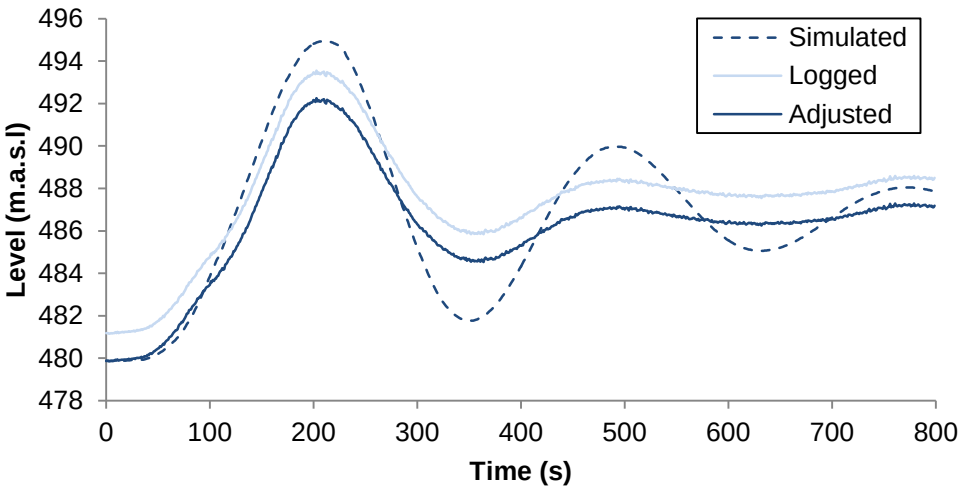

Figure 3.15: Comparisons of surge tank oscillations, validation

3.6 Throttle Design

The throttle design has multiple steps, which are accounted for in the following chapter. The foundation for simulation considerations is reviewed and the procedure is explained. Determination of throttle geometry is also included in the following section.

3.6.1 Simulation Scenarios

The worst case scenario is important to establish when investigating the effect of surge tank throttles at Tonstad HPP. There are several parameters that have an impact of the hydraulic behaviour of the power plant.

The total production of the plant determines the flow of water, and therefore also the magnitude of water hammer and mass oscillation. It is evident that maximum production will, cause the maximum flow, giving the worst case at a production of 960 MW.

The reservoir levels at Ousdal and Homstøl will affect, not only the steady state level in the surge tanks, but also the efficiency of the turbines. More discharge is needed to produce at the same power when the water levels are low, than when they are high.

The friction in the system will decrease with an increasing inflow of water to the creek intakes, because less water needs to travel the long tunnels from the reservoirs. The result of this is that the more water that flows through the creek intakes, the higher will the level be in the surge tanks. Inflow to the creek intake also contribute to the momentum during mass oscillations, which will result in higher amplitudes of the peaks, but a faster damping of the flow towards the upper reservoirs.

It can be argued that the critical situation, for a downswing of the surge tanks water table, can be a sudden load increase at already high loads. This may be true, but it is also a fact that the load increase can, and is, controlled so that the increase will happen in a manor where the opening is so slow that it does not constitute a risk for too low surge tank levels. This is safeguarded by the waterway protection system put in operation in December 2014 (Svingen, 2015). It is therefore only investigated scenarios with load rejection.

The main concern until now has been to draw air into rock trap, but it is also important to have control of the upwards movement of the water level in the surge tank. Although being important, the upwards movement at Tonstad has, to the authors knowledge, not been a problem and cannot be worsened by the installation of throttles. The critical situation for upwards movement and overflow is therefore not further investigated.

Drawdown Scenario

The scenario is configured critical for the drawdown of the water level in the surge tanks. The water levels at Ousdal and Homstøl is at LRWL, the Sirdal water level is at HRWL and there is no inflow in the creek intakes. This will, at maximum production, result in the maximum possible turbine discharge and as low levels in the surge tanks as possible. This is considered the absolute worst case scenario related to low levels in the surge tanks. When performing simulations at the absolute worst case scenario, it is however clear that the conditions are not suited for the evaluation of a throttle. The steady state level in the surge tank is drawn down into the tunnel, causing operation circumstances that are not tolerable in reality. The performance of the throttle is therefore estimated at the worst case situation found with steady state level at the current safety restriction in the surge tanks 470 m.a.s.l.

To determine the worst case scenario at 470 m.a.s.l for the drawdown, a series of emergency shutdown simulations with variations in creek inflow and plant operation is undergone. The limit for the steady state can be approached in multiple variations of water level in reservoirs, creek intake inflow and electricity generation. The examination is done by performing simulations at given reservoir water levels, adjusting the creek intake and the output power incrementally to achieve steady state 470 m.a.s.l. in the surge tanks. The simulations are done with water levels equal and unequal at Ousdal and Homstøl reservoirs, but the unequal simulations only covers water levels where Ousdal is higher than Homstøl as that is the normal situation. The emergency shutdown time is set to 12 seconds. A list of simulations performed can be found in Table 3.8.

Table 3.8: Simulations to determine worst case scenario 1

Water level Ousdal (m.a.s.l.)	Water level Homstøl (m.a.s.l.)	Q_{creek} (m³/s)	Corresponding output effect (MW)
482.0	482.0	0, 25, 75, 100	663, 714, 758, 803
485.0	485.0	0, 25, 50, 75, 100	888, 790, 837, 885, 928
488.0	488.0	0, 25, 50, 75	808, 858, 905, 952
495.5	495.5	0	959
482.0	471.0	0, 50, 75, 100	294, 425, 473, 510
488.0	482.0	0, 25, 50, 75	730, 774, 824, 870
496.7	482.0	0, 25, 50, 75	796, 846, 893, 935

The worst case scenario for each water level is determined by the lowest level in the surge tank during the mass oscillation, meaning the first local minimum. All simulations in Figure 3.16, except one, suggest that the critical inflow to the creek intakes is zero. It is noted that the response when the water level at Ousdal and Homstøl is equal is increasingly favourable with increase of the creek intake flow. The progress of the response to increased inflow to the creek intakes when looking at different water levels at Ousdal and Homstøl is not as consistent as for equal levels, but has a general tendency of being more favourable with more flow in the creek intakes.

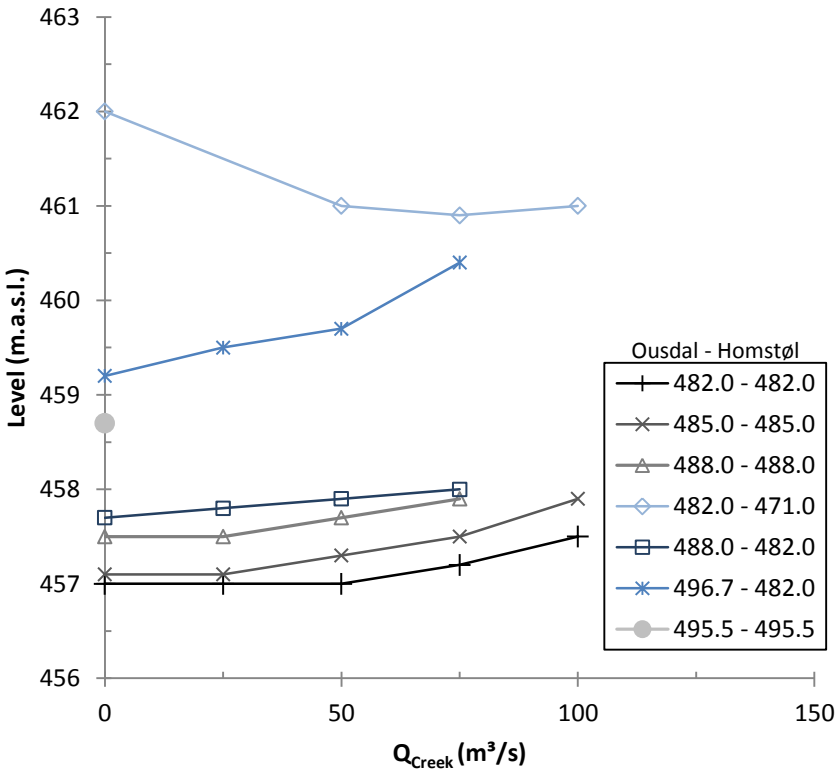

Figure 3.16: Minimum level in the surge tanks during mass oscillations

Figure 3.16 suggests that the drawdown of Homstøl reservoir will be favourable, when considering first local minimum of mass oscillations. The conclusion of the undergone simulations is that the worst case scenario for shutdown, with a steady state level in the surge tank 470 m.a.s.l., is at water levels equal in Homstøl and Ousdal 482 m.a.s.l. This is therefore considered the critical scenario for the throttle design. The boundary conditions used for the scenario is found in Table 3.9, with the turbine setting as in Table 3.10, resulting in a steady state level at 470 m.a.s.l. and a turbine discharge of 170.8 m³/s.

Table 3.9: Boundary conditions, drawdown scenario

Description	Unit	Value
Water level Ousdal	(m.a.s.l.)	482.0
Water level Homstøl	(m.a.s.l.)	482.0
Water level Sirdal	(m.a.s.l.)	49.5
Q_{Creek}	(m³/s)	0.0

Table 3.10: Turbine settings, steady state 470 m.a.s.l.

Turbine	Output effect (MW)
1	134
2	134
3	135
4	0
5	260

3.6.2 Shutdown Time

The time of shutdown is an important factor when dealing with water hammer and mass oscillations. The turbines at Tonstad HPP originally have an emergency shutdown time of 12 seconds. There is however bypass valves that will operate when the pressure in front of the turbine reaches a certain level. These bypass valves are however not included in the numerical model of Tonstad.

The bypass valves will in principle act as prolongers of the shutdown time, for shutdowns with pressures exceeding opening pressure for the valves. The valves for units 1 to 4 have opening times of about 1 seconds and a closing time of 23 seconds. Unfortunately, the capacity of the valves and the opening pressure threshold has not been acquired. It is however informed that bypass valves, in general, are dimensioned so that they in principle handle all the flow, subtracted for the flow going through the turbine in the closing (Svingen 2015, pers. comm., 28 April). This information is not verified for Tonstad HPP, so a conservative approach is taken by neglecting the effect of the bypass valves.

3.6.3 Throttle Placement and Restrictions

The throttle position is important for the effect on the hydraulics. To give the throttle maximum effect it should be placed as low as possible in the shaft, to be in effect on as low levels as possible. The placement is however restricted by practical conditions.

The lower chamber of the surge tank is included into the headrace tunnel as a side chamber. It is not favourable to build the throttle in the chamber because of the needed size, and there are no narrow sections before the lower surge chamber. The optimal placement of the surge tank throttles at Tonstad is therefore considered to be as low as possible in the surge shaft.

For the surge tanks 1 and 2, throttles in the numerical model are set 463.0 m.a.s.l., leaving 3 meters of shaft under it, for an approximate adjustment for thickness of the throttle and surrounding rock quality. With the same assumptions for surge tank 3, the throttle level is set 466.5 m.a.s.l. in the model.

The largest diameter of the throttle is restricted by available area in the shaft of the surge tanks. The shafts are, in addition to mass oscillations, used for gate manoeuvring, resulting in the need for moving equipment to pass through the throttle. It is assumed that the equipment cannot pass through the steel cone, thus enforcing a restriction of the cone diameter. In the elliptic cross-section of surge tank 1 and 2, shown in Figure 1.6, the maximum diameter of the steel cone is considered to be 3.2 meters, leaving a margin of approximately 0.5 meters. The rectangular cross-section of surge tank 3, allows for a maximum diameter of 4.0 meters, with a tolerance about 0.6 meters.

3.6.4 Alterations to LVTrans

To effectively simulate a throttle in the surge shafts at Tonstad, some alterations to elements are necessary to do in LVTrans. The procedure for calculations for the surge shaft level is embedded in LVTrans as a C++ coding field. The code is structured such that it calculates the area in the surge tank as a function of height of the water level in the surge tank and the change in this level as a function of the flow in the chamber, in an iterative manor. The iterations proceed until the increment is sufficiently small, or until the maximum number of iterations is reached.

Only small alterations are made to the code to adapt it for an approximate simulation for a throttle. Parts of the old source code and the equivalent altered parts, embedded in LVTrans, are shown below. For the ease of programming, the general loss coefficients in the bottom of the surge tank and the level of the throttle are not given as user specified parameters in the visual interface, but as numbers in the C++ coding field, market with square borders in the new code. The full, altered, script can be found in Appendix D.

Original code

```
                        ...

// Vanlig sjakt under weir
   if (L <= Lw) {
      Am = (dA*(L - L0) + A + A0)/dt;
      Q = (A + A0)*(L - L0)/dt - Q0;
      if (Q < 0.0) Cv = Cvm; else Cv = Cvp;
      F = L + Z0 + Q*abs(Q)/(2.0*Cv) - Ca + Ba*Q;
      dF = 1.0 + Am*(Ba + abs(Q)/Cv);
   };
                        ...

if (L <= Lw) {
   Q = (A + A0)*(L - L0)/dt - Q0;
   if (Q < 0.0) Cv = Cvm; else Cv = Cvp;
   Q_over = 0.0;}
                        ...
```

New Code

```
                        ...

// Vanlig sjakt under weir
   if (L <= Lw) {
      Am = (dA*(L - L0) + A + A0)/dt;
      Q = (A + A0)*(L - L0)/dt - Q0;
   if ( Lw > 1000) {
      if (Q < 0.0)
     { if (L<26.5) Cv = 8900; else Cv = Cvm;}
     else {if (L<26.5) Cv = 8900; else Cv = Cvp;}
      F = L + Z0 + Q*abs(Q)/(2.0*Cv) - Ca + Ba*Q;
      dF = 1.0 + Am*(Ba + abs(Q)/Cv);}
else {
 if (Q < 0.0)
     { if (L<20.5) Cv = 8900; else Cv = Cvm;}
     else {if (L<20.5) Cv = 8900; else Cv = Cvp;}
      F = L + Z0 + Q*abs(Q)/(2.0*Cv) - Ca + Ba*Q;
      dF = 1.0 + Am*(Ba + abs(Q)/Cv);}
```

```
    };
                                ...
if (L <= Lw) {
    Q = (A + A0)*(L - L0)/dt - Q0;
if (Lw > 1000) {
    if (Q < 0.0)
      { if (L<26.5) Cv = 8900; else Cv = Cvm;}
      else {if (L<26.5) Cv = 8900; else Cv = Cvp;}
    Q_over = 0.0;}
else {
if (Q < 0.0)
      { if (L<20.5) Cv = 8900; else Cv = Cvm;}
      else {if (L<20.5) Cv = 8900; else Cv = Cvp;}
    Q_over = 0.0;} }

                                ...
```

As can be seen from the code above, the first if-statement of the new code checks if the variable Lw is under 1000. This is a practical measure to divide surge tank 1 and 2 from surge tank 3, because the throttle height is different in surge tank 3. This can be done because the variable Lw, which is the height of an overflow weir in the surge tanks, is set so high that there will never be overflow in the surge tank. This is an assumption that, with the authors experience with the numerical model, is considered reasonable.

An extra if statement is added to the parts of the code that determines the use of the singular loss coefficient in upwards or downwards direction. The statement will check if the surge tank level is above or below the throttle level and assign the loss coefficient specified by the user for the flow situation. As a consequence, the variables Cvp and Cvm, are no longer singular losses for the whole surge tank, but only when the water level is above throttle level.

It is emphasised that the new code embedded in LVTrans is tailored for Tonstad HPP and the existing numerical model. It is therefore not possible to apply the new code on other models without altering parts of the code.

3.6.5 Numerical Simulation

To optimize the throttle losses for Tonstad HPP, several simulation steps are necessary. Initially a reference simulation of the worst case scenario for a steady state level in the surge tanks, as found in Table 3.9, is made to compare the effect of an inserted throttle. The same

scenario is used for the rest of the simulations, only varying the inlet and outlet coefficients of the surge tanks, C_{vp} and C_{vm}. A flow chart of simulation procedure is shown in Figure 3.17

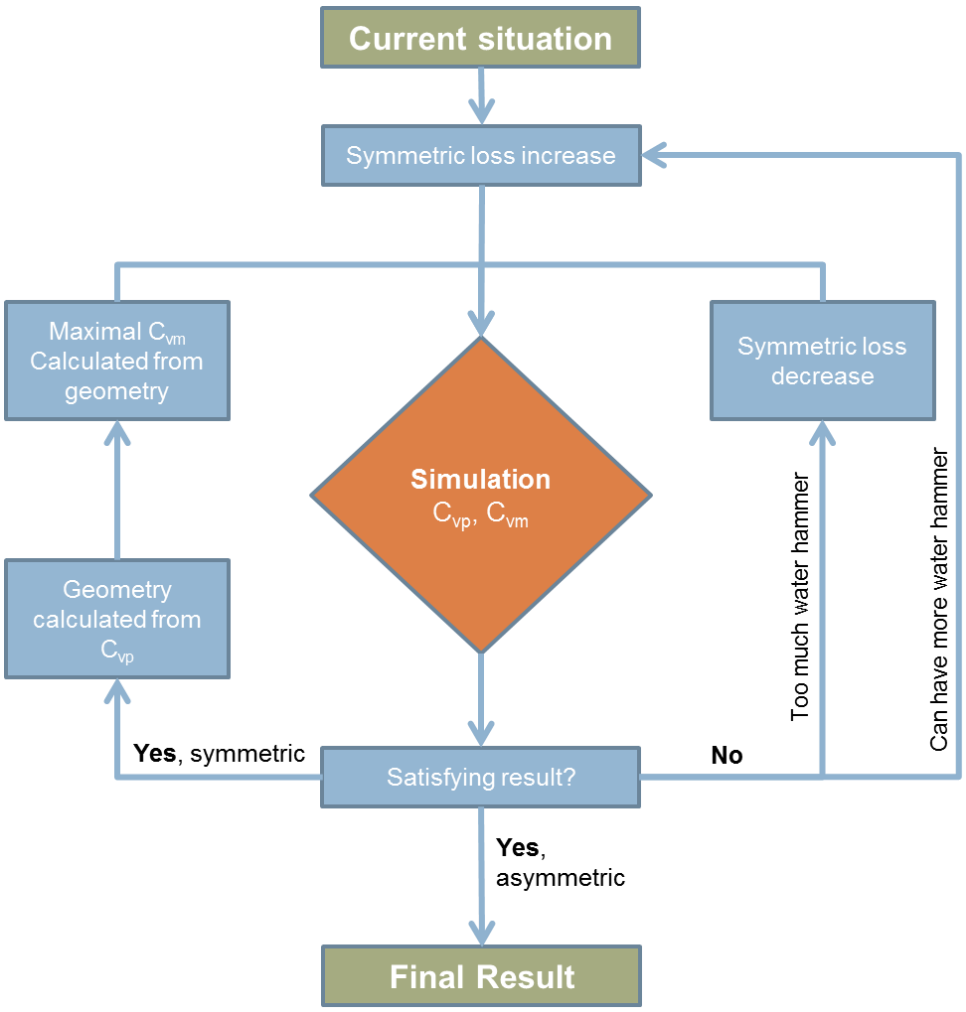

Figure 3.17: Simulation flow chart

The optimal symmetric throttle loss is found by parameter variation. The symmetric losses are incrementally increased, until the optimal symmetric throttle loss is found. This optimal loss will be the boundary for the upwards directed flow, as it is also the maximum tolerable magnitude of water hammer.

Numerically, the optimal throttle loss in the downwards direction is infinitely high, but this is however limited by practical conditions. The geometry of the surge tank limits the geometry of the throttle, forcing a maximal downwards loss, dependent on the throttles asymmetric geometry. The downwards loss is calculated by empirical tabular values, and used in a simulation, giving the final results. Table 3.11 lists representative executed simulations with C_{vp} and C_{vm}.values and their corresponding k values associated with the area of surge shafts

1 and 2. The simulations in Table 3.11 are performed with a time increment of $\Delta t = 0.001$ seconds to ensure that the water hammer pressure is correctly represented.

Table 3.11: Loss factor and resistance coefficient simulation

Simulation name	C_{vp}	C_{vm}	K_{vp}	K_{vm}
Current	8900	8900	1	1
50 - 50	50	50	240	240
25 - 25	25	25	481	481
10 -10	10	10	1202	1202
1 - 1	1	1	12017	12017
Asymmetric	25	17	481	707

Validation of New Surge Tank Water Level Restriction

The optimal throttle is found as described above, and a new water level restriction in the surge tanks is proposed. A simulation with the boundary conditions in Table 3.9 is now performed with the new restriction level, by increasing the production of the units. The turbine settings for a simulation with a steady state level in the surge tank 462 m.a.s.l. is shown in Table 3.12. This level is chosen because the lower chamber of surge tank 3 starts at this level. The shutdown time is still 12 seconds, but the time step is decreased to $\Delta t = 0.01$ seconds.

Table 3.12: Turbine settings, steady state 462 m.a.s.l.

Turbine	Output effect (MW)
1-4	153
5	313

3.6.6 Throttle Geometry

An approximate geometry of the suggested throttles at Tonstad HPP is found by calculations based on Idelchik (1986), using on loss coefficients found from simulations. It is chosen to not consider a symmetric throttle because an asymmetric throttle is hydraulically superior, and the rough methods of cost calculations, used in the thesis, fail to differentiate the asymmetric from symmetric, thus leaving the symmetric throttle less profitable.

An iterative process is necessary for the asymmetric throttle, because there are several parameters that contribute to the extent of asymmetry of the resistance coefficients. The largest throttle diameter, and the length of the throttle is restricted by the available space in the surge tanks, and the angle of the diffuser/nozzle and smallest throttle diameter is found by trial and error. A sketch displaying the throttle configuration is found in Figure 3.18.

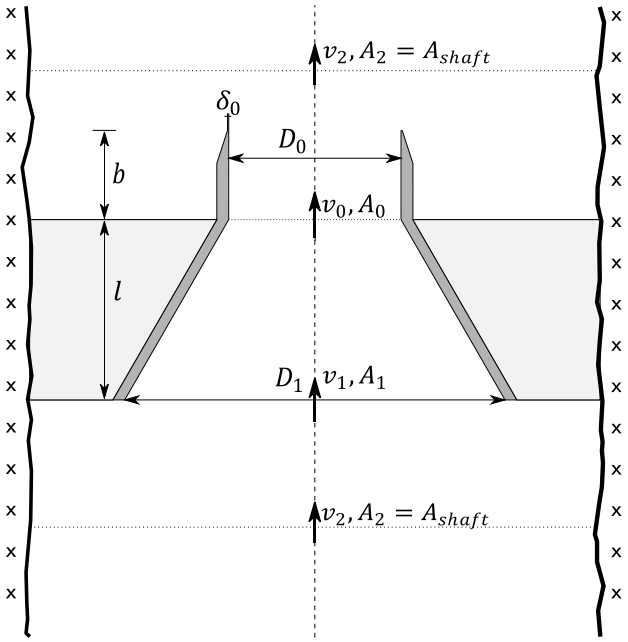

Figure 3.18: Configuration of an asymmetric throttle

Calculations show that the loss attributed to friction is very small in comparison with the local losses, when methods of Idelchik (1986) is employed. Friction losses are therefore not included in calculations of loss factors and throttle geometry.

To translate the resistance coefficient from being dependent on the throttle diameter to dependence on the surge shaft, we utilize that

$$k_{th}\frac{Q^2}{A_{th}2g} = k_{ss}\frac{Q^2}{A_{ss}2g} \qquad 3\text{-}28$$

which is independent of flow when rewritten to

$$k_{ss} = k_{th}\frac{A_{ss}}{A_{th}} \qquad 3\text{-}29$$

Asymmetric Orifice – Upwards Flow

The geometry of the asymmetric throttle is designed as a conical section connected to a straight pipe, protruding from the wall in which it is mounted, as seen in Figure 3.18. There is in the literature of Idelchik (1986), not described the exact same geometric configuration chosen for the throttle, so the resistance coefficient is calculated from composition of different flow situations.

Calculation of the resistance coefficient for the upwards flow is done by superposition of diffuser flow, sudden contraction and sudden expansion, as illustrated in Figure 3.19 A-C, with references to equations in this thesis and diagrams in Idelchik (1986). The most important term in this calculation is the sudden expansion from A_0 to A_2, which constitute approximately 90 % of the resistance to flow. The assumption of $Re > 10^4$ is made, and the velocity distribution exponent is assumed to be $m = 8$.

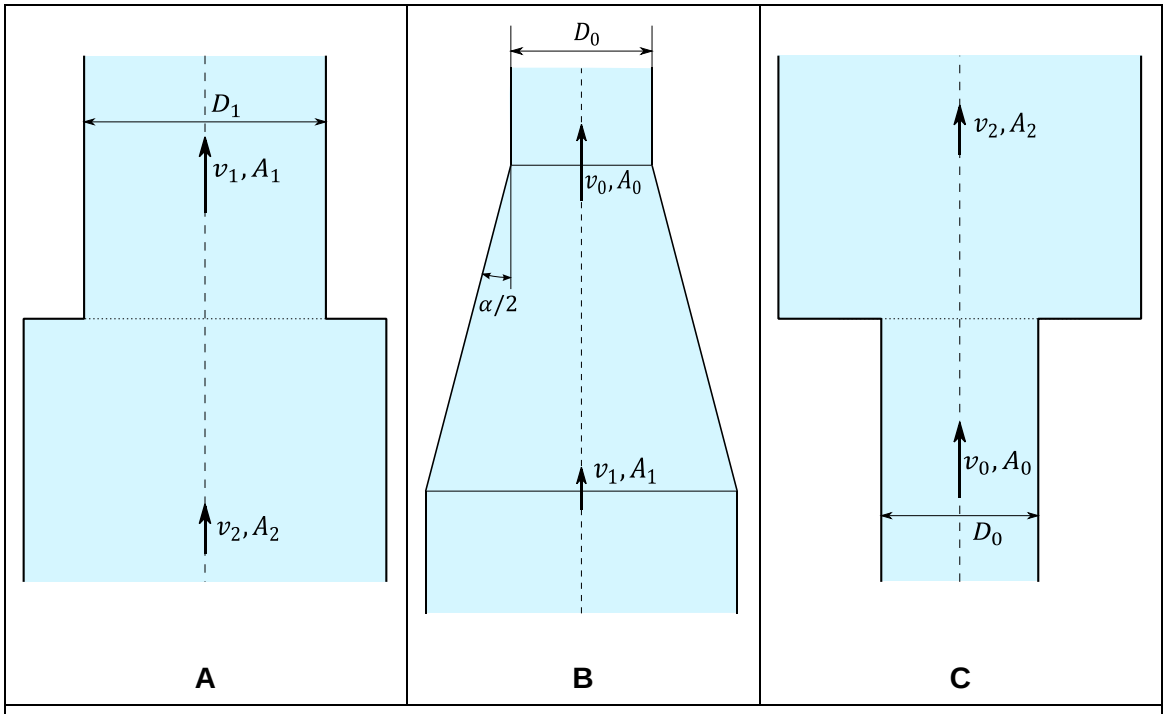

Equation reference		
2-57	2-54	2-55, 2-56

Figure 3.19: Superposition of asymmetric upwards resistance coefficient

Asymmetric Orifice – Downwards Flow

For the calculation of the downwards flow of the asymmetric throttle, the same procedure of superposition as in the upwards flow is considered. The total resistance is now found by a combination of entrance to a straight tube, conical expansion, and sudden expansion, as seen in Figure 3.20. The most important terms of the calculation is the resistance from the entrance

of the straight tube and the conical expansion. The assumption of $Re > 6 * 10^4$ is made and the velocity distribution exponent is set assumed to be $m = 8$.

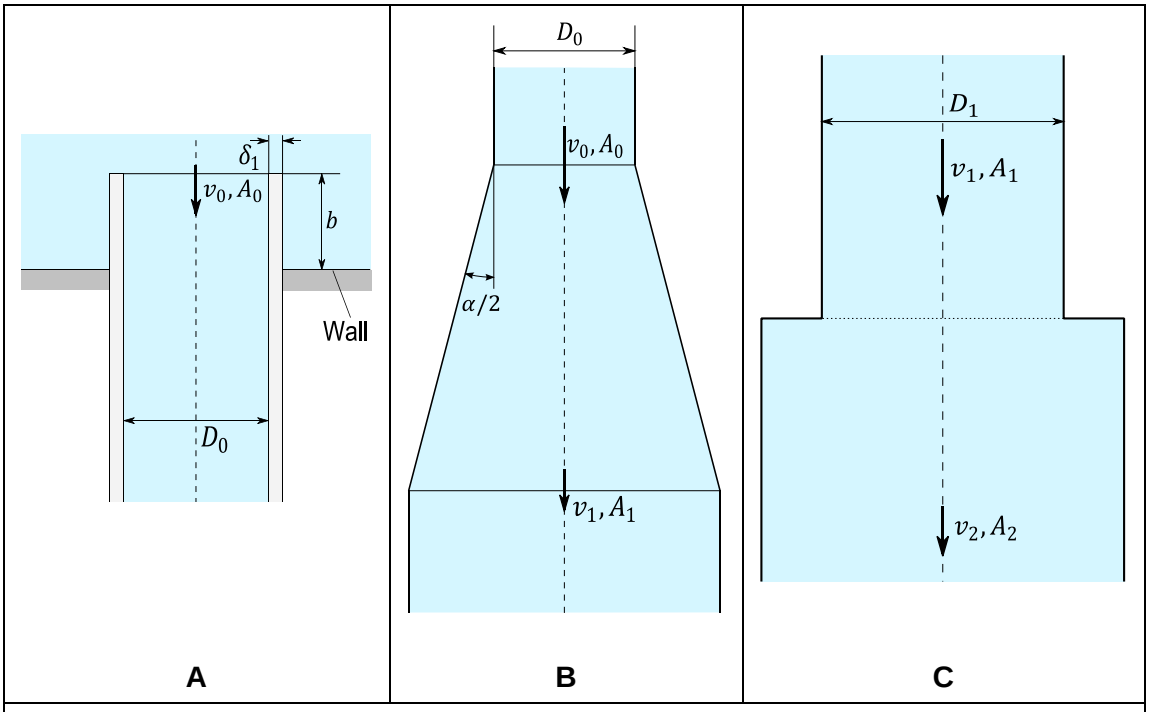

Equation reference		
-	2-52	2-55, 2-56
Diagram reference (Idelchik, 1986)		
3-2	5-2 (a), 5-2 (b/c)	

Figure 3.20: Superposition of asymmetric downwards resistance coefficient

3.7 Economic Viability

To find the economic viability of the throttle, an analysis of benefits and costs is performed. It is informed that the estimation of cost of restricted operation is the only part in the economic analysis that is within the scope of the thesis, but the considerations of throttle costs and the calculation of simple investment criteria are made, because it is the author's belief that these results are useful to put the throttle effect into an economic context.

3.7.1 Cost of Restricted Operation

The cost of restricted operation is highly dependent on the effect the throttle will have on the hydraulic system. An estimation of gained output effect is made, if the operational limit in the surge tank is reduced to 462 m.a.s.l., by finding the difference in output effect when simulating the steady state level 470 m.a.s.l. and 462 m.a.s.l. Simulations are made for equal

levels in Homstøl and Ousdal, with no inflow to the creek intake and with an inflow of 50 m³/s. Results are found in Table 3.13.

Table 3.13: Estimation of gained output effect

Reservoir levels (m.a.s.l.)	Gained effect (MW)	
	$Q_{Creek} = 0$	$Q_{Creek} = 50$
497	0 MW	0 MW
490	105 MW	10 MW
482	180 MW	174 MW

The annual cost of the restricted operation is estimated to be 2.5 million NOK by Einar Thygesen (2015, pers. comm,. 21 May), production manager at Sira-Kvina Hydropower Company, based on the estimate of gained output effect in Table 3.13. It is noted that this value is estimated with very high uncertainty, dependent on price developments, future water inflow, and the future evolution of power reserve markets.

3.7.2 Cost of Throttle

It is an extremely difficult task to estimate the cost of the throttle construction, because there is practically no basis for comparison of the operation. Such a construction is highly dependent on local conditions and the availability of tenderers for such a complex job. It is nevertheless calculated a minimum cost to be expected.

The cost of the implementation of throttles is based on a collection of average contractor expenses for Norwegian hydropower plants (SWECO Norge AS, 2010). The cost estimate assumes the construction of the throttle similar to the construction of an inlet cone from a blasted tunnel. The cost is found, from figure B.7.3 in (SWECO Norge AS, 2010), to be 90 000 NOK/m. The head is considered to be $H = 65\,m$, which is the rough distance from the maximum water level possible in the surge tank. The extremely difficult formwork and concrete situation is taken into account by adding the double cost of formwork for a hatch in a plug and the double cost of concrete for creek intakes, found in the report. This means an addition of 3000 NOK/m² formwork and 3000 NOK/m³ concrete. The additional disadvantage of working in a vertical shaft is accounted for by adding 50 % of the total construction costs.

The steel cone cost is estimated from a steel lining pipe. The lowest pressure class in diagram M.6.c is $H = 300\,m$ (SWECO Norge AS, 2010). This is still chosen because the cost of a

cone would be higher than for a simple pipe. To further account for the complex geometry and the added cost of a small order, an addition of 50% of the cone cost is made.

The design and construction management is estimated from SWECO Norge AS (2010) to be 25 %, which is the most conservative estimate. The project owner cost is set to 10 %. The addition for unforeseen costs account for all unforeseen work, including comprehensive rock bolting, cast-in pipes, guide ways for the hatch etc. Taking the very high uncertainty level of the construction process in to consideration, the unforeseen cost is set to 100 % of total contractor cost.

The cost found by using the contractor expenses is given in 2010 currency from the first quarter in NOK (SWECO Norge AS, 2010). The cost is regulated after construction cost index for road construction to first quarter 2015, with 17.4 % (Statistics Norway, 2015).

3.7.3 Cost of Plant Production Halt

The construction time of the implementation of throttles is important to assess the loss in income during production halt. The construction time is estimated on the basis of access through the top of the surge tank, with construction of rock-anchored support blocks and a concrete platform, to support the steel cone. The steel cone is lifted in in two parts and assembled on the platform, before concrete is casted to cover the conical part.

An estimate of four to eight weeks of construction is made as a guessed estimate, assuming construction work around the clock. It is emphasised that this is a very uncertain estimate.

A best guess estimate is of the cost of emptying the waterway and a production halt of 4 weeks, made by Thygesen (2015, pers. comm., 29 May), is six to seven million NOK. The dominating cost burdens are the lowering of reservoir water levels prior to the stop, the lost ability to produce if the price is high and the lost income from not being able to deliver grid auxiliary services.

The cost of production halt is set to seven million for the calculations, assuming that it is possible to finish the construction in approximately 4 weeks.

3.7.4 Investment Criteria

The investment criteria NPV, IRR and LCOE are commonly used for decision making, and are described in more detail in section 2.5. The NPV is calculated by equation 2-59, and the IRR after the definition in section 2.5. Because the estimation of the cost of restricted

operation is received as monetary value, and not as gained energy, the LCOE criterion is not calculated.

Because the calculated cost of restricted operation is a benefit of installing the throttle, it is in the analysis regarded as an annual income, and thereby a positive cash flow. The cost of throttle construction and cost of production loss at the power plant is the negative cash-flow occurring in year 0. The total cash flow is distributed over the life-time, which is assumed to be 40 years. The discount rate for the NPV is considered to be 7 %, which is known to have been used by the owners of Sira-Kvina Hydropower Company, in recent years (Thygesen 2015, pers. comm., 29 May).

4 Results

Results from the simulations and calculations are presented in this chapter. Firstly a selection of representative results from the Numerical simulation and optimization, before the calculated throttle geometry and loss coefficients. Lastly results from the economic analysis will be reported.

4.1 Numerical Simulation and Optimization

Results from numerical simulation and optimization are presented, based on methodology described in section 3.6.5.

4.1.1 Current Situation

The simulation representing the current situation at Tonstad HPP is firstly examined by the surge tank mass oscillations in Figure 4.1, and the pressure head in front of the turbine in Figure 4.2. The simulations are run according to Table 3.9, with an emergency shutdown of 12 seconds.

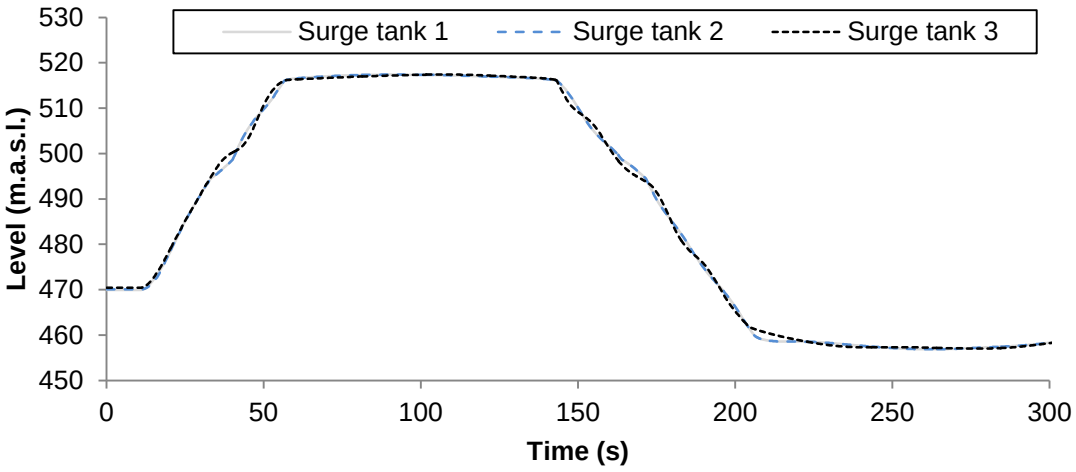

Figure 4.1: Surge tank oscillations at current situation

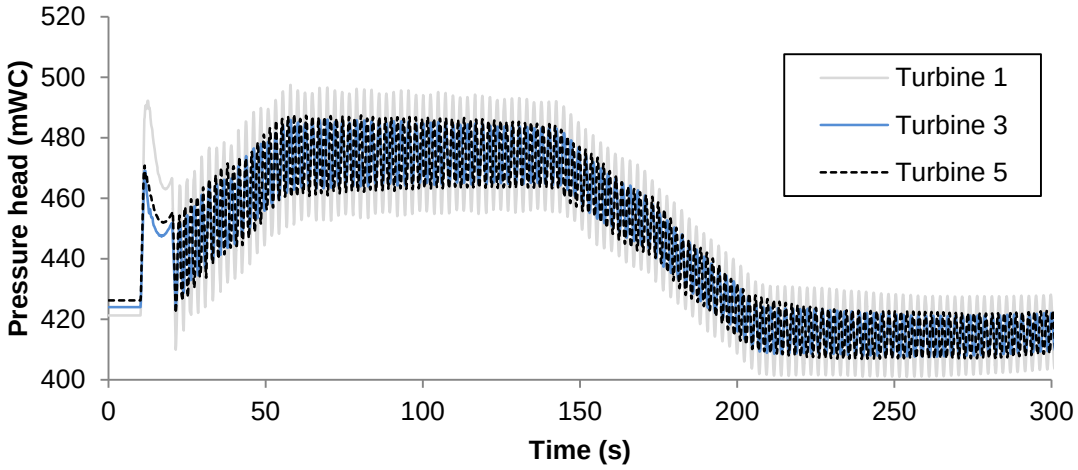

Figure 4.2: Turbine pressure head at current situation

Figure 4.2, shows that the pressure head in front of turbine 1 is larger than the pressure head in front of turbine 3 and 4, but that the progress of the surge tank oscillations of all surge tanks are approximately similar. The variations of turbine pressure head and the small variations in surge tank levels are expected, due to the variation of flow in penstocks 1, 2 and 3. The variations of surge tank levels are so low that they are, in the following comparison of different loss factors, only presented by surge tank 1.

4.1.2 Comparison of Loss Factors

The comparison of loss factors are split into simulations with symmetric loss factors in the surge chamber, meaning $C_{vp} = C_{vm}$, and asymmetric loss factors, meaning $C_{vp} \neq C_{vm}$. The investigated loss factors are listed in Table 3.11, and simulations are run according to Table 3.9 with an emergency shutdown of 12 seconds.

Symmetric Loss Factors

Figure 4.3 shows the progress mass oscillations in surge tank 1, and Figure 4.4 the pressure head in front of turbine 1 for the variation of symmetric loss factors. When taking a closer look at the first 50 seconds of the pressure head in front of turbine 1, in Figure 4.5, one can more easily observe the difference in water hammer between the different loss factor simulations.

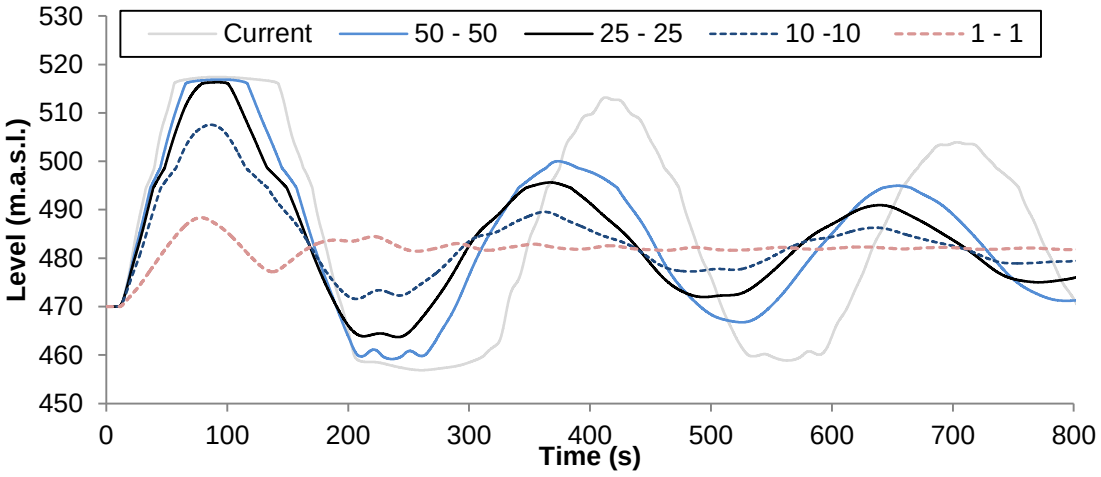

Figure 4.3: ST1 mass oscillations, symmetric loss factor comparison

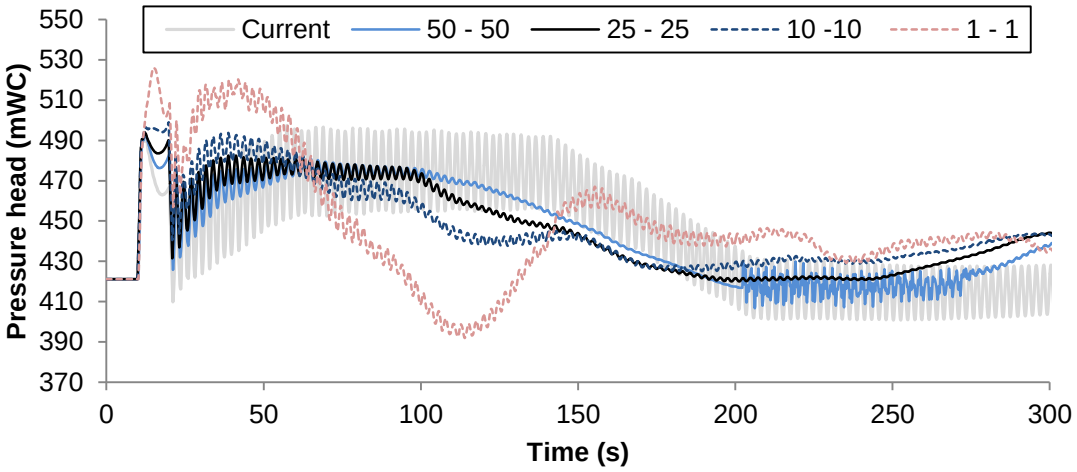

Figure 4.4: Pressure head in front of T1, symmetric loss factor comparison

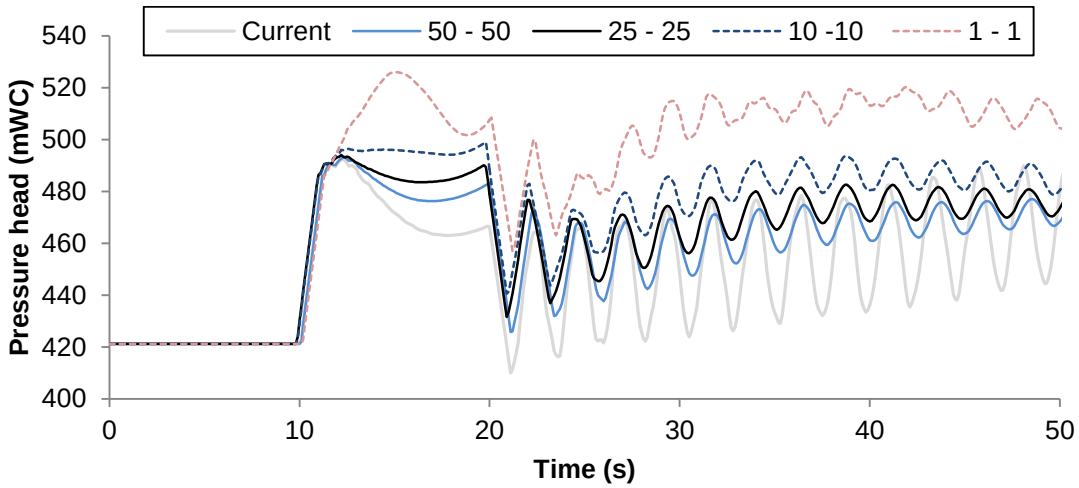

Figure 4.5: Water hammer turbine 1, symmetric loss factor comparison

Asymmetric Loss Factors

There are only reported a single simulation with asymmetric loss factors, but these are compared with simulation 25-25 and the current situation simulation. Figure 4.6 compares mass oscillations, while Figure 4.7 compares pressure head in front of the turbine. Figure 4.8 displays the first 50 seconds of the pressure head in front of turbine 1. The level of first local minimum and the difference from the simulation of the current situation is found in Table 4.1.

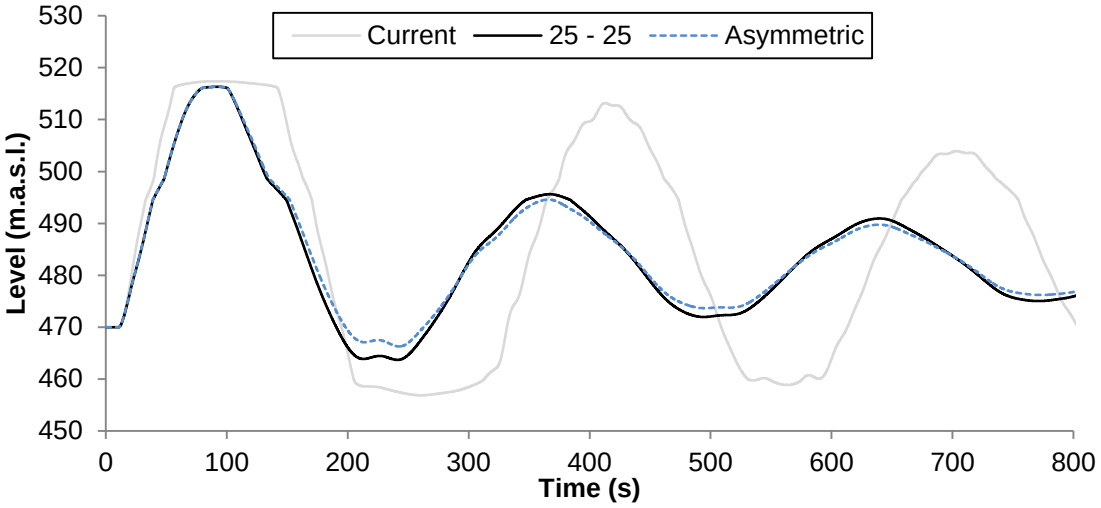

Figure 4.6: Surge tank 1 mass oscillations, asymmetric loss factor comparison

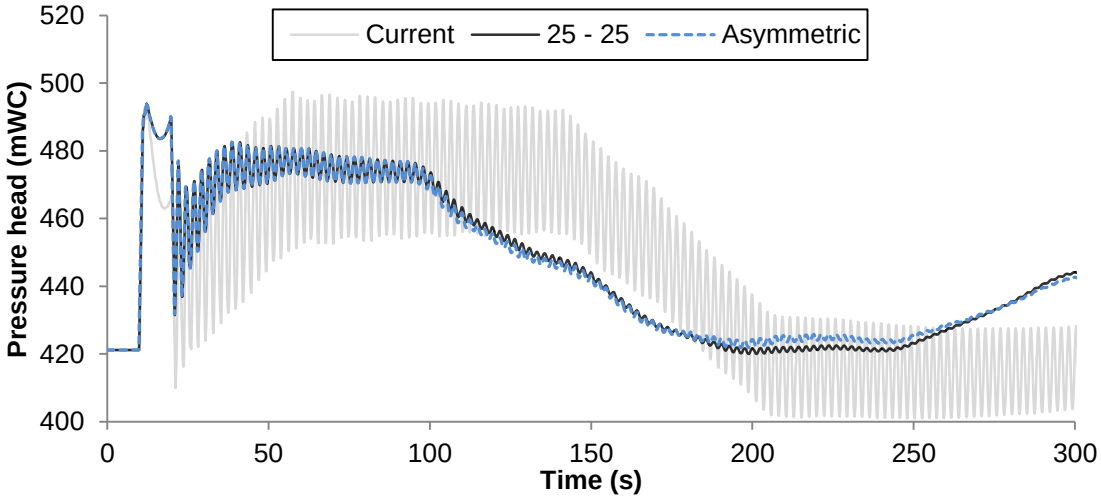

Figure 4.7: Pressure head in front of turbine 1, asymmetric loss factor comparison

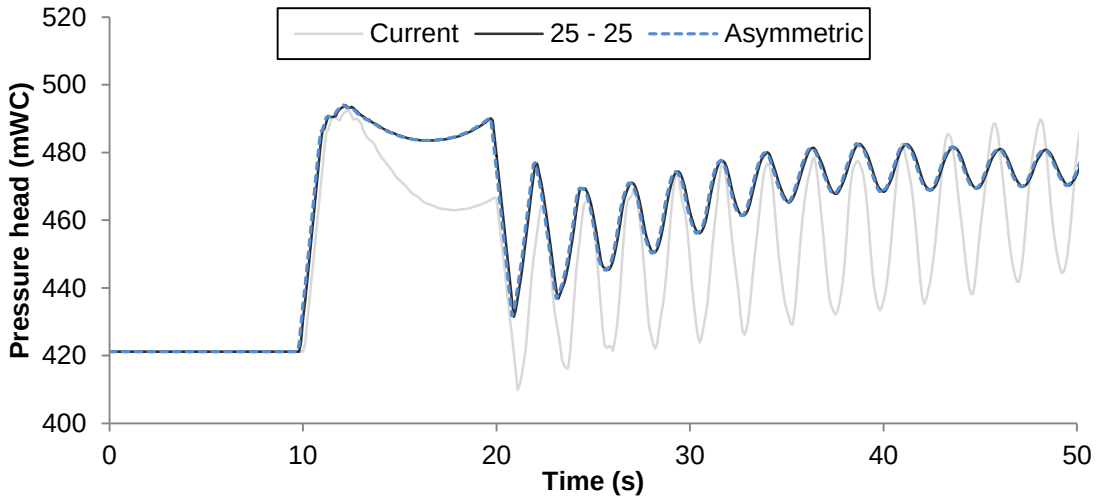

Figure 4.8: Water hammer turbine 1, asymmetric loss factor comparison

Table 4.1: Results of asymmetric simulation

Simulation	$C_{vp} – C_{vm}$	First local minimum	Difference from current simulation
	(-)	(m.a.s.l.)	(m)
Current	8900 – 8900	456.6	0
Symmetric	25 – 25	463.7	7.1
Asymmetric	25 – 17	466.2	9.6

4.1.3 Simulations of Final Asymmetric Throttle

The simulations for the final surge tank is divided, into a simulation with the current restriction level in the surge tank and with a changed restriction to 462 m.a.s.l.

Current Restriction Level

The surge tank oscillations of the three surge tanks, for the asymmetric simulation, are presented in Figure 4.9, and the pressure head in front of turbines 1, 3 and 5 in Figure 4.10. The pressure head in front of turbine 2 and 4 are assumed to be equal to the pressure head in front of turbine 1 and 3, respectively. It is some, but little variation in the surge tank levels in Figure 4.9, and differences in turbine pressure head, in Figure 4.10, is comparable to the differences in turbine pressure head without the throttle in Figure 4.2.

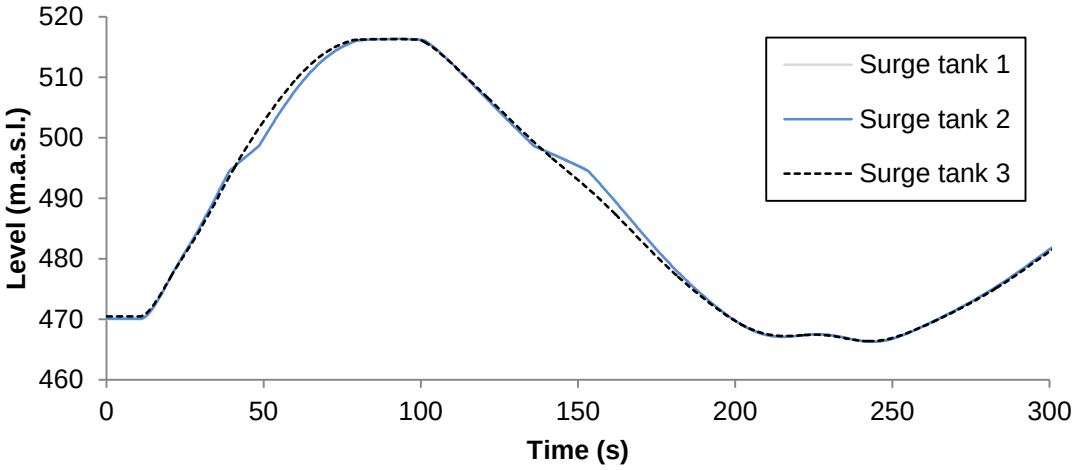

Figure 4.9: Surge tank mass oscillations, asymmetric simulation

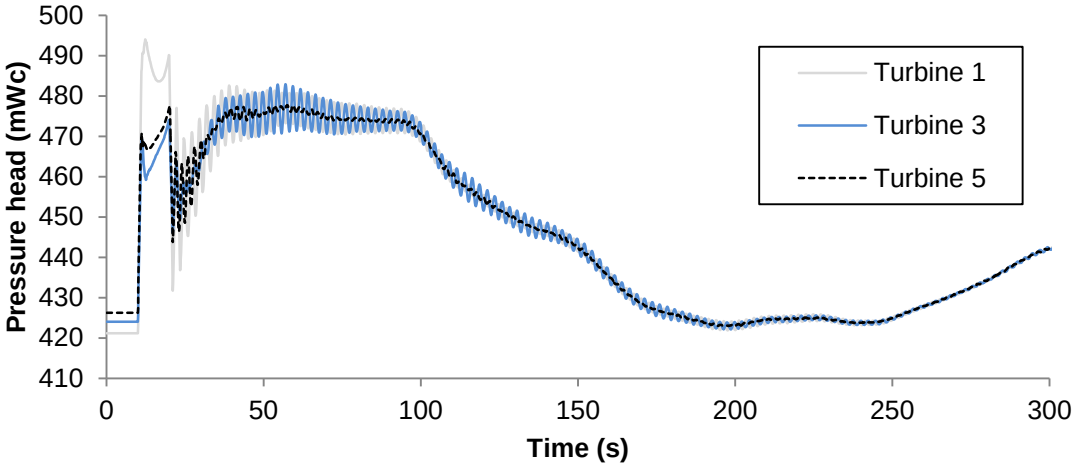

Figure 4.10: Pressure head in front of turbines, asymmetric simulation

Lowered Restriction Level

The simulations of a change in restricted steady state level in the surge tank to 462 m.a.s.l., is performed with the asymmetric throttle. The surge tank mass oscillations and pressure head in front of the turbine are shown in Figure 4.11. The first local minimum of the mass oscillation is 471.5 m.a.s.l., which is 5.3 meter higher than for a steady state 470 m.a.s.l. The maximum pressure head in front of the turbine is 516.3 mWC, 4 % higher than for the simulation of the current situation.

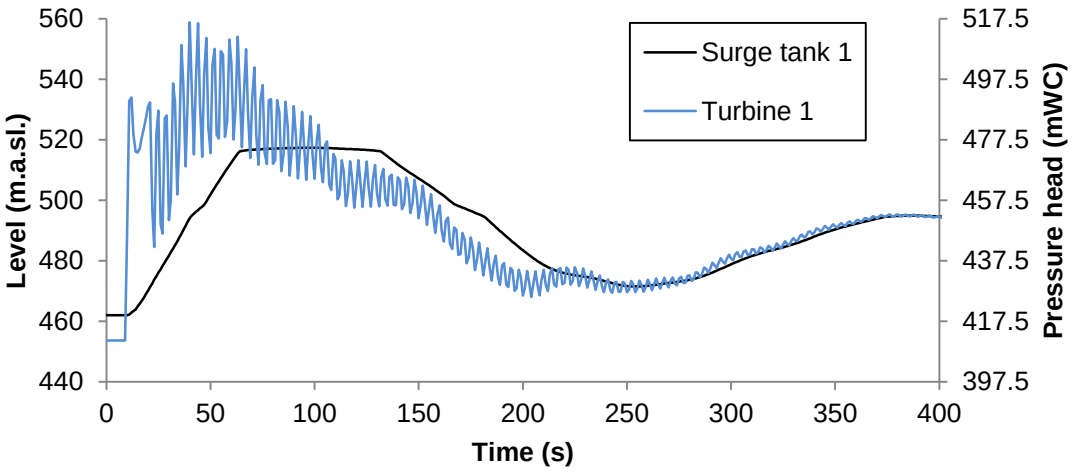

Figure 4.11: Surge tank mass oscillation and pressure head in front of turbine at steady state level 462 m.a.s.l.

4.2 Throttle Geometry

The asymmetric throttle losses in the upwards direction, found in Table 4.2, are calculated on the basis of the superposition and references found in Figure 3.19, while the asymmetric downwards throttle losses, in Table 4.3, are calculated on the basis of Figure 3.20. The resistance coefficients, k, is related to the area of the surge tank riser, $A_{shaft} = A_2$, of the representative throttles.

Table 4.2: Loss coefficients of upwards flow

Loss situation	k, ST1-2	k, ST3
Sudden contraction	10	20
Smooth contraction	49	67
Sudden expansion	428	467
Total resistance coefficient	**486**	**554**

Table 4.3: Loss coefficients of downwards flow

Loss situation	k, ST1-2	k, ST3
Inlet	403	438
Smooth expansion	305	386
Sudden expansion	12	4
Total resistance coefficient	**719**	**829**

A comparison of the total resistance coefficients k, to the loss factor C, on the form used in LVTrans is shown together with the ratio of asymmetry in Table 4.4.

Table 4.4: Loss coefficients and loss ratio for the asymmetric throttle

Description	Notation	ST1-2	ST3
Upwards resistance coefficient	k_{vp}	486	554
Downwards resistance coefficient	k_{vm}	719	829
Upwards loss factor	C_{vp}	25	25
Downwards loss factor	C_{vm}	17	17
Loss ratio	R	1 : 1.5	1 : 1.5

The loss factors found in Table 4.2 and Table 4.3, corresponds to the throttle geometry described in Table 4.5, relative to Figure 3.18.

Table 4.5: Asymmetric throttle geometry

Description	Notation	Unit	ST1-2	ST3
Diameter of inlet/straight tube	D_0	(m)	1.5	1.5
Largest diameter in diffuser/nozzle	D_1	(m)	3.2	4.0
Area of shaft	A_2	(m^2)	35	38
Divergence angle	α	(°)	60	70
length of throttle	l	(m)	1.52	1.81
Length of protruding tube	b	(m)	0.75	0.75
Thickness of tube edge	δ1	(m)	0.01	0.01

4.3 Economic Analysis

The total discounted cost of the restricted operation over the life time, together with estimated throttle construction costs and economic loss of the emptying of the waterway and production cease can be found in Table 4.6. The detailed estimation of construction costs, in Appendix E, show that a minimum cost for a single throttle is 4 MNOK, when rounded up to the nearest million.

Table 4.6: Cost of restricted operation, throttles and production halt in MNOK

Description	Value
Cost of restricted operation	33.3
3 x Cost of Throttle	11.9
Cost of production cease	7.0

Investment Criteria

The results of calculation of NPV and IRR with a discount rate of 7 % and life time of 40 years is found in Table 4.7.

Table 4.7: Result of investment criteria

Criterion	Unit	Value
NPV	MNOK	14.4
IRR	%	13.1

5 Discussion

The discussion is divided in three parts. The first part handles the topic of throttle design, with a focus on hydraulic design. The second part discusses the economic viability of a throttle, followed by a section that relates the results to application at other hydropower plants.

5.1 Throttle design

The throttle design is an iterative process with multiple steps, and many considerations. The discussion is divided thematically into four parts where the process, assumptions and results are discussed for the model validity, determination of the critical situation, simulations and throttle geometry, separately. An evaluation of uncertainties connected to the design is treated in the last sub-section.

Model Validity

The assessment of the validity of the model is based on the findings of the calibration and validation of the model. As is seen from the surge tank mass oscillations in Figure 3.9 and Figure 3.15 for the calibration and the validation, respectively, the period of mass oscillations in the simulations show very good coherence with the prototype measurements, with deviations fewer than 5 %. This indicates that the relationship between lengths, cross-sectional area of surge tanks and tunnel areas are correct.

The amplitude of the mass oscillations in the calibration and validation simulations shows large deviation when compared to the prototype reference incidents, as seen in Figure 3.9 and Figure 3.15. The deviation from simulation to prototype measurements, of the amplitude at the first local maximum and the first local minimum of the mass oscillation, are found to be 76 % and 154 % for the calibration. The validation shows deviations of 41 % and 154 %. This supports the assumption that accuracy of the results worsen increasingly with time after regulation. The difference of minus 40 MW of regulated power from the calibration to the validation incident gives an indication that the error is increasing with the size of the shutdown, although this cannot be confirmed without comparison of reference incidents shutting down at higher loads. The comparison of the model and the prototype is done under slow power regulation and partially outside of the regulation domain used for simulations. The scaling effect on the transient friction deviation, induced by of faster shutdowns at higher loads, is an uncertainty of a magnitude that has not been possible to estimate with the current prototype measurements.

The reason for the difference in steady state level from simulations to the prototype is unknown, but it is seen that it is close to constant when comparing calibration and validation. This may indicate some sort of systematic error in the data, and the curves are adjusted to fit with the calibration.

It is concluded, in the calibration, that there can be several sources of error, but none that can contribute in a way that leads to errors of the magnitude experienced. The greatest part of the deviation is hence attributed to the unsatisfactory damping of oscillatory friction in the MOC, and thereby LVTrans.

Considering substantial deviations, it is advised against an absolute interpretation of the simulation results when using the numerical model of Tonstad HPP, although the deviations contribute conservatively to the evaluation of the safety of the waterway. Yet, it is believed that the numerical model gives sufficiently accurate results when interpreted relatively.

Critical Situation

The absolute critical situation at Tonstad HPP would be a full shutdown of 960 MW with LRWL in both upstream reservoirs, HRWL in the Sirdalsvann reservoir and no inflow to the creek intakes. This would however not be possible, because the friction loss of the system would be so great that the water level in the surge tanks would be drawn down in the tunnels, even at steady state operation. With this in mind, and the fact that the model is best suited for relative comparisons, another approach was taken. Tonstad has an operational restriction with water table 470 m.a.s.l. in the surge tanks, that is causing limitations resulting in economic losses. Instead of determining a safety restriction based on absolute interpretations of simulation results, the throttle effect is determined based on the relative decrease of amplitude in the surge tank oscillations, with steady state 470 m.a.s.l.

A critical situation for emergency shutdown of Tonstad HPP is found to be with water tables at 482 m.a.s.l in Homstøl and Ousdal, 49.5 m.a.s.l. in Sirdalsvann and with no inflow to the creek intakes. This assessment is made on the basis of Figure 3.16 with the assumption that a power increase of the turbine is controlled by the waterway protection system, and that Ousdal is not at a lower level than Homstøl during operation. These assumptions are considered adequate for the normal situation at Tonstad. One can see that the general trend is that the situation for the drawdown level is improved with an increase of creek intake inflow. This is supported by the theory that, the more inflow in the creek intakes at shutdown, the more resistance is created when water flows back in the waterway. It is also, with the same

reasoning, an explanation to the increase in the first peak in the mass oscillations, because the added water from the creek intake during shutdown increase the momentum.

An important factor that is not included in the simulations is the effect of gate closure, full or partial. If the gate is closed at Homstøl, all the water is taken from Ousdal, resulting in a formidable friction loss that may very fast draw down the steady state level into the sand trap. This also limits the situation where the level at Ousdal is lower than Homstøl, because this would only be the case if the gate is partially or fully closed at Homstøl.

Another critical situation for Tonstad HPP is the overflow of the surge tanks upstream the turbines. Taking into consideration that overflow, to the authors knowledge, has not been a problem, and that a throttle implementation only would better the situation, further investigations are not prioritised.

The critical shutdown time is considered to be 12 seconds, despite the increase due to the installed safety bypass valves. These are neglected firstly because the capacity has not been verified, but also as safety measure, in case of valve malfunction. It is emphasised that the neglecting of safety valves is a highly conservative assumption.

Simulations

The simulations are run based on the boundary conditions and turbine settings found in Table 3.9 from the critical situation analysis, with an emergency shutdown time of 12 seconds.

The simulation procedure is semi-iterative following the flow chart in Figure 3.17. The simulation of the current situation in Figure 4.1 and Figure 4.2 shows what is regarded as an exaggerated response to shutting down at the critical situation, compared to the actual response at Tonstad HPP. The turbine pressure head of the current situation shows a water hammer that is approximately as high as the maximum amplitude of the mass oscillations. The difference between the oldest turbines 1 and 3 is due to the fact that flow through penstock 1 is higher than the flow through penstocks 2, caused by higher effect produced by turbines connected to penstock 1. The water hammer in association with penstock 3 is also affected by the difference in output effect, but is in addition affected by a different geometry of the surge tank. It is highly noticeable, in Figure 4.2, that different flow and geometry cause different head losses in the penstocks, when comparing the steady state levels.

To find the optimal loss factor for the throttle, several simulations with different symmetric loss factors are made. A representative collection of these simulations are found in Table 3.11, together with the resistance coefficient k, related to the shaft area. By examining the

course of the mass oscillations from the different simulations in Figure 4.3, one can clearly see that the lower loss factor, meaning increased loss, the lower is the amplitude of the mass oscillations. It is however apparent, by revision of Figure 4.4, that the simulation 1-1 causes excessive pressures in front of the turbine. It can also be seen that the pulsations within the mass oscillations are dampened faster in the throttled simulations. Simulation 1-1 is a very good example of what happens if the throttle is constructed so small that the desired effect of having a surge tank is cancelled, giving a higher water hammer pressure. Figure 4.5 better shows the immediate response to shutdown, where the difference in water hammer is clear. The first peak of the curve is at approximately the same height for all simulations, except for simulation 1-1, and the part following the first deflection is raised with higher losses. The optimal loss is usually considered to be when the maximum water hammer is equal to the peak of the mass oscillations, but it is in the case of Tonstad HPP considered to be the pressure of the first peak. With these considerations in mind, the optimal symmetrical loss factor of Tonstad HPP is found to be $C_v = 25$.

The determination of an asymmetric loss factor is done solely by maximizing the loss ratio of the geometry, restricted by the surge shaft. The results of the loss factor calculation, in Table 4.4, yields that the lowest loss factor available for downwards flow was found to be $C_{vm} = 17$, assuming a conical throttle with a protruding pipe, restricted by the geometry of the surge shaft. This leads to a loss ratio of 1:1.5 from upwards to downwards flow. The mass oscillations of the simulation of shutdown with asymmetric loss factors, in Figure 4.6, show that the asymmetry will have no effect on the first maximum, compared to simulation 25-25, but shows an improvement on the first minimum by about 2.5 meters. As can be seen from Figure 4.7 and Figure 4.8, there are no obvious change in water hammer pressure. Table 4.1 lists the difference in first local minimum water level for the symmetric and asymmetric simulation, compared to the simulation of current situation, showing that the symmetric and asymmetric throttle will reduce the global minimum of 7.1 meters and 9.6 meters, respectively. This is an indication that there is a possibility to move the water level restriction in the surge chamber, if a throttle is installed. The safety restriction is currently in the surge shaft 470 m.a.s.l., and an estimate of lowering the level by eight meters, to 462 m.a.s.l., is made. This is because it is the level at which the lower chamber of surge tank 3 starts.

A simulation of a situation where the surge tanks restricted steady state water level is moved to 462 m.a.s.l. is performed. The results, in Figure 4.11, support the safety of such a decision, because the local minimum of the surge tank oscillation is not lower than the local minimum

of the simulation with steady state level at 470 m.a.s.l. There is however experienced increased pressures in front of the turbine. This is thought to be a result of optimization of the throttle at a situation in which the flow is not maximal. The pressure increase, in front of the turbine, compared to the current situation is found to be 4 %. A brief investigation of a full shutdown, from 960 MW with $Q_{Creek} = 80\, m^3/s$, shows an increase of 5 % of maximum pressure in front of the turbines when compared to a similar simulations with no throttle. This indicates that it is still possible to optimise the loss factor, with regards to the maximum pressure in front of the turbines. A preferred procedure for finding a throttle with no excess pressure in front of the turbine would be to first check the maximum pressure tolerated, and then check the improvement on the mass oscillations. The result of an optimisation to fit a throttle with no excess pressure would be a slightly higher loss factor, and a slightly bigger throttle, leading to a little lower level of the first local minimum of the mass oscillation. The conservative assumption to exclude bypass valves, does however suggest that the pressure increase would be less in the real system. A conclusion is hence drawn, that a pressure increase of 5 % is tolerated, when assessing the throttle effect, supported by the fact that a more accurate optimization process of the throttle is recommended before a final decision is made.

Throttle Geometry

The throttle geometry is found based on the assumption that the loss factor for upwards flow is $C_{vp} = 25$ for all surge tanks. The geometry is decided by the use of superposition of tabular values from Idelchik (1986), described in section 3.6.6 for the configuration found in Figure 3.18. Due to the limitations for the largest throttle diameter, enforced by shaft geometry, the most important factor for the throttle loss has been found to be the inlet diameter. The geometry is found by trial and error, firstly by changing the configuration of the upwards loss to fit $C_{vp} = 25$, and then by maximizing the loss of downwards flow. This is mainly done by contribution of a pipe extension as the inlet of downwards flow. There is not used a tabular value for a scheme exactly similar to the proposed configuration of the throttle, because none is found and the superposition is therefore approximate.

As is seen from Table 4.2, the main contributor to the loss is the sudden expansion after the smooth contraction of the cross-section. This is a calculation that portraits a situation in very close resemblance to the actual, and the total calculation is therefore considered sufficiently accurate. The composition of downwards flow, in Table 4.3, identify the case of inlet through a pipe protruding from a wall and the smooth expansion of the cross section as the dominant

contributions to the head loss. These represent a higher degree of uncertainty to the calculated resistance coefficients, because the geometry of the cases for tabular values, show slight deviations from the planned throttle geometry. The conclusion drawn based on this is that the resistance coefficient for upwards flow is more accurate than the coefficient for downwards flows. The resistance coefficients, found in Table 4.4, are considered to have reasonable validity for the purpose of estimation. However, it is recommended that accurate resistance coefficients are optimized by experiment, or a combination of CFD and experiment, so called hybrid modelling, for a detailed design of the throttle. This method may also be used to verify the hydraulic functionality of the throttle.

Uncertainties of the Throttle Design

A qualitative evaluation of the most important uncertainties is summed up in Table 5.1. The evaluation of each uncertainty is made, with regards to magnitude and effect on the results.

Table 5.1: Evaluation of uncertainties of the throttle design process

Uncertainty	Evaluation
Deviations of the amplitude of mass oscillations from simulation to prototype measurements	The deviation, mostly attributed to unsatisfactory description of transient friction, is considered to be conservative, when results are interpreted absolutely. Because the simulations show that the minimum level of the surge tank mass oscillations are not reached absolutely, it is confidently considered to have a conservative outcome.
Calibration outside the simulation domain	The calibration outside the simulation domain is a problem, because the deviation from prototype cannot be quantified with precision. This effect is, however, limited because all throttle optimisation simulations are carried out with the same flow, and should therefore have the same magnitude of error. The faster damping of the system for a greater throttling does slightly increase uncertainty of transient friction. This uncertainty cannot be assumed to have a conservative outcome, without further analysis.
Creek inflow	The effect of inflow to the creek intakes is an uncertainty that has a great effect on the simulation results if deviation from measurement is high. The inflow is calculated, with what is perceived as sufficient quality. The deviation in creek inflow may affect the accuracy of the error estimate from calibration, but does not affect simulation results, as the most conservative value for creek inflow is chosen for all simulations.

Exclusion of bypass valves	The exclusion of the bypass valves leaves a high uncertainty. The effect of this uncertainty is very conservative with regards to the safety of the mass oscillations, although it may increase the estimated effect of the throttle, because more flow through the throttle will cause higher losses.
Pressure increase	The pressure increase, when lowering the restriction to 462 m.a.s.l. impose little uncertainty to the results, as the increase is considered sufficiently small.
Exclusion of gate operation	The operation of gates highly affect the hydraulic response. The simulations are performed with open gates, and are therefore only valid for this situation.
Geometry calculations	The calculations of throttle geometry include some uncertainty of the resistance coefficient in the downwards direction. This mainly because it is not optimised to fit a given resistance coefficient, but to give as high coefficient as possible. The geometry is possible to further optimise for a higher downwards loss, but it is believed that the main loss contributors are included. This uncertainty leaves simulations conservative.

A general evaluation of the total uncertainty of the results, based on the combination of components of Table 5.1, yields that the simulation results have a degree of uncertainty, some of which may be eliminated by further investigations. However, the total assessment of these uncertainties give grounds to deem the result conservative towards the safety of the minimum level mass oscillations in the surge tank, provided that all gates are fully open in the system. There is a higher uncertainty of the actual throttle effect, but a decreased restriction in the surge tank to 462 m.a.s.l., is considered to be safe with the optimised throttle.

The uncertainty of the model with respects to optimisation, caused by exclusion of bypass valves and gate operation, is high and may affect the optimisation of the throttle as well as the profitability. It is therefore, for further investigations, recommended to include these variables in the simulations.

5.2 Economic Viability

A brief assessment of the economic viability is made, to convey the throttle effect to an economic context. It is emphasised that all the economic considerations made are rough and for the most part based on experience founded estimates, resulting in very high uncertainty connected to results.

The total discounted cost of the restricted operation of 33.3 MNOK, found in Table 4.6, shows that there is a great potential for economic profit by lowering the safety restriction water level in the surge tank. The increased income is not due to the increase of water inflow, but as a result of more flexible operation, making it very dependent on future market development. Because expected future market situation of (Statnett SF, 2014) is an increasing demand for flexible power, it is possible that the throttling of the surge tanks would be profitable. If, philosophically, the electricity price would be a flat tariff, then the throttle would be worthless.

The estimate of the cost of one throttle is found to be 4 MNOK. It is important to emphasise that this is a minimum of the cost that needs to be expected for the throttle construction. This may double depending on local conditions and availability of qualified contractors. The cost of production halt and emptying of the waterway is also a very uncertain factor, which is extremely dependent on the runoff and market situation during the construction period. The investment criteria in Table 4.7 show, given that all assumptions hold, that the implementation of throttles is profitable with a good margin, with a NVP of 14.4 MNOK and an IRR of 13.1 %. One can see from this that the throttle cost could be doubled and still be considered profitable, according to the NVP and IRR model, using the assumption of 40 years lifetime and 7 % discount rate.

Although the rough estimations show an economic profitability for the installation of surge tank throttles at Tonstad HPP, there is one major uncertainty with this. The authors work with the numerical model of Tonstad HPP, has shown that the current safety restriction of water level in the surge tank is decidedly conservative in many situations. It is observed that the inflow from the creek intakes, reservoir water levels and gate operation highly affect the mass oscillations of the system. This has led to the perception that the absolute restriction of water level is an uneconomic and unnecessary method of ensuring the safety. This is also backed by the conclusion of a report describing guidelines for operational limitation with different gate openings at the reservoirs (Ellefsrød, 2001). It is therefore highly recommended that investigation of critical situations with different reservoir levels, runoff situations and gate settings is performed, with the goal of making an operation scheme dependent on these factors. Such a scheme would determine when the restriction level can be broken, resulting in higher flexibility, while the safety of the waterway is ensured. The implementation of an operational scheme may have a drastic impact on the profitability of the installation of surge

tank throttles. This is because with a more optimal base case, the earnings would be less than if compared to the current situation.

5.3 General Considerations

The evaluation of a surge tank throttle at Tonstad HPP shows that throttle implementation may have a great economic benefit, by giving more flexibility to the operation. As the energy markets in Norway is gradually changing, with the expectation of more peaking operation and more reserve capacity needed, more stability may be required for existing power plants. The ability of adaptation to a changing electricity market may turn out to be an important factor for the profitability of an upgrading and rehabilitation project. It is estimated by Norges vassdrags- og energidirektorat (2015), that the total theoretical potential for upgrading and rehabilitation projects in Norway is 15 TWh, whereof only two TWh is interesting, with the present market situation.

The implementation of a throttle can definitively enhance a high head hydraulic systems response to regulation, dependent on the scheme in question, as exemplified with the case of Tonstad HPP. This renders a possibility for an existing regulation power plant to more efficiently exploit the water in the reservoir, for more profitable operation, and at the same time possibly offer improved grid stability.

The use of complex throttles should be a prioritised activity when designing a new high head hydropower plants surge tanks. An optimal throttle will reduce the required size of a surge tank, and thereby cost, compared to a solution with no throttle. The development in computational power has enabled the use hybrid modelling, combining one-dimensional and CFD modelling with physical models, for smoother and faster optimizations of surge tanks and throttles.

6 Conclusion

In this thesis a study on the effect of surge tank throttling has been made, by utilization of the one-dimensional computer program LVTrans to design and simulate the effect of the installation of a throttle in the surge tanks of Tonstad HPP. It is established that the design of an optimal surge tank throttle can be used to induce a favourable singular loss that will contribute to the dampening of transient behaviour, without severely increasing pressure on the penstock.

The numerical model of Tonstad HPP is currently running on site, and shows good results as a superset regulator. There is however, by calibration and validation, found large deviation from the amplitude of mass oscillations when comparing with plant measurements of shutdown incidents. These deviations are attributed to the insufficient representation of the frequency-dependent friction, during transient behaviour, in the MOC. Although being highly conservative, the model is not recommended for absolute interpretation, but is considered sufficiently accurate for relative applications, when a conservative approach is taken.

The simulations are performed for the worst case scenario of the normal situation, excluding gate closure at Homstøl and Ousdal, and thereby water levels where Ousdal is lower than Homstøl. Interpretations are made relatively by comparing simulation of the current situation with simulations using different throttle losses, provided a steady state water level in the surge tank at the imposed safety restriction at 470 m.a.s.l. The results of simulations show that an optimised asymmetric throttle with loss ratio 1:1.5, from upwards to downwards flow, will result in an increase of the minimum level of the surge tanks mass oscillation by 9.6 meters, without increasing penstock pressure. Simulation with a decrease in safety restriction level in the surge tank of 8 meters confirms functionality, of an installed throttle.

The evaluation of uncertainties of the throttle design shows that there are sources of error that substantially contributes to the uncertainty of the throttle effect, but that the sum of all conservative assumptions leaves reasonable ground to move the restricted water level to 462 m.a.s.l.

The current water level restriction, in the surge tanks at Tonstad HPP, results in an economic loss roughly estimated to 2.5 million NOK a year, when compared to a restriction level of 462 m.a.s.l. It is estimated that the profitable installation of surge tank throttles can carry a cost of approximately 33 million NOK. An estimation of throttle minimum expected costs, shows that the installation of surge tank throttles is profitable with the assumptions made.

The analysis of the effect of surge tank throttling at Tonstad HPP, exemplifies the benefits that may be achieved by detailed throttle design. The throttling of existing hydropower plants may give more flexibility to meet an electricity market, where peaking operation is becoming more important. Throttle design for new hydropower plants should be considered as it may be a considerable cost saver.

Recommendations for Future Work

The author has, in his work with numerical model of Tonstad HPP, discovered that the absolute restriction of the level in the surge tanks is very conservative. The inflow from the creek intakes, the levels in the reservoir and gate operation highly affect the behaviour of the hydraulic system. It is therefore recommended to do a total mapping of under which circumstances the restriction may be broken, before considering installation of a surge tank throttle. An operational scheme from such a mapping is expected to improve operational flexibility, thus reducing the profitability of a throttle.

There were, during calibration and validation, found unexpected values for the water level at Sirdalsvann. It is therefore suggested to verify recent logged values from the superset regulator against known levels, to uncover possible errors.

As the inflow to the creek intakes has a great significance on the dampening of transients, it is recommended to install instrumentation to log the flow from each intake. It is then possible to further improve the model, eliminate uncertainties with regards to creek intake flow and enhance the monitoring of an operational scheme.

For detailed design of a throttle it is recommended to further optimize and verify the hydraulic functionality by hybrid modelling, using a combination of CFD, one-dimensional and physical modelling. The inclusion of gate operation and effect of bypass valves is endorsed in such an analysis. It is also suggested to save the superset regulator log if a large shutdown should occur, so the deviations from model to prototype can be better estimated. The improvement of the production analysis, throttle cost calculation and estimate of costs of lost production is recommended to more accurately portrait the economic viability of throttle installation.

References

BREKKE, H. 1984. *A stability study on hydro power plant governing including the influence from a quasi nonlinear damping of oscillatory flow and from the turbine characteristics.* Dr.Techn. thesis, Norges Tekniske Høgskole.

BØE, A. E., FODSTAD, L. A. & UNDHEIM, M. 2013. *Diamantar varer evig,* Tonstad, Sira-Kvina Kraftselskap.

CROWE, C. T., ELGER, D. F., WILLIAMS, B. C. & ROBERTSON, J. A. 2009. *Engineering fluid mechanics,* Hoboken, N.J., Wiley.

ELLEFSRØD, T. 2001. Vannveisdynamikk, Rettledning for drift ved strupning i inntak Homstølvann. Larvik: Norconsult.

FEATHERSTONE, R. E., NARULLI, C. & MARRIOTT, M. 2009. *Civil Engineering Hydraulics,* Chichester, Wiley-Blackwell.

GABL, R., ACHLEITNER, S., NEUNER, J., GÖTSCH, H. & AUFLEGER, M. 2011. 3D-numerical optimisation of an asymmetric orifice in the surge tank of a high-head power plant. *34th IAHR World Congress.* Brisbane, Australia.

GOMSRUD, D. 2014. Numerical Simulation of Surge Tank Throttle. Tonstad Hydropower Plant. Trondheim: Norwegian University of Science and Technology.

IDELCHIK, I. E. 1960. *Handbook of Hydraulic Resistance: Coefficients of Local Resistance and of Friction,* National Technical Information Service.

IDELCHIK, I. E. 1986. *Handbook of hydraulic resistance,* Washington, Hemisphere Publ.

INDUSTRIDEPARTEMENTET 1963. Tillatelse for Sira-Kvina Kraftselskap til å foreta reguleringer og overføringer i Sira- og Kvinavassdragene.

INTERNATIONAL ENERGY AGENCY 2014. World energy outlook 2014. Paris: OECD.

LONGVA, P. & TVERSTØL, A. 2014. Rundskriv R-109/14, Prinsipper og krav ved utarbeidelse av samfunnsøkonomiske analyser mv.: Det kongelige finansdepartement,.

NABI, G., HABIB-UR-REHMAN, KASHIF, M. & TARIQ, M. 2011. Hydraulic Transient Analysis of Surge Tanks: Case Study of Satpara and Golen Gol Hydropower Projects in Pakistan. *Journal of Engineering & Applied Science,* Vol. 8.

NATIONAL INSTRUMENTS 2014. LabVIEW™ 2014. Version 14.0f1 ed.

NIELSEN, T. K. 1990. Dynamisk dimensjonering av vannkraftverk. Trondheim: SINTEF.

NORGES VASSDRAGS- OG ENERGIDIREKTORAT. 2015. *Opprustning og uvidelse* [Online]. Available: http://www.nve.no/no/Energi1/Fornybar-energi/Vannkraft/Opprusting-og-utvidelse/ [Accessed 29th May 2015].

OLJE- OG ENERGIDEPARTEMENTET 1990. Lov om produksjon, omforming, omsetning, fordeling og bruk av energi m.m. (energiloven).

PINDYCK, R. S. & RUBINFELD, D. L. 2005. *Microeconomics,* Upper Saddle River, N.J., Pearson Prentice Hall.

RICHTER, W. 2015. Sketch of throttle at Obervermuntverk II. Unpublished.

RICHTER, W., DOBLER, W. & KNOBLAUCH, H. 2012. Hydraulic and Numerical Modelling of an Asymetric Orifice Within a Surge Tank. *4th IAHR International Symposium on Hydralic Structures.* Porto, Portugal.

RICHTER, W., ZENZ, G., SCHNEIDER, J. & KNOBLAUCH, H. 2015. Surge tanks for high head hydropower plants - Hydraulic layout - New developments. *Geomechanics and Tunnelling,* Vol. 8.

SHORT, W., PACKEY, D. J. & HOLT, T. 1995. A Manual for the Economic Evaluation of Energy Efficiency and Renewable Energy Technologies. Golden, Colorado: National Renewable Energy Laboratory.

SIRA-KVINA KRAFTSELSKAP 2008. Magasin/Avløp Sira Kvina, Systemskisse for flomberegniger.

SIRA-KVINA KRAFTSELSKAP. 2014. *Tonstad* [Online]. Available: http://www.sirakvina.no/Prosjekter-og-anlegg/Kraftstasjoner/Tonstad/ [Accessed 25th January 2015].

SIRA-KVINA KRAFTSELSKAP. 2015. *Kort om Sira-Kvina* [Online]. Available: http://www.sirakvina.no/Om-Sira-Kvina/Kort-om-Sira-Kvina/ [Accessed 29th April 2015].

STATISTICS NORWAY 2015. Construction cost index for road construction, table 08662. 24th April ed.: Statistics Norway.

STATNETT SF. 2013a. *Sekundærreserver (FRR-A)* [Online]. Available: http://www.statnett.no/Drift-og-marked/Markedsinformasjon/sekundarreserver/ [Accessed 18th March 2015].

STATNETT SF. 2013b. *Tertiærreserver (FRR-M)* [Online]. Available: http://www.statnett.no/Drift-og-marked/Markedsinformasjon/RKOM1/ [Accessed 28th May 2015].

STATNETT SF. 2014. Systemdrifts- og markedsutviklingsplan 2014-20.

STEYRER, P. 1999. Economic Surge Tank Design by Sophisticated Hydraulic Throttling. *28th IAHR Congress.* Graz, Austria.

SVINGEN, B. 2003. Dokumentasjon for LVTrans (LabView Transient Pipe Analysis). SINTEF Energiforskning AS.

SVINGEN, B. 2007. Manual LVTrans for versjon 8_1.2.4. SINTEF.

SVINGEN, B. 2015. Overordnet regulator og vannvegsvern i Tonstad kraftverk. *Produksjonsteknisk konferanse.* Trondheim.

SWECO NORGE AS 2010. Kostnadsgrunnlag for vannkraftanlegg. Oslo: Norges vassdrags- og energidirektorat.

VEREIDE, K., RICHTER, W., ZENZ, G. & LIA, L. 2015. Surge Tank Research in Austria and Norway. *WasserWirtschaft Extra*, 1**,** 58-62.

WYLIE, E. B. & STREETER, V. L. 1993. *Fluid transients in systems,* Englewood Cliffs, NJ, Prentice Hall.

Appendix A

References for Relevant Construction Drawings

A.1 Waterway Drawings

Name	Number	Year
Tonstad Kraftverk Tilløpstunel Homstøl - Tonstad	2717	Unknown
Tonstad Kraftverk, Utvidelse Trykksjakt Stikning, spregning	KT2.323.001.B06014	1984
Tonstad Kraftverk, Utvidelse Hovedstikningsplan Oversikt, lengdesnitt	KT2.321.000.B06018	1985
Tonstad Kraftverk Vannveier m/ plan	KT1.321.001.B08093	1997

A.2 Surge Tanks 1 and 2 Drawings

Name	Number	Year
Tonstad Kraftverk Fordelingsbasseng og inntak trykksjakter Plan og snitt	KT1.323.001.B00325	1965
Tonstad Kraftverk Stigesjakter og utjevningsbasseng Sprengningsplan	KT1.841.001.B00345	1965
Tonstad Kraftverk Øvre fordelingsbasseng Dekke over stigesjakter. Forskaling	KT1.322.000.B00656	1966
Tonstad Kraftverk Øvre fordelingsbasseng Fjellbolter i stigesjakt, innstøping av føringer for lukeopptrekk	KT1.322.000.B00658	1966
Tonstad Kraftverk Øvre fordelingsbasseng m/ trykksjakter Oversikt	KT1.322.001.B00699	1967

A.3 Surge Tank 3 Drawings

Name	Number	Year
Tonstad Kraftverk, Utvidelse Tverrslag Toppen Stikning, spregning	KT2.321.015.B06019	1985
Tonstad Kraftverk, Utvidelse Tilløpstunnel nedre svingekammer stinking, sprengning	KT2.322.000.B06023	1985
Tonstad Kraftverk, Utvidelse Inntaksluke Arrangement, spregning	KT2.322.001.B06034	1985
Tonstad Kraftverk, Utvidelse Inntaksluke lukekammer Forskaling	KT2.322.000.B06101	1986
Tonstad Kraftverk, Utvidelse Tilløpstunnel Øvre svingkammer m/ lukekammer Stikning, Sprengning	KT2.322.001.B06050	1986

Appendix B

Construction Details

B.1 Vertical elevation of surge tank 1 and 2

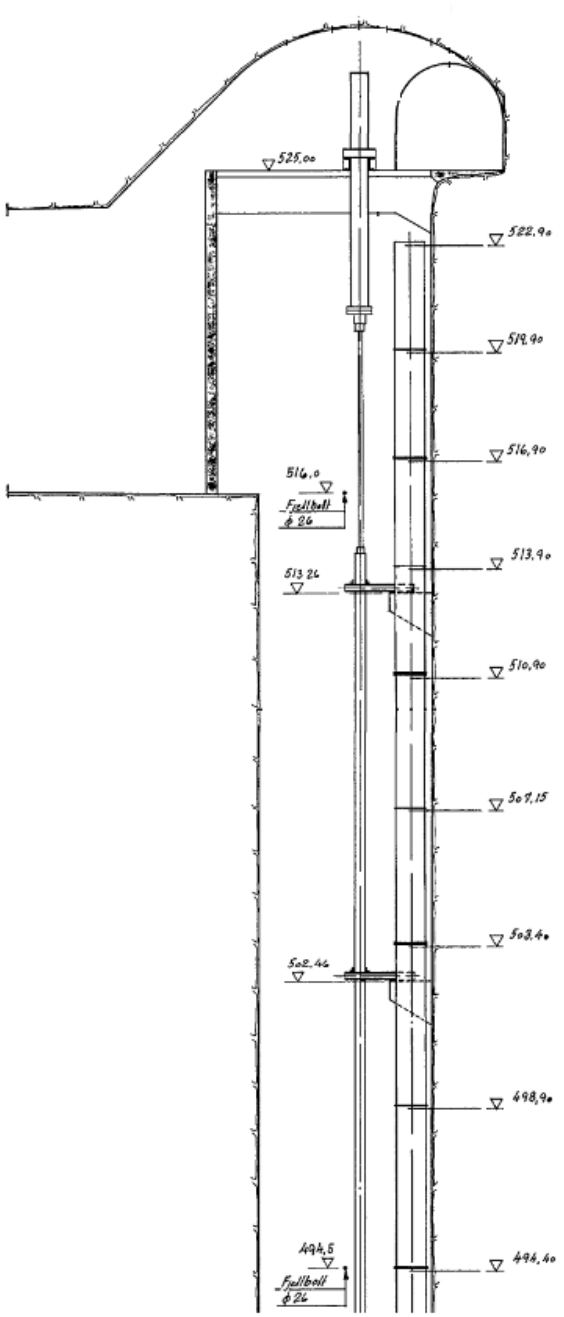

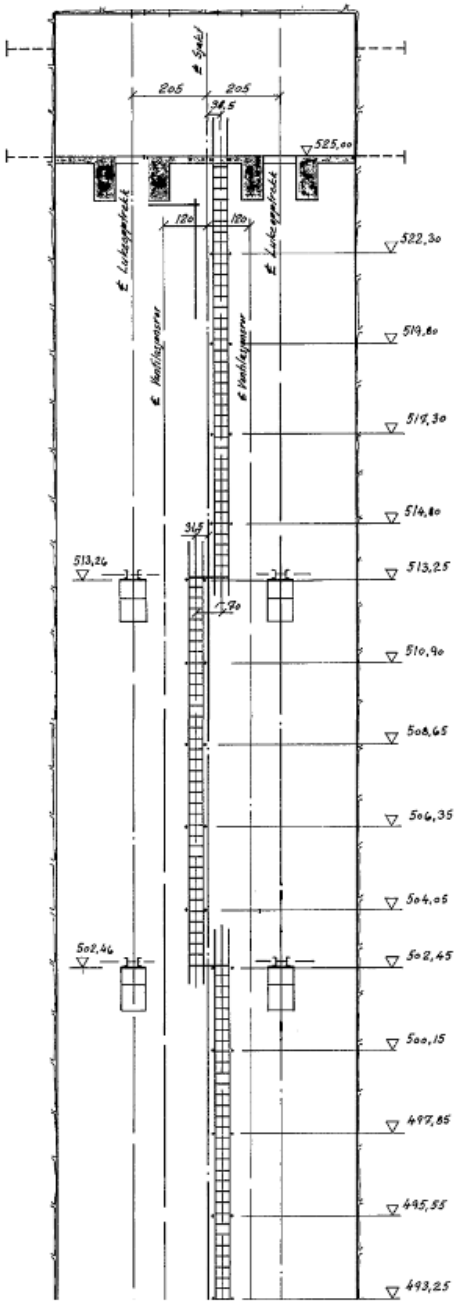

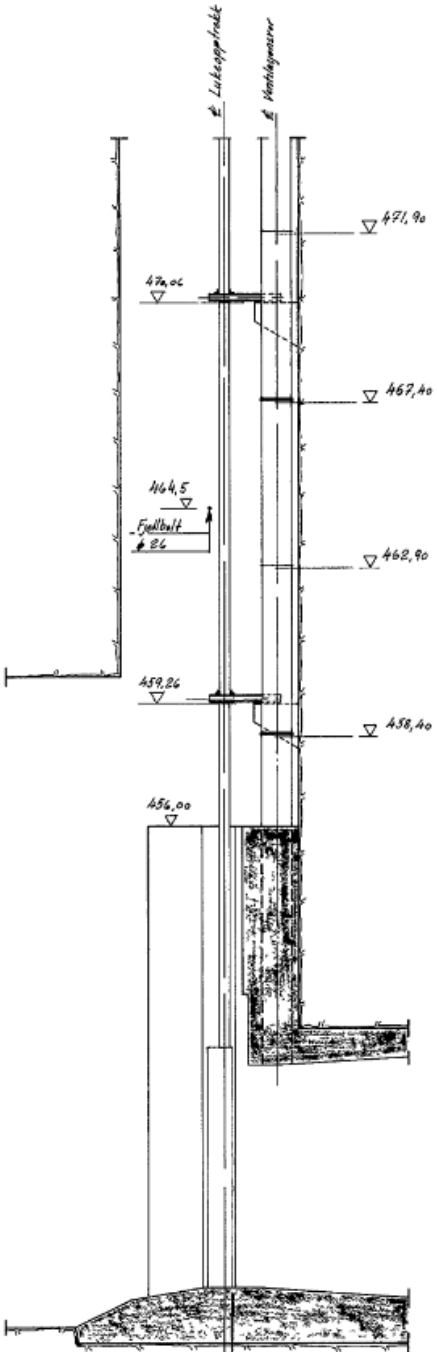
Luftspjutrör
Vattenmanometer
471,90
470,05
467,40
464,5
Fjädbult
ø 26
462,90
459,26
458,40
456,00

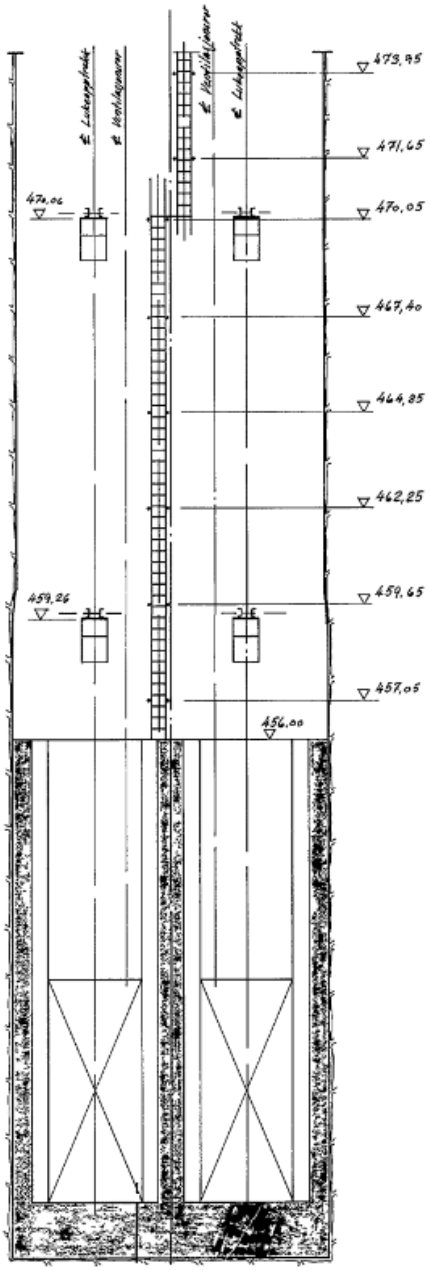
Luftspjutrör
Vattenmanometer
Vattenmanometer
Luftspjutrör
473,95
471,65
470,05
470,05
467,40
464,85
462,25
459,65
459,26
457,05
456,00

B.2 Construction Details Sand Trap

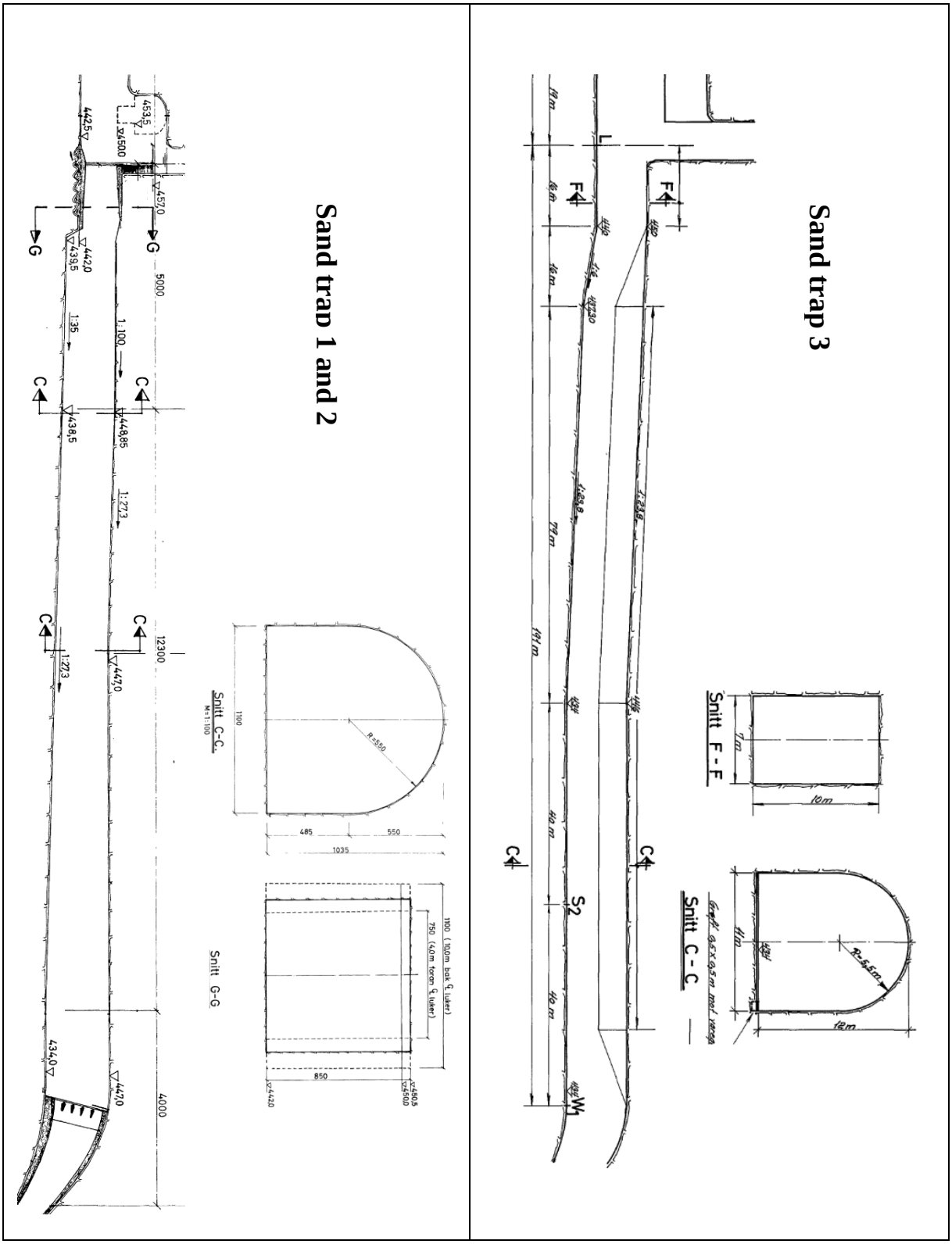

Appendix C

LVTrans Input Parameters

C.1 Input Parameters for Variable Surge Tank in LVTrans

Parameter	Unit	SST12 & SST34	SST5
H0	m	30.0	30
B-with	m	10	10
C-cnst	m	1.8	1.8
L-weir	m	100	1100
L0	m	9.50	7.50
L1	m	11.00	10.00
L2	m	14.50	16.50
L3	m	17.50	19.50
L4	m	52.00	73.60
L5	m	52.05	74.30
L6	m	56.10	75.00
L7	m	56.15	76.00
L8	m	73.50	77.00
L9	m	74.30	78.00
A0	m	2000.0	2000.0
A1	m	285.0	505.0
A2	m	285.0	505.0
A3	m	35.0	37.5
A4	m	35.0	37.5
A5	m	75.0	1270.0
A6	m	75.0	1270.0
A7	m	35.0	1270.0
A8	m	35.0	1270.0
A9	m	595.0	1270.0

C.2 Input Parameters for Turbines in LVTrans

Parameter	Unit	Turbin 1-4	Turbin 5
Qr	m^3/s	42.5	80.0
Hr	m	430.0	430.0
Hr_design	m	430.0	430.0
Nr	rpm	375	300
Tr	Nm	4295729.0	1010759.0
Er	Nm	4295729.0	1010759.0
a1r(deg)	^{o}	10.9	13.1
b1r(deg)	^{o}	49.5	54.7
r1	m	1.8253	2.2817
r2	m	1.0186	1.27332
Ta	s	6.0	6.94
Twt	s	0.1	0.1
Rq	-	0.00	0.00
Rm	-	0.03	0.03
Rd	-	0.04	0.04
eta_h	-	0.96	0.96
eta_r	-	0.94	0.94
Nturb	-	1.0	1.0
Poles	-	16	20
D_grid	-	0.0	0.0
delta_r	rad	0.785	0.785
F_grid	Hz	50.0	50.0
eve_mod	-	0.2	0.2

C.3 Input parameters for PID regulators in LVTrans

Parameter	Unit	Turbin 1-4	Turbin 5
Pr	MW	168,693	317.54
Nr	rpm	375	300
SP_Power	MW	160	320
PID P_n_grid	-	2.0	1.0
PID Ti_n_grid	-	4.0	10.0
PID Td_n_grid	-	0.0	0.0
PID P_n_island	-	1.0	1.0
PID Ti_n_island	-	5.0	10.0
PID Td_n_island	-	0.0	0.0
Ti_power	s	5.0	5.0
T_ramp	s	153.85	200
Rp_droop	-	0.06	0.06
T_close_hi	s	12.0	12.0
T_close_low	s	12.0	12.0
T_open_hi	s	12.0	12.0
T_open_low	s	12.0	12.0
kap_change	-	0.5	0.5
a	-	0.0	0.0
b	-	1.0	1.0
c	-	0.0	0.0

Appendix D

Source Code for the Altered Variable Surge Tank Element

```
float64 Cv, L0, A, A0, dA, Am, dL, Ba, Ca, Sb, Sc, dF, F, Ha, Q0;
float64 g = 9.82;
float64 eps = 0.00001;
int32 N = 0;
Sc = Cp1/Bp1 + Cm2/Bm2;
Sb = 1.0/Bp1 + 1.0/Bm2;
Ca = Sc/Sb;
Ba = 1.0/Sb;

Q0 = Q;
L0 = L;
L = 2.0*L - L00;

//  Finner A(L0)
if (L0 <= L_h[0]) A0 = A_h[0];
else if ((L0 >= L_h[0]) && (L0 < L_h[1])) A0 = dA_h[1]*(L0 - L_h[0])
+ A_h[0];
else if ((L0 >= L_h[1]) && (L0 < L_h[2])) A0 = dA_h[2]*(L0 - L_h[1])
+ A_h[1];
else if ((L0 >= L_h[2]) && (L0 < L_h[3])) A0 = dA_h[3]*(L0 - L_h[2])
+ A_h[2];
else if ((L0 >= L_h[3]) && (L0 < L_h[4])) A0 = dA_h[4]*(L0 - L_h[3])
+ A_h[3];
else if ((L0 >= L_h[4]) && (L0 < L_h[5])) A0 = dA_h[5]*(L0 - L_h[4])
+ A_h[4];
else if ((L0 >= L_h[5]) && (L0 < L_h[6])) A0 = dA_h[6]*(L0 - L_h[5])
+ A_h[5];
else if ((L0 >= L_h[6]) && (L0 < L_h[7])) A0 = dA_h[7]*(L0 - L_h[6])
+ A_h[6];
else if ((L0 >= L_h[7]) && (L0 < L_h[8])) A0 = dA_h[8]*(L0 - L_h[7])
+ A_h[7];
else if ((L0 >= L_h[8]) && (L0 < L_h[9])) A0 = dA_h[9]*(L0 - L_h[8])
+ A_h[8];
else if (L0 >= L_h[9]) A0 = A_h[9];
```

```
do {
   //   Finner  A(L) og dA
   if (L <= L_h[0]) {A = A_h[0]; dA = dA_h[0];}
   else if ((L >= L_h[0]) && (L < L_h[1])) {A = dA_h[1]*(L - L_h[0])
+ A_h[0]; dA = dA_h[1];}
   else if ((L >= L_h[1]) && (L < L_h[2])) {A = dA_h[2]*(L - L_h[1])
+ A_h[1]; dA = dA_h[2];}
   else if ((L >= L_h[2]) && (L < L_h[3])) {A = dA_h[3]*(L - L_h[2])
+ A_h[2]; dA = dA_h[3];}
   else if ((L >= L_h[3]) && (L < L_h[4])) {A = dA_h[4]*(L - L_h[3])
+ A_h[3]; dA = dA_h[4];}
   else if ((L >= L_h[4]) && (L < L_h[5])) {A = dA_h[5]*(L - L_h[4])
+ A_h[4]; dA = dA_h[5];}
   else if ((L >= L_h[5]) && (L < L_h[6])) {A = dA_h[6]*(L - L_h[5])
+ A_h[5]; dA = dA_h[6];}
   else if ((L >= L_h[6]) && (L < L_h[7])) {A = dA_h[7]*(L - L_h[6])
+ A_h[6]; dA = dA_h[7];}
   else if ((L >= L_h[7]) && (L < L_h[8])) {A = dA_h[8]*(L - L_h[7])
+ A_h[7]; dA = dA_h[8];}
   else if ((L >= L_h[8]) && (L < L_h[9])) {A = dA_h[9]*(L - L_h[8])
+ A_h[8]; dA = dA_h[9];}
   else if (L >= L_h[9]) {A = A_h[9]; dA = dA_h[10];}

   // Vanlig sjakt under weir
   if (L <= Lw) {
      Am = (dA*(L - L0) + A + A0)/dt;
      Q = (A + A0)*(L - L0)/dt - Q0;
   if ( Lw > 1000) {
      if (Q < 0.0)
     { if (L<26.5) Cv = 8900; else Cv = Cvm;}
     else {if (L<26.5) Cv = 8900; else Cv = Cvp;}
      F = L + Z0 + Q*abs(Q)/(2.0*Cv) - Ca + Ba*Q;
      dF = 1.0 + Am*(Ba + abs(Q)/Cv);}
else {
 if (Q < 0.0)
     { if (L<20.5) Cv = 8900; else Cv = Cvm;}
     else {if (L<20.5) Cv = 8900; else Cv = Cvp;}
      F = L + Z0 + Q*abs(Q)/(2.0*Cv) - Ca + Ba*Q;
      dF = 1.0 + Am*(Ba + abs(Q)/Cv);}
   };

   // Weir at Lw
```

```
   if (L > Lw) {
      Am = 1.5*B_w*C_w*sqrt(L - Lw) +  (dA*(L - L0) + A + A0)/dt;
      if (L0 >= Lw)
         Q = B_w*C_w*pow((L - Lw),1.5) + B_w*C_w*pow((L0 - Lw),1.5)
+ (A + A0)*(L - L0)/dt - Q0;
         else Q = B_w*C_w*pow((L - Lw),1.5) + B_w*C_w*pow(0.0,1.5) +
(A + A0)*(L - L0)/dt - Q0;
      if (Q < 0.0) Cv = Cvm; else Cv = Cvp;
      F = L + Z0 + Q*abs(Q)/(2.0*Cv) - Ca + Ba*Q;
      dF = 1.0 + Am*(Ba + abs(Q)/Cv);
   };

   dL = -F/dF;
   L = L + dL;
   N++;
}
while (abs(dL) > eps && N < 100);

//   Finner  A(L) og dA
   if (L <= L_h[0]) A = A_h[0];
   else if ((L >= L_h[0]) && (L < L_h[1])) A = dA_h[1]*(L - L_h[0])
+ A_h[0];
   else if ((L >= L_h[1]) && (L < L_h[2])) A = dA_h[2]*(L - L_h[1])
+ A_h[1];
   else if ((L >= L_h[2]) && (L < L_h[3])) A = dA_h[3]*(L - L_h[2])
+ A_h[2];
   else if ((L >= L_h[3]) && (L < L_h[4])) A = dA_h[4]*(L - L_h[3])
+ A_h[3];
   else if ((L >= L_h[4]) && (L < L_h[5])) A = dA_h[5]*(L - L_h[4])
+ A_h[4];
   else if ((L >= L_h[5]) && (L < L_h[6])) A = dA_h[6]*(L - L_h[5])
+ A_h[5];
   else if ((L >= L_h[6]) && (L < L_h[7])) A = dA_h[7]*(L - L_h[6])
+ A_h[6];
   else if ((L >= L_h[7]) && (L < L_h[8])) A = dA_h[8]*(L - L_h[7])
+ A_h[7];
   else if ((L >= L_h[8]) && (L < L_h[9])) A = dA_h[9]*(L - L_h[8])
+ A_h[8];
   else if (L >= L_h[9]) A = A_h[9];

if (L <= Lw) {
   Q = (A + A0)*(L - L0)/dt - Q0;
if (Lw > 1000) {
```

```
   if (Q < 0.0)
     { if (L<26.5) Cv = 8900; else Cv = Cvm;}
     else {if (L<26.5) Cv = 8900; else Cv = Cvp;}
   Q_over = 0.0;}
else {
if (Q < 0.0)
     { if (L<20.5) Cv = 8900; else Cv = Cvm;}
     else {if (L<20.5) Cv = 8900; else Cv = Cvp;}
   Q_over = 0.0;} }

if (L > Lw) {
    if (L0 >= Lw)
       Q = B_w*C_w*pow((L - Lw),1.5) + B_w*C_w*pow((L0 - Lw),1.5) +
(A + A0)*(L - L0)/dt - Q0;
       else Q = B_w*C_w*pow((L - Lw),1.5) + B_w*C_w*pow(0.0,1.5) +
(A + A0)*(L - L0)/dt - Q0;
   if (Q < 0.0) Cv = Cvm; else Cv = Cvp;
   Q_over = B_w*C_w*pow((L-Lw), 1.5);}

Hb = Z0 + L;
Ha = Hb + Q*abs(Q)/(2.0*Cv);
HPin = Ha;
HPup = Ha;
HPout = Ha;
QPin =  (Cp1 - Ha)/Bp1;
QPout = (-Cm2 + Ha)/Bm2;
QPup = Q;
LP = L;
```

Appendix E

Throttle Cost Calculation

	COST ESTIMATE FOR THROTTLE					
	Description	Unit	Unit cost (1000 NOK/unit)	Number of units	Cost (1000 NOK)	Comment
1	Throttle					
1.1	Steel cone	m	90	2.25	203	Fig. M.6.c, H=300 m, D=3500 mm
1.2	Addition, geometry	%		50	101	Addition for more complex geometry of cone. % of steel cone
1.3	Steel cone construction	m	330	1.5	495	Fig. B.7.3, H<80 m, A=35 m^2
1.4	Addition very complex formwork	m^2	3	35	105	Addition of Double of the of the assumed formwork cost, for hatch
1.5	Addition difficult concrete situation	m^3	3	52.5	158	Addition of Double the assumed concrete cost for creek intake.
1.6	Additional cost, vertical shaft work	%		50	379	Addition for working in a shaft instead of a tunnel, % of total construction cost
2	**Total Contractor Cost**				**1440**	
3	Additions					
3.1	Design & construction management	%		25	360	
3.2	Project owner costs	%		10	144	
3.3	Unforseen	%		100	1440	
4	Total Cost (2010-NOK)				3384	
5	**Total Cost (2015-NOK)**				**3973**	**Increase 17.4 % from 2010 to 2015**

Appendix F

Correspondence

F.1 Email from Einar Thygesen to Kaspar Vereide 21th May 2015

Daniel Gomsrud

Emne: VS: strupning svingekammer

From: Einar Thygesen [mailto:Einar.Thygesen@sirakvina.no]
Sent: 21. mai 2015 11:44
To: Kaspar Vereide
Cc: Rolv Guddal; Sigurd Netlandsnes
Subject: SV: strupning svingekammer

Hei,

Jeg estimerer etter beste skjønn en årlig gevinst (med effekt økning som beskrevet i tabellen under) på ca 2,5 mill. NOK.
Størrelsen på gevinsten er belemret med svært stor usikkerhet. Den avhenger av fremtidige priser og prisforskjeller (f.eks. dag/ natt og vinter/ sommer), fremtidige tilsig samt hvordan kapasitetsmarkedet for FRR og RK utvikler seg.

Mvh Einar

Fra: Kaspar Vereide [mailto:kaspar.vereide@ntnu.no]
Sendt: 18. mai 2015 15:06
Til: Einar Thygesen
Kopi: Rolv Guddal; Sigurd Netlandsnes; Daniel Gomsrud
Emne: RE: strupning svingekammer

Hei igjen Einar,

Takk for hyggelig telefonsamtale tidligere i dag. Vi har nå beregnet hvor mye ekstra effekt man kan kjøre i Tonstad dersom man kan senke restriksjon på vannstand i svingekammer fra kote 470 til kote 462. Dette er selvsagt avhengig av vannstand i inntaksmagasinene, og vannføring fra bekkeinntak. Under er tabell som viser økt mulig effekt for forskjellige situasjoner. Som du kan se så har strupningen høyest effekt ved lav magasinvannstand, og liten vannføring fra bekkeinntakene:

Magasinvannstand	Vannføring fra bekkeinntak = 0 m3/s	Vannføring fra bekkeinntak = 50m3/s
497	0 MW	0 MW
490	105 MW	10 MW
482	180 MW	174 MW

Håper da du kan gi oss et enkelt estimat på fortjenesten dersom man struper svingekammerne.

Hilsen Kaspar

From: Einar Thygesen [mailto:Einar.Thygesen@sirakvina.no]
Sent: 18. mai 2015 09:40
To: Kaspar Vereide
Cc: Rolv Guddal; Sigurd Netlandsnes
Subject: SV: strupning svingekammer

Hei,

Jeg har tenkt en del på dette siden jeg så e-posten din.

1

Dette er veldig utfordrende å svare på.
Å kunne kjøre ned til 462 har jo som du påpeker en økonomisk gevinst. Men det har ingen praktisk betydning når det er mye vann i inntakene eller mye tilsig til bekkeinntakene, da er det dagens installerte effekt på 960 MW som er begrensningen. Resten av tida vil det gi en økt fleksibilitet til å kunne kjøre hardere enn i dag, men det er jo kjøring på dårlig virkningsgrad.

Det vil så langt jeg kan se være aktuelt å benytte en mulighet til å kjøre ned mot 462 istedenfor 470 i følgende situasjoner:

- Ved høye priser (effektpriser/ overraskende høye priser) vil vi kunne kjøre hardere enn i dag (i tilfeller hvor 470 og ikke 960 MW er begrensningen). Prisene må da være så høye at det forsvarer den dårlige virkningsgraden, det vil si ca 40% eller mer over vannverdi)
- Ved ønske om å tappe inntakene til Tonstad langt ned fort (for å kunne sluke store tilsig som er i vente eller kunne stå på lave priser fram i tid). Da vil kjøring på dårlig virkningsgrad bety lite, for vannverdien vil være veldig lav.
- For å kunne kjøre mer FCR/ FRR i Tonstad enn i dag selv om inntakene er lave/ tilsiget til bekkeinntakene er lavt. (Vi vil da ha muligheten til å svinge ned mot 462 istedenfor 470. Dette vil bare gi kortvarige forverringer av virkningsgraden ved oppregulering.

Å komme med noe tallestimat på hvilken økonomisk gevinst dette vil kunne gi er svært vanskelig. Generelt har denne gevinsten gått ned etter ansettelse av produksjonsplanlegger og hydrolog samt innføring av optimaliseringsprogrammet Shop og installasjon av Overordnet regulator/ Vannvegsvern. Alle disse faktorene har gjort det mulig å utnytte Tonstad kraftstasjon bedre uten å gå under 470 ved hjelp av kontinuerlig overvåking og produksjonsplanlegging.

Men verdien av fleksibilitet er alltid stor.
Jeg ønsker å snu spørsmålsstillingen: Hva koster din installasjon?

Ta gjerne en telefon

Mvh Einar
Mob: 40 00 12 34

Fra: Kaspar Vereide [mailto:kaspar.vereide@ntnu.no]
Sendt: 18. mai 2015 08:08
Til: Einar Thygesen
Kopi: Daniel Gomsrud
Emne: strupning svingekammer

Hei Einar!

Nå er det en stund siden vi hadde en kort prat i gangen på hovedkontoret, angående studie på strupning av svingekammeret på Tonstad kraftverk.
Masterstudent Daniel Gomsrud begynner å få resultater fra studiet sitt, og det ser ut som at en slik strupning har en positiv effekt på svingningene.

Kort fortalt viser studien at man redusere dagens restriksjoner på kjøring av tonstad kraftverk. Dagens restriksjon på laveste vannstand i svingekammeret på 470 kan senkes til 462 (som var restriksjonen fra gammelt av). Dette vil jo ha en økonomisk gevinst, og vi ønsker gjerne å få tall på denne, slik at vi kan gi en vurdering på om tiltaket bør gjennomføres.

Har du mulighet til å gi oss en rask vurdering av en slik økonomisk gevinst? Den trenger ikke være omfattende, men skal brukes til å gi en pekepinn på om strupning bør vurderes videre.
Håper du har mulighet!

Vennlig hilsen,
Kaspar Vereide

****
Civil Engineer and Ph.D. candidate
Department of Hydraulic Engineering and Environmental Science
Norwegian University of Science and Technology (NTNU)
Kaspar.vereide@ntnu.no
+47 926 981 09

F.2 Email from Einar Thygesen to Kaspar Vereide 29th May 2015

Subject **SV: kostnader installering av strupning**

From Einar Thygesen <Einar.Thygesen@sirakvina.no>

To 'Kaspar Vereide' <kaspar.vereide@ntnu.no>

Cc Daniel Gomsrud <danielgo@stud.ntnu.no>, Rolv Guddal <Rolv.Guddal@sirakvina.no>, Sigurd Netlandsnes <Sigurd.Netlandsnes@sirakvina.no>

Date 2015-05-29 15:36

Hei Kaspar, jo takk nå er jeg frisk igjen.

Man er nok litt heldig hvis man helt unngår vanntap med en 25 dagers stans, i snitt må man nok påregne noe vanntap.
Dette kan vi beregne ganske nøyaktig ved å studere tilsigshistorikken nøye.
Blir vanntapene små, er de dominerende kostnadene:

- Kostnad ved å kjøre ned magasinene forut for utetida (man må kjøre på litt dårligere pris og litt dårligere virkningsgrad forut for utetida).
- Pristap under utetida (det er alltid en mulighet for at sommerprisen blir såpass høy at det lønner seg å kjøre litt på god virkningsgrad).
- Tap ved å ikke kunne kjøre systemtjenester i Tonstad (og i begrenset grad i Tjørhom og Solhom).

Havari i Tonstad på 4 uker i uke 29 er tidligere beregnet til å kost 11,7 mill i utetidskostnad (uke 29 er billigst mulige havaritidspunkt).
Da har man ikke anledning til å kjøre ned magasinene ekstraordinært på forhånd. Tap på systemtjenester er imidlertid ikke medregnet.
Best Guess fra min side er ca5-6 mill NOK i utetidskostnader for en planlagt totalstans på Tonstad 4 uker midt på sommeren.

Jeg vet ikke hvilken neddiskonteringsrente som benyttes av eierne våre nå, men antar at du kan legge til grunn 6-7% (dette benyttet eierne våre for noen år tilbake i hvert fall). Levetida for strupe-innretningen kjenner du best selv. Kan du ikke sette 25 år (eksisterende tunnel-systemene til Tonstad lever vel minst 25 år til)?

Dersom du ønsker mer eksakte tall, så kan vi få en av eierne eller Sintef til å regne nøyaktig på dette.
Økonomiavdelingen eller eierne våre kan eventuelt gi mer nøyaktige tall på diskonteringsrente og antall år som benyttes for nedskrivning.

Mvh Einar

Fra: Kaspar Vereide [mailto:kaspar.vereide@ntnu.no]
Sendt: 29. mai 2015 14:10
Til: Einar Thygesen
Kopi: Daniel Gomsrud; Rolv Guddal
Emne: kostnader installering av strupning

Hei Einar, håper helsa er på rett kjøl igjen!

Vi prøver å beregne kostnad for strupningen, og lurer på om du har noen formening om hvor mye man bør regne som økonomisk tap per dag som Tonstad er stengt?
Vi antar nå at man kan regne en mindre sum per dag så lenge magasinene ikke er fulle + et stort tillegg per dag magasinene er fulle.

I 2010 var Tonstad stengt i 25 dager under revisjon, uten at man hadde flomtap fra hverken Homstøl og Ousdal.
Man kjørte da ned magasinene og produserte totalt 1 900 MWh (som man sikkert ikke fikk maksimal pris for) i forkant.
Dersom man ikke har flomtap, hvilke kostnader er dominerende da?

I tillegg lurer vi på hva dere bruker som diskonteringsrente og levetid for prosjekter? Vi ønsker å bruke det